Environmental Modelling & Software 99 (2018) 170–209

Contents lists available at ScienceDirect

Environmental Modelling & Software

journal homepage: www.elsevier.com/locate/envsoft

Development, implementation, and validation of a generic nutrient recovery model (NRM) library

C. Vaneeckhaute [a, b, c, *], F.H.A. Claeys [d], F.M.G. Tack [e], E. Meers [e], E. Belia [f], P.A. Vanrolleghem [a, c]

[a] modelEAU, Département de génie civil et de génie des eaux, Université Laval, 1065 Avenue de la Médecine, Québec, QC, G1V 0A6, Canada
[b] BioEngine, Research Team on Green Process Engineering and Biorefineries, Chemical Engineering Department, Université Laval, 1065 Avenue de la Médecine, Québec, QC, G1V 0A6, Canada
[c] CentrEau, Centre de recherche sur l'eau, Université Laval, 1065 Avenue de la Médecine, Québec, QC, G1V 0A6, Canada
[d] MIKE By DHI Software for Water Environments, Guldensporenpark 104, 9820 Merelbeke, Belgium
[e] Ecochem, Laboratory of Analytical and Applied Ecochemistry, Ghent University, Coupure Links 653, 9000 Ghent, Belgium
[f] Primodal Inc., 145 Rue Aberdeen, Québec, QC, G1R 2C9, Canada

ARTICLE INFO

Article history:
Received 13 October 2016
Received in revised form
14 July 2017
Accepted 8 September 2017
Available online 14 November 2017

Keywords:
Generic physicochemical model framework
Reduced PHREEQC
Resource recovery
Mathematical modelling
Numerical solution
Water chemistry
Anaerobic digestion model

ABSTRACT

The reported research developed a generic nutrient recovery model (NRM) library based on detailed chemical solution speciation and reaction kinetics, with focus on fertilizer quality and quantity as model outputs. Dynamic physicochemical three-phase process models for precipitation/crystallization, stripping and acidic air scrubbing as key unit processes were developed. In addition, a compatible biological-physicochemical anaerobic digester model was built. The latter includes sulfurgenesis, biological N/P/K/S release/uptake, interactions with organics, among other relevant processes, such as precipitation, ion pairing and liquid-gas transfer. Using a systematic database reduction procedure, a 3- to 5-fold improvement of model simulation speeds was obtained as compared to using full standard thermodynamic databases. Missing components and reactions in existing standard databases were discovered. Hence, a generic nutrient recovery database was created for future applications. The models were verified and validated against a range of experimental results. Their functionality in terms of increased process understanding and optimization was demonstrated.

Software and database availability

Name	Nutrient Recovery Model (NRM) library + Nutricover.dat database
Contact	Céline Vaneeckhaute, BioEngine, Research team on green process engineering and biorefineries, Chemical Engineering Department, Université Laval, 1065 avenue de la Médecine, Pavillon Adrien-Pouliot, Québec, QC, Canada, G1V 0A6, Tel. 1 418 656 28 59, E-mail: celine.vaneeckhaute@gch.ulaval.ca
Year first available	2016
Software required	WEST or Tornado (http://www.mikepoweredbydhi.com/products/west) and/or PHREEQC (http://wwwbrr.cr.usgs.gov/projects/GWC_coupled/phreeqc/)
Programming language	Modelica and C
Availability	Source code and databases can be obtained on request by contacting the corresponding author
Cost	Free

1. Introduction

In the transition from waste (water) treatment plants (WWTPs) to water resource recovery facilities (WRRFs), mathematical models are becoming important tools to hasten nutrient recovery process implementation and optimization (Vanrolleghem and Vaneeckhaute, 2014). Indeed, models may aid in technology development, process operation, optimization, and scale-up in a cost-effective way (Rieger et al., 2012; Yu et al., 2011). Although to

* Corresponding author.
E-mail addresses: celine.vaneeckhaute@gch.ulaval.ca (C. Vaneeckhaute), fhcl@dhigroup.com (F.H.A. Claeys), Filip.Tack@ugent.be (F.M.G. Tack), Erik.Meers@ugent.be (E. Meers), belia@primodal.com (E. Belia), peter.vanrolleghem@gci.ulaval.ca (P.A. Vanrolleghem).

http://dx.doi.org/10.1016/j.envsoft.2017.09.002

date many processes for the recovery of nutrients from waste(-water) have been proposed and applied to varying degrees, for example, struvite precipitation, ammonia stripping and acidic air scrubbing (Vaneeckhaute et al., 2017a), no generic models for nutrient recovery aiming at the construction and optimization of treatment trains for resource recovery are currently available (Vaneeckhaute et al., 2017b). Moreover, existing model libraries for WWTPs, e.g., activated sludge models (ASMs) provided by the International Water Association (IWA) (Henze et al., 2000; Gernaey et al., 2004), do not allow the integration of nutrient recovery unit processes and/or the coupling of a nutrient recovery treatment train. This is due to the omission of key fundamental physicochemical components and transformations that are essential to describe nutrient recovery unit processes (Batstone et al., 2012; Brouckaert et al., 2010; Flores-Alsina et al., 2015). Critical elements to be dealt with include accurate descriptions of acid-base reactions, slow precipitation kinetics, liquid-gas exchange and sorption/desorption in the complex mixture of chemical species that the resource recovery systems in place deal with (Batstone et al., 2012). Consequently, the potential to use models to adequately put together an optimal treatment train of unit processes and set the operating conditions that maximize nutrient recovery and fertilizer quality is missing.

Over the last 10 years, important progress was made towards the development and integration of a physicochemical modelling framework compatible with the current more biological process-oriented modelling frameworks provided by IWA (Flores-Alsina et al., 2016; Hauduc et al., 2015; Lizarralde et al., 2015; Mbamba et al., 2016). However, the scope of the existing studies stops at the anaerobic digestion of WWTP sludge, where it mainly aims at the prediction of uncontrolled struvite precipitation during digestion through phosphorus modelling. At the start of this research, no generic models were available that may allow to predict, optimize and control under dynamic conditions the recovered product quality (e.g., macronutrient content, particle size, density), yield and process performance of a series of nutrient recovery technologies following digestion of various waste(water) flows (manure, sludge, food waste, etc.).

The reported research aimed at developing a library of generic integrated biological-physicochemical three-phase mathematical process models for the most established nutrient recovery systems currently available as selected in Vaneeckhaute et al. (2017a), as well as a compatible model for anaerobic digestion. The models are based on detailed solution speciation and reaction kinetics, as brought forward in Vaneeckhaute et al. (2017b). This nutrient recovery model (NRM) library is a synthesis of the large body of knowledge on nutrient recovery processes that is currently available from research studies and operational experience. In contrast to existing model libraries for waste(water) treatment, e.g., the ASM library (Henze et al., 2000; Gernaey et al., 2004), the scope of the proposed NRM library starts at the anaerobic digester and focusses on the nutrient recovery treatment train following the digester.

In addition to the development of a generic physicochemical modelling framework, a critical and challenging step when combining biological and physicochemical differential equations is their numerical solution (Lizarralde et al., 2015). This is due to the stiffness that arises when considering reactions with very different conversion rates, i.e. the range of system time constants is large (Batstone et al., 2012; Brouckaert et al., 2010; Lizarralde et al., 2015; Musvoto et al., 2000; Rosen and Jeppsson, 2006; Sotemann et al., 2005). Previous attempts towards inclusion of a physicochemical modelling framework in existing WWTP models (e.g., Flores-Alsina et al., 2016; Hauduc et al., 2015; Mbamba et al., 2016; Takács et al., 2006) applied a limited literature-based selection of chemical species and reactions for self-implementation in the modelling software and used self-coded numerical solvers that have shown difficulties with convergence (Flores-Alsina et al., 2015). Moreover, when one wants to extend these models with new species and reactions, time-consuming and complicated programming work is required. Model flexibility is, however, particularly important for modelling of WRRFs due to the variability of waste (water) flows in time and between different facilities (Vanrolleghem and Vaneeckhaute, 2014). Lizarralde et al. (2015) proposed the coupling of an external existing geochemical software tool for inclusion of some basic speciation calculations in dynamic process models. The use of an external geochemical software tool with designated thermodynamic databases is interesting for accurate calculation of chemical speciation and pH. Software tools as PHREEQC and MINTEQ are generally accepted tools for equilibrium water quality modelling and have a dedicated and proven solver for chemical speciation calculations (Allison et al., 1991; Parkhurst and Appelo, 2013). However, simulation times using the full PHREEQC/MINTEQ thermodynamic databases for chemical speciation may be longer than when dedicated program code is used (Lizarralde et al., 2015). Hence, an important challenge exists in the development of an efficient methodology for including and solving the stiff equations related to the chemical speciation submodel in nutrient recovery models. A compromise should be found between model accuracy and simulation times.

The present paper describes the specifications, the development methodology and the implementation of the generic NRM framework. A systematic procedure to allow for inclusion of accurate chemical speciation in dynamic nutrient recovery process models at minimal computational effort is proposed. Model functionality in terms of increased process understanding and optimization is demonstrated through testing and validation. Recommendations for further experimental research required to fully calibrate the model dynamics, as well as case-specific potential model extensions, are provided.

2. Nutrient recovery model (NRM) building methodology

The methodology used for development of the NRM library can be represented by six steps, shown in Fig. 1 and described in detail in the sections below.

The proposed generic models are based on mass balances to describe physicochemical and biochemical transformation and transport processes, as well as an accurate calculation of water chemistry in order to correctly define solution speciation and driving forces for component transformation. Two key features of the models should be stressed. First, a dynamic modelling approach, i.e. one that accounts for time-dependent changes in the state of the system, was applied, because the models should be applicable to time-varying situations and variable operating conditions, such as i) periodical load variations, e.g., truck loads of waste, sludge treatment during working hours only, and seasonal variations, ii) individual disturbances, e.g., rain events and incorrect manipulations, and iii) systems that are operated intermittently or cyclically as is the case for multiple nutrient recovery processes, e.g., intermittent aeration in stripping systems and (semi-) batch processes to obtain target fertilizer specifications, e.g., a predefined ammonium sulfate (AmS) concentration in an acidic air scrubber. Second, the geochemical software tool PHREEQC was used for two purposes in the development of the NRM library:

1) **PHREEQC for NRM building** (Section 2.2.1), which involves the selection of species and reactions to be included in the models, the preparation of a reduced PHREEQC model database, and the definition of PHREEQC selected outputs;

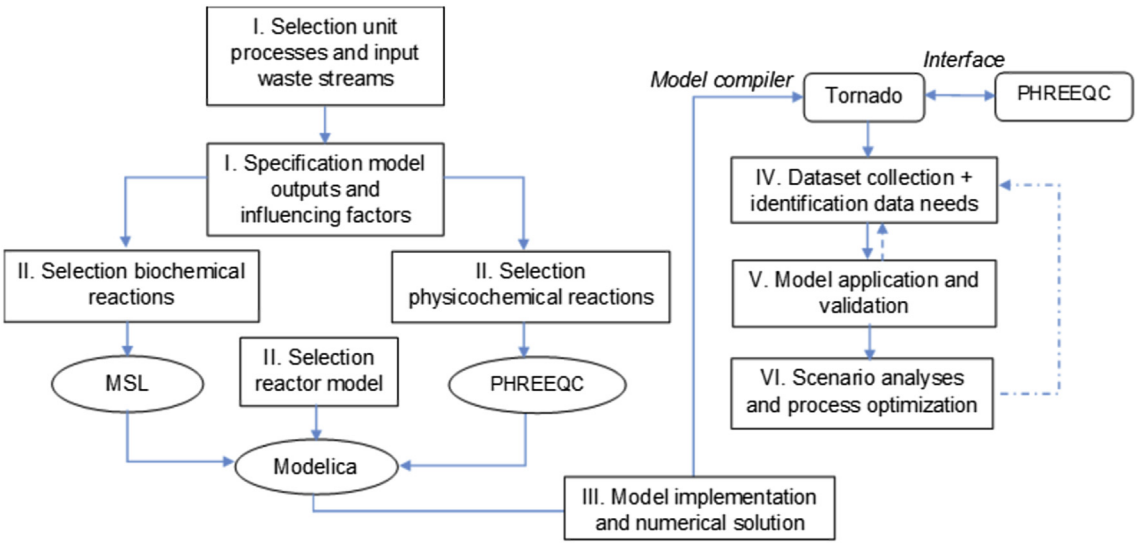

Fig. 1. Six-step model development scheme. Step I: definition of modelling objectives; Step II: theoretical model development; Step III: model implementation and numerical solution; Step IV: data collection and identification of data needs; Step V: model application and validation; Step VI: scenario analyses and process optimization; MSL = model specification language.

2) **PHREEQC for NRM simulation** (Section 2.3), which involves the tight coupling of the reduced PHREEQC model to a kinetic and dynamic mass balance model in order to accurately and efficiently calculate speciation and driving forces for component transformations at each time step during the model simulations.

As opposed to previously used speciation modelling methodologies (e.g., Flores-Alsina et al., 2016; Hauduc et al., 2015; Mbamba et al., 2016; Takács et al., 2006), the proposed methodology guarantees convergence and flexibility (Lizarralde et al., 2015). In order to reduce simulation times, a systematic procedure for thermodynamic model database reduction was proposed. Finally, it should be noted that in the following sections, variables will be defined with their dimension given in straight brackets: [*M*] for mass, [*L*] for length, and [*T*] for time.

2.1. Step I: definition of modelling objectives

2.1.1. Selection of considered/included unit processes and input waste streams

A literature review on nutrient recovery technologies (Vaneeckhaute et al., 2017a) was conducted in order to select the best available technologies as key unit processes for modelling (Table 1: four key units). The selection was made based on the economic feasibility, full-scale application at this stage, and the potential to produce marketable end products for agricultural applications. With the purpose of modelling treatment trains, four ancillary units were additionally selected (Table 1).

Table 1
Key units and ancillary units included in the nutrient recovery model (NRM) library.

Type	Unit	Model name
Key unit	Anaerobic digester	NRM-AD
Key unit	Precipitation/crystallization unit	NRM-Prec
Key unit	Stripping unit	NRM-Strip
Key unit	Air scrubber	NRM-Scrub
Ancillary unit	Settling tank	NRM-Settle
Ancillary unit	Storage tank	NRM-Store
Ancillary unit	Chemical dosing unit	NRM-Chem
Ancillary unit	Heat exchanger	NRM-Heat

As mentioned above, in contrast to existing studies, the scope of the present research starts at the anaerobic digestion unit and focusses on the nutrient recovery treatment train following the digester. No recycle flows to upstream facilities in the WRRF, e.g., to an activated sludge (AS) system, were currently considered. In later stages, the proposed NRM models could be coupled to activated sludge models (ASMs), if a generic physicochemical framework is also integrated in the ASMs.

As input waste stream to the digester, manure and sludge (primary and secondary sludge, and mixtures of these) from WWTPs removing nitrogen (N) and chemical oxygen demand (COD) were considered. Digestate, the remaining product after digestion, was considered as input stream to the key units for controlled nutrient recovery following the digester. Next to manure, WWTP sludge was selected since the current most advanced models for anaerobic digestion originate from the municipal wastewater and sludge treatment sector. Nevertheless, for future applications, the generic NRM-AD implementation allows easy extension to co-digestion of other organic-biological wastes, e.g., using the general integrated solid waste co-digestion (GISCOD) modelling tool proposed by Zaher et al. (2009). The NRM-AD model can also be extended to allow for specific reactions occurring during the treatment of sludge from enhanced biological phosphorus (P) removal (EBPR) as, e.g., in Ikumi (2011) or Wang et al. (2016), but this was considered to be outside the scope of this paper.

2.1.2. Specification of model outputs and influencing factors

In order to develop valuable tools for process optimization, the desired model outputs and factors that may affect these outputs were defined for each NRM key unit on the basis of a detailed literature review (Vaneeckhaute et al., 2017b).

Obviously, the total content of **principal macronutrients**, N, P, and potassium (K), in the fertilizer product and the amount of **biogas produced** are important model outputs, so as to quantitatively and qualitatively determine the overall resource recovery. Next to the three principal macronutrients, N, P, and K, previous studies have shown the relevance of the **secondary macronutrient**, sulfur (S), in the context of nutrient recovery (Vaneeckhaute et al., 2014). Some motivations for inclusion of S in the models were: i) the demand for S fertilization in agriculture is increasing, hence its recovery deserves

attention (Till, 2010), ii) S may precipitate with iron (Fe), making Fe less available for P precipitation, iii) sulfate reducing bacteria (SRBs) compete with methane (CH_4) producing bacteria for the same substrate, hence CH_4 production may be reduced at high S concentrations (Oyekola et al., 2007), iv) hydrogen sulfide (H_2S) is an important inhibitor of CH_4 producing bacteria (Oyekola et al., 2007), and v) high biogas H_2S values cause important concerns (toxicity, corrosion, biogas pollution), e.g., in the paper industry (Reiter and Piccot, 2004). Calcium (Ca) and magnesium (Mg) are also of importance, mainly for their soil improving properties and their interaction with P (Vaneeckhaute et al., 2016).

For all nutrient recovery systems, the **percentage recovery of the target nutrient** is a key performance measure. It was calculated using Equation (1):

$$\%\ Recovery\ = \frac{S_i^{in} \cdot Q_{in} - S_i^{out} \cdot Q_{out}}{S_i^{in} \cdot Q_{in}} \cdot 100 \quad (1)$$

in which S_i^{in} and S_i^{out} are the in- and outgoing liquid flow concentrations for component i [M L^{-3}], and Q_{in} and Q_{out} are the in- and outgoing flow rates [L^3 T^{-1}].

Furthermore, the **macronutrient use efficiency** (N, P, K, S) in the fertilizer end products is an important factor in determining the agronomic potential and sustainability of the produced fertilizers. It was evaluated as the percentage available or mineralized nutrient content over the total nutrient content, e.g., NH_4-N/total N and ortho-P/total P. This percentage can be obtained by means of a chemical solution speciation calculation (Section 2.2.1). Next, the fertilizer pH and **salt content** are of important concern as they may impact soil quality. The pH was directly calculated from solution speciation. Salts were characterized using the sodium adsorption ratio (SAR), i.e. the relative amount of available sodium (Na) over divalent cations, Ca and Mg (Hillel, 2008).

Factors that may additionally determine the value of the recovered product are the **particle size** (for solid fertilizers), the **density** (for liquid fertilizers), and the **product purity**. In this work the particle size was evaluated as mean particle diameter (Section 2.2.2), but in future research one may be interested in particle size distributions (PSDs) (Nopens et al., 2014; Perez et al., 2008).

For the NRM-Prec unit, product purity was evaluated by calculating the fraction of precipitated target mineral(s) over the total product collected, taking in account the presence of multiple competing and concurrent precipitation reactions. To this end, also the precipitation of principal **micronutrients** occurring in waste(-water) treatment, such as Fe and aluminium (Al), were evaluated, since these precipitates may negatively impact the fertilizer P release in the soil (Vaneeckhaute et al., 2016). Moreover, pollution with **organics** was accounted for (see Section 2.2.1). For the NRM-Strip/NRM-Scrub units, purity was evaluated by calculating the amount of volatile target component(s) captured over the total amount of gas/liquid captured.

Finally, the **formation of scale** within the treatment unit is an important operational bottleneck for multiple nutrient recovery technologies. Especially calcium carbonate ($CaCO_3$) and magnesium carbonate ($MgCO_3$) formation in the stripping and scrubbing units are of concern. To determine scale formation, the amount of $CaCO_3$ and $MgCO_3$ precipitates formed were evaluated, next to other relevant precipitation reactions. The scaling potential was then examined by using the scaling criteria of the Ryzner Index (Tchobanoglous et al., 2003).

2.2. Step II: theoretical model development

The dynamic mathematical model of each unit process was built using (Fig. 2): i) the definition of a chemical speciation model by means of geochemical modelling software (PHREEQC for model building, Section 2.2.1), ii) the description of a kinetic physicochemical and biochemical transformation model tailored to the models developed in the first step (Section 2.2.2), and iii) the selection of a reactor mass balance model to describe the (time-dependent) process conditions (Section 2.2.3).

2.2.1. Chemical speciation model: PHREEQC for NRM building

In order to describe the water chemistry in each system, first the potentially present chemical components and species were identified (step 1), and the possible heterogeneous physicochemical

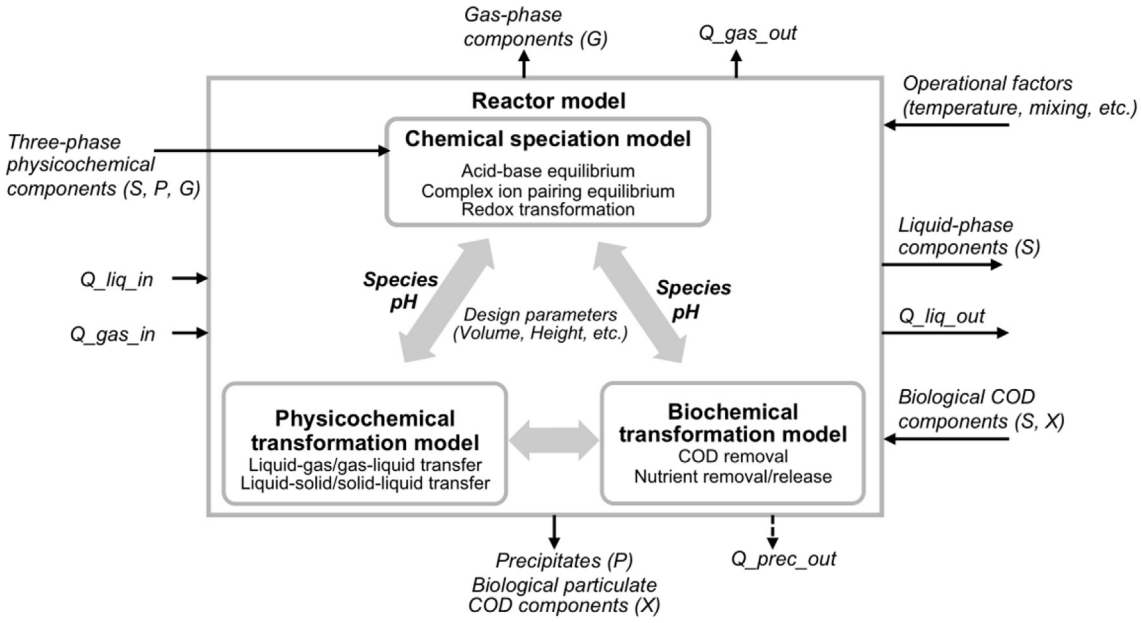

Fig. 2. Development of combined physicochemical-biological three-phase (liquid-solid-gas) process models. COD = chemical oxygen demand; G = gas; P = precipitate; Q_gas = gas flow rate; Q_liq = liquid flow rate; Q_prec = precipitate extraction rate (for NRM-Prec); S = soluble; X = biological particulate COD.

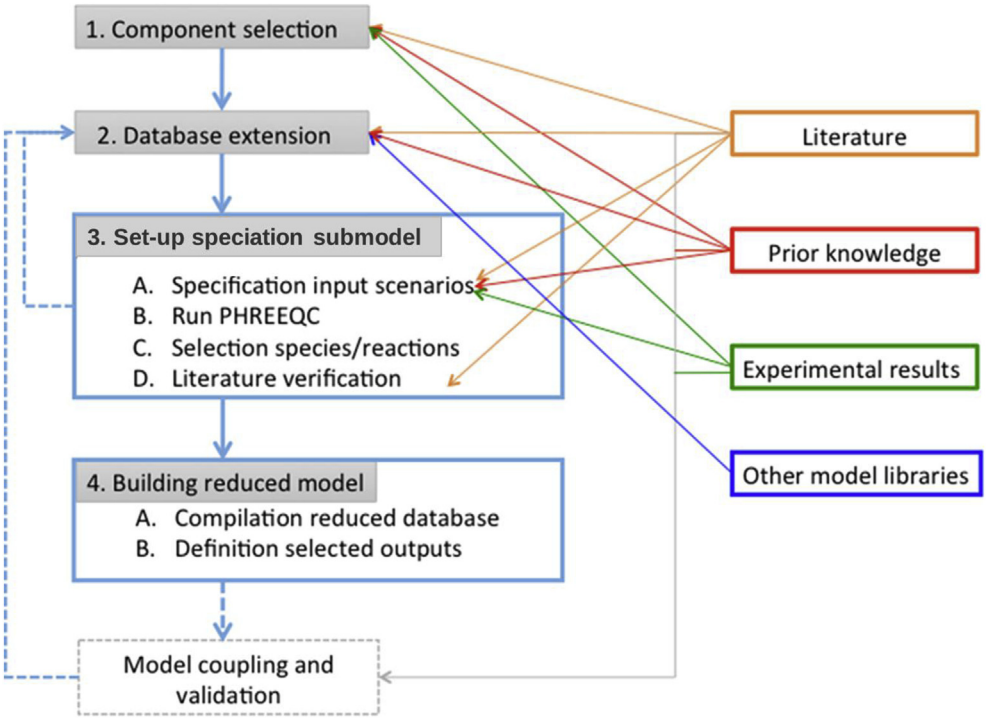

Fig. 3. Methodology for selection of relevant species and reactions per key unit and development of a reduced PHREEQC chemical speciation model for inclusion in the NRM library.

transformation reactions (gas transfer, precipitation) were selected using generally accepted geochemical software for equilibrium water quality modelling, PHREEQC 3.0.6 (Parkhurst and Appelo, 2013). Visual MINTEQ 3.1 was used as a control (Allison et al., 1991). Since the involved homogeneous reactions (acid-base, ion pairing) in a speciation calculation are very rapid compared to heterogeneous physicochemical reactions and biological reactions, instantaneous equilibrium can be assumed adequate for solving water chemistry in NRMs (Batstone et al., 2012).

In order to compromise between model accuracy and simulation times when coupling the speciation model to the dynamic mass balance model, a reduced PHREEQC database and input script with defined selected model outputs were developed for each key unit (Section 2.3.1). The four-step procedure proposed for NRM building, involving the selection of the relevant species/reactions and the preparation of the reduced PHREEQC chemical speciation model, is presented in Fig. 3 and further described below.

2.2.1.1. Step 1 - selection of relevant components for each unit process. Based on literature, collected experimental data and prior knowledge, the most important physicochemical dissolved components to include in models for nutrient recovery from both (digested) manure and sludge were selected for each key unit process (Table 2). In line with the selected model outputs (Section 2.1.2), it was aimed to represent **five important component classes**: 1) All important macronutrients for recovery in line with the findings in Vaneeckhaute et al. (2014) (~impact recovery efficiency and fertilizer value); 2) Gaseous compounds (~impact biogas production, volatilization, odors, greenhouse gas emissions, among other); 3) Salts (~impact ionic strength and soil quality); 4) Inorganic and organic carbon compounds (~impact biogas production, product purity, and scaling); 5) Micronutrients that may occur in large quantities in waste(water) treatment, e.g., Fe and Al as a result of coagulation/flocculation practices (~impact product purity and recovery potential).

Since redox reactions were also considered, components that exist in more than one valence state in solution were identified by their component name followed by their valence. For instance, i) the component S_C_4_ (carbon +IV) constitutes CO_3^{2-} plus HCO_3^- plus H_2CO_3 (or $CO_{2,aq}$) plus various other carbonate complexes present in the solution, such as $MgCO_3$ and $CaHCO_3^+$, and ii) S_N_min3_ (nitrogen −III) constitutes both NH_4^+ and dissolved NH_3, as well as its various complexes. Only for Fe, the two valence states, Fe (+II) and Fe (+III), were lumped together into one component for total Fe, since the measurement of its valence is complicated and generally not provided in practice in WRRFs, nor in literature. Yet, in the speciation calculation, the Fe (+II) /Fe (+III) redox equilibrium was considered, as calculated from the occurring redox potential. The input Fe redox states, e.g., Fe(+III)Cl_3 and Fe(+II)SO_4, can optionally be specified, if such data are available.

As it is well-known that the presence of organic compounds may influence the purity of recovered products (Kozic et al., 2011), relevant interactions between inorganic and organic components were also accounted for. Among the organic biological components considered (see Section 2.2.3), volatile fatty acids (VFAs) up to valerate were included as individual components in the physicochemical models. Oh and Martin (2010) indeed emphasized the particular importance of their physicochemical behaviour in WRRFs. The remaining soluble organic chemical oxygen demand (COD) fractions (see Section 2.2.3) were lumped into one component, i.e. dissolved organic carbon (DOC; 1 g DOC ≈ 0.33 × g COD). For DOC, the complexation with metals (Ca, Mg) was computed using a competitive Gaussian model for dissolved organic matter (DOM; 1 mol DOC ≈ 8.6×10^{-2} mol DOM; USEPA, 1999). This simplified approach may be further refined for future applications, if more insights in the physicochemical behaviour of each particular COD fraction become available.

Finally, it should be remarked that heavy metals, such as cadmium (Cd), copper (Cu), and zinc (Zn), were not yet included in the speciation models. Nevertheless, heavy metals and the

Table 2
Dissolved physicochemical components selected for each key unit in the nutrient recovery model (NRM) library. AD = anaerobic digestion; Prec = precipitation/crystallization; Strip = stripping; Scrub = scrubbing. Component names are given by their valence state.

Symbol	Component	AD	Prec	Strip	Scrub	Symbol	Component	AD	Prec	Strip	Scrub
S_Acetate	Acetate	X	X	X	–	S_K	Potassium	X	X	X	–
S_Al	Aluminium	X	X	X	–	S_Mg	Magnesium	X	X	X	–
S_Butyrate	Butyrate	X	X	X	–	S_Na	Sodium	X	X	X	–
S_Ca	Calcium	X	X	X	–	S_N_min3_	Nitrogen (-III)[f]	X	X	X	X
S_C_4_	Carbon (+IV)[a]	X	X	X	X	S_N_0_	Nitrogen (0)[g]	X	(X)[l]	X	X
S_Cl	Chloride	X	X	X	–	S_N_5_	Nitrogen (+V)[h]	X	X	X	X
S_C_min4_	Carbon (−IV)[b]	X	–	X	X	S_O_0_	Oxygen (0)[i]	–	(X)[l]	X	X
S_DOM	Dissolved OM[c]	X	X	X	–	S_P	Phosphorus	X	X	X	–
S_Fe	Iron	X	X	X	–	S_Propionate	Propionate	X	X	X	–
S_H_0_	Hydrogen (0)[d]	X	–	X	X	S_S_min2_	Sulfide (-II)[j]	X	X	X	X
S_H_I_	Hydrogen (+I)[e]	X	X	X	X	S_S_6_	Sulfate (+VI)[k]	X	X	X	X
S_H2O	Water	X	X	X	X	S_Valerate	Valerate	X	X	X	–

[a] Carbonate species.
[b] CH_4(aq).
[c] OM = organic matter.
[d] H_2(aq).
[e] Refers to pH.
[f] Ammonia species.
[g] N_2(aq).
[h] Nitrate species.
[i] O_2(aq).
[j] Sulfide species.
[k] Sulfate species.
[l] Values between brackets represent the use of air instead of chemicals for pH-adjustment.

corresponding reactions are available in PHREEQC. Hence, the generic approach used for chemical speciation allows easy extension of the models to incorporate heavy metals for future applications.

2.2.1.2. Step 2 - addition of relevant components/species/reactions to generic geochemical databases. To verify completeness, the generic PHREEQC (Phreeqc.dat) and MINTEQ (minteq.v4.dat) databases were compared with each other, as well as with prior knowledge and with literature. Two observations were made: 1) the generic MINTEQ database is more complete than the PHREEQC one in view of WRRF modelling, 2) some important components, species, and reactions that can be expected in WRRFs are not included in either database. Hence, the generic database files were extended prior to use for speciation calculation (Table 3). The corresponding acid-base constants, ion pairing constants, solubility products, and other thermodynamics were taken from literature or other model libraries, as indicated in Table 3.

It should be noted that in the context of nutrient recovery from waste(water) flows as fertilizer products, the database extensions provided concern a fundamental contribution to the field. For example, K-struvite is, next to N-struvite, an interesting fertilizer, though its precipitation reaction is not included in the standard databases. Also precipitation of aluminium phosphate ($AlPO_4$) is highly important in waste(water) treatment since Al-salts are often dosed for sludge conditioning, whereas the precipitation reaction of ammonium sulfate, $(NH_4)_2SO_4$, is essential for description of the scrubbing process. Noteworthy is also the clear impact of the omission of the species monosodium phosphate, i.e. NaH_2PO_4(aq), on the simulation results, as was observed during model validation of the NRM-Prec (see Section 3.4.1). The generic extended database in view of nutrient recovery was named *'Nutricover.dat'* and will be made available for inclusion in future PHREEQC and MINTEQ software packages.

2.2.1.3. Step 3 - setting up the speciation submodel = selection of relevant species and reactions. The following methodology was used for selection of the relevant species and reactions:

A. Specification of input scenarios (components + operational conditions);
B. Run PHREEQC under the various conditions defined in A;
C. Select relevant species and reactions based on the PHREEQC outputs;
D. Verify the selection of species and reactions with literature.

***A. Specification of input scenarios*:** Realistic ranges for the input component concentrations and operational conditions (e.g., pH and temperature) for the speciation calculations were adopted from literature and experimental data as described in Section 2.4, as well as through contact with technology providers. The operational conditions and input streams tested for each key unit process are the following:

➢Anaerobic digestion: no oxygen, pH: 5–8.5, temperature: 20–55 °C, input: sludge and manure;
➢Precipitation unit: pH: 7–11, temperature: 20–50 °C, with and without $Ca(OH)_2$, CaO, $MgCl_2$, $Mg(OH)_2$, or MgO dosing (0–500 mol m^{-3}), input: digestate;
➢Stripping unit: pH: 7–11, temperature: 20–70 °C, with and without NaOH, $Ca(OH)_2$, CaO, $Mg(OH)_2$, or MgO dosing for pH-increase (0–500 mol m^{-3}), input: digestate;
➢Air scrubber: H_2SO_4-solution at pH: 1–4 and temperature: 15–25 °C, input: stripped air.

Table 3
Extensions made to the generic PHREEQC (P; Phreeqc.dat) and/or MINTEQ (M; minteq.v4.dat) database files, and the reference for thermodynamic data. DOM = dissolved organic matter.

Extension	Name	Database	Reference
Components	acetate, butyrate, propionate, valerate, DOM	P	M, USEPA (1999)
Species	$Ca(acetate)^+$, $Ca(butyrate)^+$, $CaCl^+$, Ca-DOM, $CaNH_3^{2+}$, $Ca(NH_3)_2^{2+}$, $Ca(propionate)^+$, $Ca(valerate)^+$, $FeH_2PO_4^+$, $FeNH_3^{2+}$, $Fe(NH_3)_2^{2+}$, H(acetate), H(butyrate), H-DOM, H(propionate), H(valerate), K(acetate), KCl(aq), KOH, KPO_4^{2-}Mg(acetate)$^+$, $Mg(butyrate)^+$, $MgCl^+$, Mg-DOM, $Mg(NH_3)_2^{2+}$, $Mg(propionate)^+$, Na(acetate), NaCl(aq), NaH_2PO_4(aq)	P	M, USEPA (1999)
	NH_2COO^-	P + M	Hafner and Bisogni (2009)
Precipitates	FeS(ppt), Mackinawite (FeS)	P	M
	$AlPO_4$, $K_2NH_4PO_4{:}6H_2O$, $(NH_4)_2SO_4$	P + M	NIST (2001)
	K-struvite ($MgKPO_4{:}6H_2O$)	P + M	Chauhan et al. (2011)

PHREEQC makes calculations using an input script in which the problem is specified via 'KEYWORDS' and associated data blocks. First, all possible realistic scenarios were introduced using the maximum/minimum values of all considered operational factors and input variables for each unit separately. Next, for each unit the composition of 20 different possible input flows (from literature: Astals et al., 2013; Bhuiyan et al., 2007; Cesur and Albertson, 2005; Martin, 2003; Mattocks et al., 2002; Tchobanoglous et al., 2003; Vaneeckhaute et al., 2012, 2013a, 2014; Vlaco, 2012; Zaher et al., 2009) was used for simulation under variable operating conditions. To this end, a PHREEQC input script was developed for each unit, involving the identification of the input waste flows (PHREEQC data blocks: 'SOLUTION' and/or 'GAS'). A batch reaction calculation was also coded in case there is both a gas and liquid input, i.e. for the stripper and scrubbing unit (PHREEQC data block: 'REACTION'). Then, one factor at a time was allowed to increase within its range (e.g., PHREEQC code: REACTION_TEMPERATURE 20.0–70.0 in 51 steps), while the other factors were kept fixed. As such, a broad range of input scenarios was screened. Note that currently no alternative strategy is available in PHREEQC for selection of the various simulation scenarios (Parkhurst D. personal communication 2014). Yet, the development of an adequate, but more time-efficient, procedure to go through a multidimensional set of factors will be aspect of further research.

B. Run PHREEQC: Speciation calculations in PHREEQC/MINTEQ are made using designated thermodynamic databases that include a wide range of data for mineral phases and compounds. The calculations are based on three types of equations: 1) equilibrium relationships, 2) concentration conditions or mass balances (one per component), and 3) electro-neutrality conditions or charge balances (Chapra, 2008; Stumm and Morgan, 1996). By inclusion of oxidation/reduction reactions in the database, also the components' redox states were defined in the speciation calculations. The pH may be defined or adjusted according to the charge balance. The Davies equation was selected for ion activity correction in the NRMs, similar to Ali and Schneider (2008), Galbraith et al. (2014), Lizarralde et al. (2015), Ohlinger et al. (1998) and Flores-Alsina et al. (2016). The Davies ion activity correction was also recommended by Hafner and Bisogni (2009) above other relevant approaches, such as the Pitzer ion interaction approach. Moreover, the Peng-Robinson equation of state, which corrects for the non-ideal behaviour of gases, was used for calculating partial pressures (p) and solubility (Parkhurst and Appelo, 2013). Furthermore, the temperature dependency of the thermodynamic equilibrium coefficients was expressed by means of the Van't Hoff relationship (Zumdahl, 2005), while the value of the water dissociation constant (K_w) at different temperatures (other than 25 °C) was computed using the equation of Harned and Hamer (1933).

C/D. Selection criteria + verification: From the speciation calculations the distribution of aqueous species (= ion activities) and saturation indices (SI) for phases (= driving forces for precipitation and gas transfer) were obtained. Soluble species with an insignificantly low activity, i.e. less than 0.01% of the total component activity in all scenarios, were excluded from the NRMs. Solids that may potentially precipitate ($SI \geq |0|$) as well as gases that may volatilize (partial pressure (p) > 0) in the different units were selected. Conditions (pH, temperature) and rates for precipitation of the various forms of the selected minerals were also researched in the literature. The aim was to confirm the exclusion of the selected insignificant species and precipitates, while further identifying potential species and reactions that should be included in the database for each unit. The number of species and reactions that were found to be relevant according the speciation calculations and that were included in each NRM are presented in Table 4a. The list of species involved and the transformation reactions included in each model are presented in Appendix 1 (Table A1.1 and Tables A1.2–1.6, respectively).

2.2.1.4. Step 4 - building of a reduced model. Knowing that the generic geochemical model databases contain more than 3000 species (Allison et al., 1991), it was expected that the elimination of irrelevant species and reactions can have a significant impact on the simulation speed. As such, with the purpose of reducing model complexity and simulation times when coupling PHREEQC for NRM simulation (Section 2.3), a new PHREEQC database file including only the selected reactions and species was set up for each unit process. Moreover, a 'SELECTED_OUTPUT' data block was coded in the input script for each unit in order to transcribe only the appointed species and driving forces to the resulting output file. The latter is required for efficient coupling of the selected outputs to the kinetic and mass balance model (Section 2.3).

Finally, simulation results and speeds using the reduced model were compared with results and speeds obtained by running the developed chemical speciation scripts using the full Phreeqc.dat (P) and minteq.v4.dat (M) databases available in the PHREEQC 3.0.6 release.

2.2.2. Physicochemical transformation model

Heterogeneous physicochemical reactions, such as liquid-gas transfer and precipitation, occur much slower than the homogeneous reactions involved in the speciation calculations presented above. Hence, a kinetic approach was applied in order to allow for dynamic variation of the constituents.

Gas exchange processes in resource recovery systems can occur passively, i.e. without intensive gas bubbling (NRM-AD), or actively, i.e. with gas bubbling driven by an external air flow (NRM-Strip, NRM-Scrub). In each case similar kinetic gas exchange formulations based on the concentration driving force between the liquid and gas phases apply (Eq. (2)):

Table 4a
Number of selected species and reactions for each key unit in the nutrient recovery model (NRM) library resulting from speciation calculations using PHREEQC (and Visual MINTEQ as control) modelling software. AD = anaerobic digestion; Prec = precipitation/crystallization; Strip = stripping; Scrub = scrubbing.

	NRM-AD	NRM-Prec	NRM-Strip	NRM-Scrub
No. of dissolved ionic species	80	86(87)[a]	80	18
No. of reactions				
Acid-base reactions	12	11	10	6
Ion pairing	48	55	47	2
Redox reactions	6	4/(5)[a]	7	6
Precipitation/Dissolution	27	28	30	1
Liquid-gas/Gas-liquid exchange	7	0/(5)[a]	7	7

[a] Values between brackets represent the use of air instead of chemicals for pH-adjustment.

$$\rho_{T,i}\left[\mathrm{M\ L^{-3}\ T^{-1}}\right] = K_{L/G,i}\cdot a\cdot\left(S_{liq,i} - H_{T,i}\cdot p_{gas,i}\right) \quad (2)$$

where $S_{liq,i}$ is the liquid phase activity of component i [M L^{-3}], $p_{gas,i}$ is the partial pressure in the gas phase of component i (atm), $H_{T,i}$ is the temperature-dependent Henry coefficient [M L^{-3} atm^{-1}], $H_{T,i}\cdot p_{gas,i}$ represents the saturation concentration of gas component i in the liquid, $K_{L/G,i}$ is the overall liquid-gas mass transfer coefficient [L T^{-1}], and a is the specific surface of the gas bubbles per reactor volume [L^{-1}]. Temperature dependency of H was described by a Van't Hoff relationship (Powers et al., 1987), while temperature dependency of $K_{L/G,i}a$ was described using the Arrhenius equation (Chapra, 2008). Through the coupling with PHREEQC (Section 2.3.1), both $S_{liq,i}$ and $p_{gas,i}$ can be calculated at every time step during the simulations. The total gas phase pressure was computed using Dalton's law of partial pressures (Stumm and Morgan, 1996). For calculation of $K_{L/G,i}a$, a distinction was made between active and passive systems, since the values may differ significantly in practice (Chapra, 2008; Sotemann et al., 2006; Tchobanoglous et al., 2003). Moreover, a second distinction was made depending on the solubility of the gas considered, which determines whether mass transfer is liquid film controlled (for low to moderate soluble gases: $H > 0.55$, i.e. for CH_4, CO_2, H_2, H_2S, N_2, O_2 = all gases considered in the NRMs, except for NH_3) or gas film controlled (for very soluble gases: $H < 0.55$, e.g., for NH_3). As such, **four potential mass transfer scenarios** were considered, which are described in detail in Appendix 2: 1) Active liquid-gas/gas-liquid transfer (NRM-Strip, NRM-Scrub) of low to moderately soluble gases; 2) Active liquid-gas/gas-liquid transfer (NRM-Strip, NRM-Scrub) of very soluble gases; 3) Passive liquid-gas/gas-liquid transfer (NRM-AD) of low to moderately soluble gases; 4) Passive liquid-gas/gas-liquid transfer (NRM-AD) of very soluble gases.

The **kinetic liquid-solid/solid-liquid transfer mechanisms** described in all NRMs are nucleation (= birth of crystals), crystal growth, and redissolution. All reactions were represented by an empirical power law (Eq. (3)) using **relative supersaturation ($S - 1$)** as driving force (Ali and Schneider, 2008; Galbraith et al., 2014; Harrison et al., 2011; Nielsen, 1984):

$$\rho_{T,i}\left[\mathrm{M\ L^{-3}\ T^{-1}}\right] = k_T\cdot(S-1)^n \quad (3)$$

in which S is the saturation ratio ($= \left(\frac{IAP}{K_s}\right)^{1/\nu}$), ν refers to the stoichiometric precipitation coefficient which represents the total number of species involved in the precipitation reaction, IAP is the ion activity product [M L^{-3}], K_s is the solubility product [M L^{-3}], k_T is the temperature dependent transfer coefficient [M L^{-3} T^{-1}], and n is the reaction order. The value of S was directly derived from the saturation index, $= \log\left(\frac{IAP}{K_s}\right)$, which is calculated by PHREEQC at every time step during model simulations. The temperature dependency of the reaction rate was modelled by means of the Arrhenius equation (Greenberg and Tomson, 1992; Nielsen, 1984).

Using literature values for the molecular weight (MW) and density of the different precipitates, the total volume ($V_{fertilizer}$), total mass/moles ($M_{fertilizer}$), and MW ($MW_{fertilizer}$) of the recovered fertilizer product (composed of the various precipitates) was calculated at every time step. The time-dependent number of particles (N_{part}) was then determined using the Avogadro constant ($N_A = 6.022 \times 10^{23}$ mol^{-1}). The mean particle diameter (d_p) of the precipitates was calculated assuming spherical particles using Equation (4):

$$d_p\ [\mathrm{L}] = \sqrt[3]{\frac{V_{fertilizer}}{N_{part}\cdot\frac{\pi}{6}}} \quad (4)$$

The kinetic precipitation/dissolution coefficient k_T and the reaction order n in Equation (3) were adjusted according to the liquid-solid/solid-liquid transfer mechanism occurring: $k_{G,T}$ and n_G for growth, $k_{B,T}$ and n_B for nucleation, $k_{D,T}$ and n_D for dissolution. The prevalent mechanism depends on the value of S and the amount of seed material in the reactor. Hence, these values were checked at every time step. As such, four possible scenarios were considered, which are described in detail in Appendix 2: 1) Supersaturation occurs ($S > 1$; $SI > 0$) and seed material is available; 2) Supersaturation occurs ($S > 1$; $SI > 0$), but no seed material is available and/or the crystal size is not large enough to have any influence on the process, i.e. the induction time is not exceeded; 3) The solution is undersaturated ($S < 1$; $SI < 0$) and precipitate is present in the system; 4) Equilibrium occurs ($S = 1$; $SI = 0$).

Finally, for the NRM-Prec, a generic mechanism for **agglomeration and floc break-up** through the effect of mixing was included using the spherical particle model for macroscale flocculation (Crittenden et al., 2012, Appendix 2). A time-dependent agglomerate number balance was also provided (Section 2.2.4). By division of the total fertilizer volume by the number of agglomerates, the agglomerate volume was obtained. The mean agglomerate diameter can then be computed in the same way as the particle diameter (Eq. (4)).

It should be remarked that mixing energy may also have to be included in Equation (3). Growth can be assumed surface integrated controlled when the system is well mixed, so the mixing effect can be neglected for the growth equations in unit processes with proper mixing (Galbraith et al., 2014; Rahaman et al., 2014). However, mixing may affect the nucleation mechanism and induction time through microscale flocculation (Ohlinger et al., 1998). This mechanism is very site and species specific, hence it was considered out of the scope of the present generic model development study. However, by selecting a generic empirical equation based on S (Eq. (3)), the models could easily be extended to include mixing effects (Galbraith et al., 2014; Perez et al., 2008), if

appropriate parameter correlations are available. As mentioned above, future extensions may also involve particle size distributions (PSDs) (Nopens et al., 2014; Perez et al., 2008).

2.2.3. Biochemical transformation model

Biochemical processes and state variables are clearly important for the NRM-AD model. The description, stoichiometry, and kinetics of biochemical transformations that may be expected in the NRM-AD were based on the Anaerobic Digestion Model No. 1 (ADM1; Batstone et al., 2002), resulting in a total of 19 processes (Appendix 3: Table A3.1). pH, H_2, and NH_3 inhibition expressions were taken from Batstone et al. (2002). Over the last ten years, various WRRF modellers (e.g. Flores-Alsina et al., 2016; Mbamba et al., 2016; Solon et al., 2015; Wang et al., 2016) have developed extensions of ADM1, mainly focused on the inclusion of a limited selection of chemical species and reactions to predict unwanted struvite precipitation and S inhibition in the digester. Since pH plays a critical role in anaerobic digestion modelling (Batstone et al., 2012; Solon et al., 2015; Vaneeckhaute et al., 2017b), inclusion of a more accurate and complete chemical speciation calculation, with associated efficient numerical solution procedure, to predict pH and driving forces for physicochemical and biochemical transformations is highly relevant.

In this study, ADM1 was for the first time extended with all essential physicochemical components and processes (acid-base reactions, ion pairing, liquid-solid transfer, liquid-gas transfer, redox transformations) that significantly impact anaerobic digester performance and digestate quality, selected in Section 2.2.1 (Appendix 3: Table A3.1, Extension 1). Ion pairing of cations with VFAs was also accounted for. On top of being important for predicting anaerobic digestion pH and performance, inclusion of such detailed physicochemical framework is essential for predicting process performance and product quality of physicochemical nutrient recovery unit processes that follow the digester. Indeed, the output digestate characteristics from the anaerobic digestion model should be sufficiently specified and compatible with the required input to the nutrient recovery unit process models. Similar as in Lizarralde et al. (2010), biological sulfate reduction (= sulfurgenesis) was incorporated based on the model proposed by Knobel and Lewis (Appendix 3: Table A3.1, Extension 2). An inhibition term for H_2S was incorporated in the appropriate biokinetics (I_{H2S}), and its transfer to the gas phase was included as described in Section 2.2.2. The decay of SRBs was included in the same way as the decay of other organisms described in the ADM1 model (Batstone et al., 2002). N, P, K, and S release from biomass, as well as nutrient uptake by growing biomass was accounted for (Appendix 3: Table A3.1, Extension 3). Modelling of EBPR sludge was considered beyond the scope of this study (Section 2.1.1), but for future applications the NRM-AD could be further extended using equations from, e.g., Ikumi (2011), Flores-Alsina et al. (2016) or Wang et al. (2016) (Appendix 3: Table A3.1, Potential Extension 4). Finally, N and P release through disintegration of complex particulates, P release from lipid hydrolysis, N release from protein degradation and amino acid uptake, as well as the N and P content of soluble and particulate inerts were also included. The detailed stoichiometric matrix and kinetic transformation equations proposed can be found in Appendix 3 (Tables A3.2-A3.4).

In this study, the biological solids leaving the digester were supposed to end up mainly in the solid fraction after solid-liquid separation of the digestate. Hence, in the subsequent key units for nutrient recovery, it was assumed that biochemical particulate transformations do not play a significant role. Nevertheless, in order to allow coupling of NRMs to activated sludge models (ASMs) in a later stage (through return liquors, for instance), the biological state variables were integrated in all NRMs. Note that the physicochemical interactions with the remaining soluble COD components were included in all models (Section 2.2.1).

2.2.4. Reactor model

The used reactor design and the default specifications and features for each unit process are compiled in Appendix 4. For each unit process, a mass balance was written, not only for all components in the liquid phase (S), e.g., Equation (5), but also for all components in the gas phase (G), all precipitated components (P), and all particulate biological solids (X), including both a transport term (based on in- and outgoing flow rates) and a transformation term (involving liquid-gas/gas-liquid transfer, liquid-solid/solid-liquid transfer, and biochemical transformations):

$$\frac{d\left(S_{liq,i}\cdot V_{liq}\right)}{dt}\left[\mathrm{M\ T^{-1}}\right] = S_{liq_{in},i}\cdot Q_{liq_{in}} - S_{liq,i}\cdot Q_{liq_{out}} + V_{liq}\cdot\sum_{j=1:n}\rho_j\cdot\nu_{i,j} \quad (5)$$

where $\sum_{j=1:n}\rho_j\cdot\nu_{i,j}$ is the summation of the specific kinetic process rates for process j (ρ_j, [M L^{-3} T^{-1}]) multiplied by the stoichiometric coefficient for component i on process j ($\nu_{i,j}$, [M M^{-1}]), $Q_{liq_{in}}$ and $Q_{liq_{out}}$ are the in- and outgoing liquid flow rates [L^3 T^{-1}], V_{liq} is the bulk reactor volume [L^3], and $S_{liq_{in},i}$ and $S_{liq,i}$ refer to the activities of the in- and outgoing liquid components [M L^{-3}].

In addition, a mass balance for the seed material in the reactor was included, similar as Equation (5). The mass of seed material was adjusted in time according to the mass of precipitates present in the reactor and the liquid volume. Hence, it was assumed that newly formed crystals act as seed material for precipitation, similar as was experimentally discovered by Le Corre et al. (2007). External seed material can also be added.

For the precipitation unit (NRM-Prec), also particle and agglomerate number balances were implemented. The number of free precipitated particles was assumed to reduce according to the agglomerates formed, as in Crittenden et al. (2012). Note that agglomeration was only accounted for when mixing is present in the reactor (Section 2.2.2).

2.3. Step III: model implementation and numerical solution

2.3.1. Model coding and state vector definition

The main coding language used in this study was Modelica, which is a high-level, declarative, and object-oriented modelling language (Claeys et al., 2006; Elmqvist et al., 1999). It is similar to the model specification language (MSL), which is currently used in Tornado/WEST (mikebydhi.com; Vanhooren et al., 2003), one of the most common software packages used in waste (water) quality modelling. However, Modelica has a better readability and expressiveness, and because of the more important industrial use (Audi, Ford, Siemens, etc.) of Modelica compared to MSL, the modelling community using Tornado/WEST recently decided to convert all conventional models for waste (water) treatment from MSL to the more powerful and more widely supported Modelica coding language. Tornado/WEST supports the use of both MSL and Modelica languages (Claeys et al., 2006).

As mentioned above (Section 2.2.1), a PHREEQC script was written for each unit process separately in order to include water chemistry. A 'SELECTED_OUTPUT' statement involving the selected species activities, saturation indices (*SI*'s), partial pressures (*p*'s), as well as the pH, temperature, alkalinity, and ionic strength was defined. The obtained *SI*'s and *p*'s are then used as driving forces for

precipitation and gas transfer in the Modelica code describing the slow transformation processes (Eqs. (2) and (3)).

Since only small differences exist between the selected components for the different NRMs (Table 2), it was decided to define one generic component state vector for each different phase. As such, five different NRM component state vectors were enumerated (Appendix 5: Table A5.1): 1) *Components_S1*: the components in the liquid phase, i.e. the main waste flow; 2) *Components_S2:* the components in the H_2SO_4-solution used in NRM-Scrub; 3) *Components_G:* the components in the gas phase; 4) *Components_P*: the components in the precipitated phase; 5) *Components_X*: the particulate biological solids. The *Components_S1* state vector was further split into a *Components_S1_PC* and a *Components_S1_Bio* state vector in order to describe physicochemical transformations and biological COD transformations separately. All state variable quantities involved in the physicochemical calculations (*Components_G*, *Components_P*, *Components_S1_PC*) were expressed on a molar base, whereas the state variables only involved in biological transformations (*Components_X*, *Components_S1_Bio*) were expressed on a COD-base. Moreover, for each model separately, a species state vector was enumerated referring to the PHREEQC selected output, which is different for each unit process.

Parameters and equations for the (slow) physicochemical and biochemical transformations, and mass balances for all total components were implemented in Modelica using a multi-matrix structure. The Tableau method matrix implementation of Morel and Herring (1993) was used as generic method for linking total soluble component activities to species activities and total precipitated component concentrations to precipitate concentrations in the NRMs, whereas the Gujer (2008) matrix implementation was used to describe the biochemical reactions involved.

2.3.2. Numerical solution and model execution procedure

To overcome problems related to the numerical solution of stiff systems (see Section 1), the slower reactions (Sections 2.2.2–2.2.4) and mass balances (Section 2.2.5) were represented by ordinary differential equations (ODE) coded in Modelica, while the fast reactions (Section 2.2.1) were assumed to reach steady state instantaneously and were calculated algebraically by use of algebraic equations (AE) at each iteration step using the software tool PHREEQC (Parkhurst and Appelo, 2013). In contrast to other WRRF modellers (e.g., Flores-Alsina et al.,2016; Hauduc et al.,2015; Mbamba et al., 2016; Takács et al., 2006) that implemented their own water chemistry module, the use of PREEQC to solve water chemistry was brought forward in this study (see Section 2; Vaneeckhaute et al., 2017b). PHREEQC has a dedicated and proven solver (Newton Raphson-based) for the complex set of implicit non-linear equilibrium equations involved. PHREEQC was preferred over other geochemical models (e.g., MINTEQ, WHAM, and WATEQ4F), because of its ease of integration with diverse scripting languages and other model libraries, next to its more precise methodology for precipitation calculations (Charlton and Parkhurst, 2011). Recently, a C-callable API (Application Programming Interface) for the PHREEQC engine has become available under the name IPhreeqc. It allows for easily coupling of the PHREEQC engine to software developed in other programming languages. The API provides direct access to the geochemical processes in the PHREEQC library, as well as support for new PHREEQC specification keywords that allow for easier manipulation of PHREEQC input and output data (Charlton and Parkhurst, 2011).

The models coded in the Modelica language, with invocations of the PHREEQC engine for speciation calculation, were then executed through the Tornado/WEST framework for modelling and virtual experimentation on the basis of sets of complex ODEs and AEs. A generic mechanism for calling PHREEQC from Modelica-specified

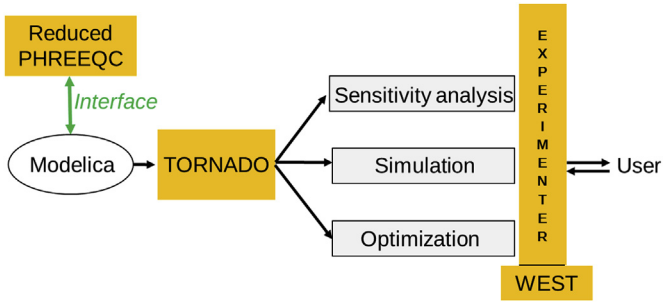

Fig. 4. Tight coupling of reduced PHREEQC to Modelica code and model execution in Tornado.

models using Tornado was developed (Fig. 4). It consists of a Tornado-specific PHREEQC wrapper library containing only a predefined set of methods to be used in Tornado/WEST, as well as a reduced PHREEQC database and a PHREEQC script with selected outputs (Section 2.2.1). Any PHREEQC code can now be run, using input data supplied by Tornado/WEST and providing output data to be used by Tornado/WEST, in a flexible manner without the need for any case-specific C/C++ code modifications by the user. As a result, the combined kinetic-equilibrium models can now be used for simulation and other tasks such as parameter estimation, optimization, scenario analysis, Monte Carlo simulation, sensitivity analysis, and steady-state analysis, through the Tornado CUI (Command-line User Interface) tool, the user-friendly Tornado Experimenter GUI (Graphical User Interface), or WEST (Fig. 4).

Finally, for numerical solution in Tornado, two different solvers, RK4ASC (Runge Kutta 4 Adaptive Step size Control integration algorithm; Press et al., 1992) and VODE (Variable-coefficient Ordinary Differential Equation solver; Brown et al., 1989), were compared. The RK4ASC algorithm was retained, since simulation times were much faster and results more stable. This is likely related to its higher ability to solve models with certain discontinuities (i.e. sharp switches in behaviour, e.g., transitions in precipitation mechanisms as function of the saturation index) and dynamic inputs/disturbances (Claeys, 2008).

2.3.3. PHREEQC-Tornado interface

In order to connect state vectors used by PHREEQC (C code) and Tornado (Modelica code), a PHREEQC-Tornado interface was developed (Fig. 5). The interface makes special use of the data defined by the 'SELECTED_OUTPUT' data blocks (Section 2.3.1), and allows this array of data to be returned to Tornado without the necessity to read or write files. Hence, the data can be transferred between PHREEQC and Tornado through internal computer memory. This method of tight model coupling has significant merits with respect to calculation time and programming: a PHREEQC instance is only created once and is subsequently reused, preserving its internal state. In general, an order of magnitude decrease in run times is obtained compared to a loosely-coupled model, which requires starting PHREEQC as an external process for each time step (Müller et al., 2011). On top of that comes the gain in simulation time by using the developed reduced PHREEQC databases and scripts instead of full PHREEQC (Section 2.2.1). Hence, a reduction of execution time is obtained at two critical points during model simulations: i) the uploading and reading of database and input files, and ii) the transfer of data between PHREEQC and Tornado.

2.3.4. Model verification and debugging

After implementation, the models were subjected to a battery of tests to ensure implementation correctness, also referred to as

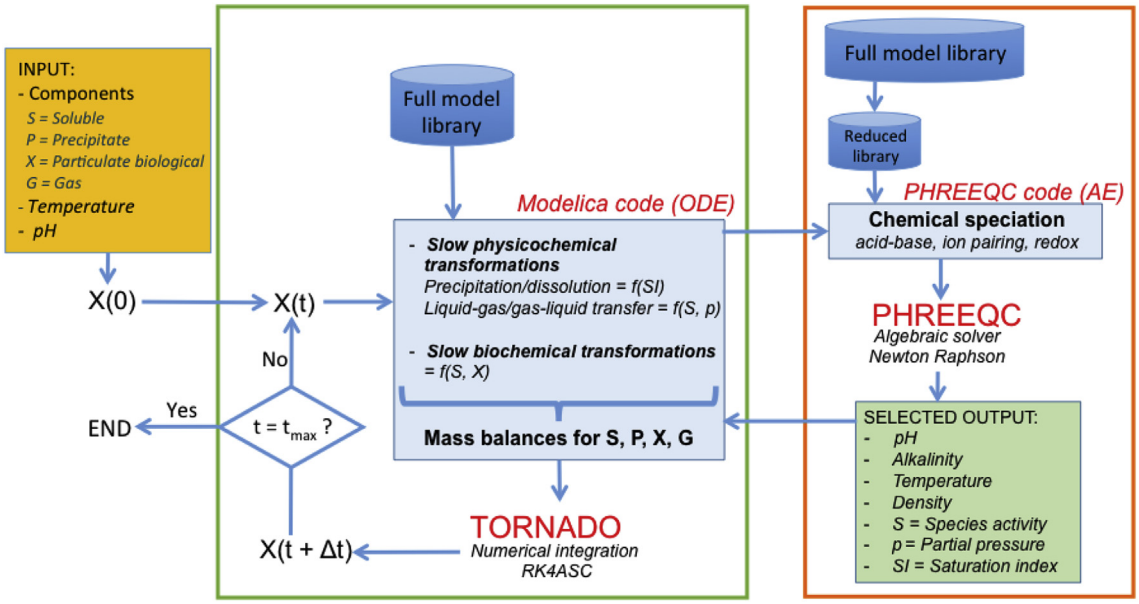

Fig. 5. Overview of the PHREEQC-Tornado interface coupling chemical speciation calculations to slow physicochemical and biochemical dynamic transformations at every time step. AE = algebraic equations; ODE = ordinary differential equations; X(0) = initial state of the system; X(t) = state of the system at time t.

model verification (Dochain and Vanrolleghem, 2001). A generic **six-step procedure for model verification** of NRMs was developed and applied to each unit process separately:

1. Verification of the PHREEQC-Tornado interface: Comparison of speciation calculations in Tornado through tight coupling to reduced PHREEQC, with simulation results from the independent full PHREEQC engine;
2. Verification of the physicochemical transformation model: Implementation of slow physicochemical transformations in Modelica code, execution in Tornado, and mass balance check;
3. Verification of the biochemical transformation model: Implementation of slow biochemical reactions in Modelica code, execution in Tornado, and i) mass balance check, ii) check against independent implementations, e.g., ADM1 (Batstone et al., 2002) and the Lizarralde et al. (2010) model for anaerobic S degradation;
4. Verification(/validation) at steady state: Performance of steady state simulations using different initial values from literature and comparison with experimental literature results;
5. Verification(/validation) of dynamics: Performance of dynamic simulations using realistic databases and checking the effect of disturbances (e.g., different loading scenarios) on model outputs through comparison with prior knowledge and literature;
6. Verification of the generic NRM implementation: Comparison of simulation results obtained with two different independent implementations of each unit process model: one based on all separate individual equations and one compact implementation based on vectors and matrices.

As such, typing errors, inconsistencies, gaps, and conceptual errors were eliminated, while software bugs were discovered and dealt with.

2.4. Step IV: dataset collection and identification of data needs

One of the issues in the development of new models is the necessity to provide data for the estimation of model parameters and for the input variables. The different types of data required for each key NRM and the datasets that were used are provided in Appendix 6 (Table A6.1).

First, a thorough review of literature and existing models was conducted to provide default values for the different parameters involved (Appendix 6: Table A6.2-A6.5). Physicochemical stoichiometry and thermodynamic parameters are incorporated in the PHREEQC and Visual MINTEQ modelling software, where they are mainly taken from the National Institute of Standards and Technology (NIST, 2001) database. Default values for the kinetic precipitation coefficients were taken from literature, while default values for biomass kinetic coefficients were taken from the ADM1 model (Batstone et al., 2002), except for the SRB kinetics for which the parameters were taken from Knobel and Lewis (2002) and Lizarralde et al. (2010).

Next to literature studies, also new experimental data aiming at NRM validation were collected through lab/pilot-scale testing and contact with industry. For NRM-AD, full-scale data at steady state from an anaerobic reactor treating S-rich paper mill primary sludge located at the WRRF Holmen Paper, Madrid, Spain has been obtained from the Center of Studies and Technical Research (CEIT, San Sebastian, Spain; Appendix 6: Table A6.6). An input fractionation was conducted following the procedure proposed by Grau et al. (2007).

For validation of the NRM-Prec, lab tests were conducted for P recovery from digestate under different operating conditions, i.e. different Mg:P-ratios and contact time notably. For this purpose, two different digestates were sampled at the full-scale biogas plants of SAP Eneco Energy (Houthulst, Belgium) and Wittevrongel Eneco Energy (Aalter, Belgium), which both treat agricultural wastes, mainly manure. A detailed input characterization was performed prior to the experiment (Appendix 6: Table A6.7). The precipitate was separated from the effluent by means of a centrifuge (5 min at 2000 rpm; Heraeus megafuge 1.0, Kendro Laboratory Products, Hanau, Germany), after which both fractions were also physicochemically analyzed. The P recovery efficiency (%) was then

calculated using the P recovery of a control (no Mg addition) as a reference. For detailed methodology and experimental results, reference is made to De Corte (2012).

To obtain data for the NRM-Strip/NRM-Scrub, a technical and financial survey for a case treating 2000 m^3 d^{-1} of digestate at 200 mol NH_4-N m^{-3} (more details: Appendix 6: Table A6.8) was carried out with various key suppliers in the field. As such, insights in the variability of the processes available to date were obtained, e.g., different target ammonium sulfate concentrations, operational pH and temperature, consumables, among other. These detailed data provided by the suppliers were used for further model refining and validation.

Finally, it should be stated that during model development new data needs appeared for which to date literature references are lacking. Such data gaps were identified and recommendations for future experiments and data collection are provided further in this paper (Section 3.5).

2.5. Step V: model validation

Model validation was performed in four different ways: i) validation against prior knowledge, ii) validation against existing models, iii) validation against literature or technical inquiries, and iv) validation against collected experimental results. In all cases, the default stoichiometric and kinetic parameter values determined in Section 2.4 were used. Input waste stream compositions, design data, and operational conditions were taken from the dataset involved. During the validation procedure, attention was given to the reduced PHREEQC database used in order to assure that all required species and reactions are included in the calculations. If required, an additional evaluation was conducted using the full PHREEQC and/or MINTEQ database, and missing species/reactions were additionally added to the reduced database.

2.6. Step VI: scenario analyses and process optimization

To gain more insight into the results and to further explore the model outcomes, scenario analyses were performed in Tornado/WEST (Claeys, 2008). Moreover, the applicability of the models for process optimization was demonstrated by running optimization experiments in Tornado/WEST (Claeys, 2008).

3. Results and discussion

The implementation of the models developed in Section 2 was verified and validated. First, simulation times for the reduced models are evaluated in Section 3.1. General verification results and verification examples showing the correctness of the PHREEQC-Tornado interface are presented in Section 3.2. An example of model validation against experimental results, including scenario analyses and/or process optimization, is given for each NRM in Sections 3.3–3.5. Finally, recommendations for further research are provided in Section 3.6.

3.1. Evaluation of reduced PHREEQC simulation times

A comparison of simulation times of the developed scripts for each unit process model using the full databases and the corresponding reduced database is presented in Table 4b.

A 3- to 5-fold average improvement of model simulation speeds was obtained using the reduced database as compared to full Phreeqc.dat and minteq.v4.dat, respectively. The observed deviation in simulation times between PHREEQC and MINTEQ shows again the higher completeness of the MINTEQ database. Note that the presented simulation times in Table 4b concern the chemical speciation model only, so without the coupling to the kinetic and mass balance model. Yet, this model reduction is clearly relevant for simulation of WRRFs, since the speciation model is run at every time step during NRM model simulations (Section 2.3.3). As such, running a complete digestate treatment train under dynamic conditions for one year would take approximately 15 min (depending on the operating conditions and input characterization) using the reduced PHREEQC model, whereas it would take 45 min using the full PHREEQC model, both with tight model coupling (Section 2.3.3) to the kinetic model. As mentioned above, it is important for model validation to keep in mind that a model reduction was performed. As such, for example, it was discovered during initial validation of the NRM-Prec model that the species NaH_2PO_4(aq) was lacking, though essential for correct prediction of P recovery (Section 3.4.1).

3.2. Model verification

3.2.1. General results and issues

During model verification, various software bugs were discovered and communicated to DHI, Merelbeke, Belgium, who successfully resolved the issues. As such, this research also contributed to the development of the Tornado/WEST software kernel.

Each step in the verification procedure was completed successfully. First, the PHREEQC-Tornado interface was found to be effective (see Section 3.2.2). Next, the mass balance check provided good results for each NRM. The step-by-step comparison of the Gujer matrix with other digester model implementations showed that the biochemical reactions were correctly implemented. Tests performed to check the ability of the models to realistically respond to model inputs, both under steady state and dynamic conditions, allowed eliminating small implementation errors. Some examples of tests and effects performed for model verification/validation can be found in Appendix 7. Finally, simulation results obtained from the two different independent implementations of the same model for each unit process, i.e. one using individual equations and one using a multi-matrix structure, were identical.

During model verification, three important general issues were observed to which future WRRF model developers must pay attention. First, it was found that some components, species, and precipitates that are highly important for modelling of WRRFs are not yet included in the generic PHREEQC and/or MINTEQ databases (Section 2.2.1: Table 3). Hence, for each new nutrient recovery model, the chemical speciation calculation should be verified with

Table 4b
Simulation times (s) and speed-up factor using the reduced PHREEQC database as compared to the full Phreeqc.dat (P) /minteq.v4.dat (M) databases for simulation of the chemical speciation scripts developed for each key unit in the nutrient recovery model (NRM) library. AD = anaerobic digestion; Prec = precipitation/crystallization; Strip = stripping; Scrub = scrubbing.

Key unit	Simulation time (s) Reduced PHREEQC	Simulation time (s) Full PHREEQC (P) /MINTEQ (M)	Speed-up factor
NRM-AD	0.031	0.094 (P) /0.185 (M)	3 (P) /6 (M)
NRM-Prec	0.047	0.094 (P) /0.172 (M)	2 (P) /4 (M)
NRM-Strip	0.047	0.156 (P) /0.172 (M)	3.5 (P) /4 (M)
NRM-Scrub	0.020	0.066 (P) /0.157 (M)	3.5 (P) /4.5 (M)

Table 5
Verification PHREEQC-Tornado interface: example NRM-Scrub. Left: gas phase speciation (atm). Right: ammonium sulfate fertilizer speciation (mole m^{-3}) after gas-liquid exchange. log(p) = logarithm of the partial pressure (p) in the gas phase.

Gas	Input p (atm)	Output full PHREEQC log(p) (atm)	Output Tornado[a] log(p) (atm)
CH_4	0.001	−6.12	−6.12
CO_2	0.006	−7.55	−7.55
H_2	0.001	−6.13	−6.13
H_2S	0.001	−1.43	−1.43
H_2O	0.0001	−1.50	−1.50
N_2	0.1	−0.03	−0.03
NH_3	0.8	−6.23	−6.23
O_2	0.09	−71.0	−71.0

Soluble species	Output full PHREEQC (mole m^{-3})	Output Tornado[a] (mole m^{-3})
NH_3	0.0361	0.0361
$NH_4SO_4^-$	0.00179	0.00179
NH_2COO^-	1.96	1.96
NH_4^+	6.46	6.46

[a] With tight coupling to the developed reduced PHREEQC model.

multiple software packages, with literature, and with prior knowledge in order to comprehensively select which components, species, and precipitates should be included in the model and which ones can be excluded. Secondly, if an input to PHREEQC is set to 0 or if a species is not defined or not present in the calculation, then a value of −999.999 is printed as output for this component's species distribution and the corresponding saturation indices and partial pressures. In the Modelica code, these outputs are then used as driving forces for slow transformations, leading to incorrect calculations. This issue was solved by introduction of an if-then-else statement in the PHREEQC-Tornado interface. Finally, attention should be paid to the use of units for input and output variables. Input concentrations in PHREEQC are expressed by default as mole m^{-3}, whereas the outputs are given by default as kmole m^{-3}. Deviations from these standard units should be declared in the PHREEQC script.

3.2.2. Verification of PHREEQC-Tornado interface

When comparing simulation results using the stand-alone full PHREEQC engine and Tornado (with tight coupling to reduced PHREEQC), identical model outputs were obtained for all NRMs. As an example, the results for the NRM-Scrub are given in Table 5. An initial gas phase flow with high NH_3 load (coming from the NRM-Strip) was used as input to the NRM-Scrub and brought into contact with a sulfuric acid solution for NH_3 absorption. The outputs, i.e. the logarithm of the partial pressures (log(p), atm) in the purified gas phase and the activities (mole m^{-3}) of some species in the ammonium sulfate solution after gas-liquid exchange, obtained with both the stand-alone PHREEQC engine and Tornado-PHREEQC are presented. It can be concluded that the implementation of the PHREEQC-Tornado interface and the PHREEQC invocation in Modelica are correct.

3.3. NRM-AD validation

3.3.1. Case study anaerobic reactor at Holmen Paper Madrid (Spain)

The NRM-AD model was validated using experimental data collected under steady state conditions from an anaerobic digester for treatment of S-rich paper mill primary sludge at a full-scale WRRF (Holmen Paper, Madrid, Spain). The same case was previously used for validation of the Lizarralde et al. (2010) model for anaerobic S reduction. The input sludge characteristics, design parameters, initial reactor state variables, and operating conditions are given in Appendix 6 (Table A6.6). Kinetic and stoichiometric parameters were set at default (Section 2.4). A comparison of experimental and simulation results using the NRM-AD and the model proposed by Lizarralde et al. (2010) is given in Table 6.

Simulation results using the NRM-AD show good agreement with the experimental results for COD removal and biogas CH_4 and CO_2 composition at a particular pH. The model also seems to give a very good prediction of the digestate pH and P content, and a relatively good prediction for NH_4-N in the digestate. The slightly higher digestate nutrient value for NH_4-N obtained with the NRM-AD may be attributed to losses of NH_3 during digestate sampling and analysis, although potential model deficiencies may not be excluded.

The NRM-AD seems to underpredict the biological SO_4 removal and corresponding H_2S production by SRBs, as will be explored below. However, from a pure validation perspective (note: no parameters were calibrated!), when comparing with the Lizarralde et al. (2010) model, overall the performance of the NRM-AD is significantly better, very probably due to the underlying more detailed chemical speciation and the inclusion of multiple competing physicochemical transformation reactions.

3.3.2. Exploration of hypotheses regarding S cycle measurements

Through model scenario analyses, four potential hypotheses were tested to explore the underestimation of biological SO_4 removal in the above case study. First, it was observed that the biogas H_2S concentration was very sensitive to variations in pH (cfr. Al-Zuhair et al., 2008). Model simulations were carried out at the digestate pH (7.21). However, the input pH was significantly lower (6.66) and the digestate pH may be influenced through contact with air. Hence, there exists some uncertainty about the actual reactor pH.

To explore this hypothesis, a scenario analysis was conducted in order to evaluate the effect of pH (variable) on the % CH_4, CO_2, and H_2S in the biogas at fixed waste input COD:SO_4-ratio. Assuming that the pH in the reactor ranged from 6.66 (waste input pH) to 7.21 (digestate pH), the biogas composition varied from 61% CH_4, 34% CO_2, 2.94% H_2S to 80% CH_4, 16% CO_2, 1.90% H_2S. Hence, with the present implementation, it was not possible to obtain 6% H_2S in the biogas at a pH in that range.

It should be remarked that the experimentally obtained biogas H_2S content of 6% is extremely high compared to literature values. Typical biogas H_2S values for similar concentrated sulfurous streams from the paper industry range between 1 and 2% H_2S (Reiter and Piccot, 2004). Hence, a second reason for the uncertainty may be related to the H_2S analysis itself, conducted by the operators.

A third explanation may be the exclusion of lactate in the present NRM-AD implementation. Lactate is a preferred substrate for sulfate reducing bacteria and would thus aid in increasing SO_4 removal and H_2S production (Oyekola et al., 2007). This may explain the slight overestimation of biogas CO_2 production and underestimation of H_2S production. In the present case, no lactate measurements were available, but future research should consider this component.

Furthermore, the non-consideration of reactions (precipitation/ion pairing) with Al and Fe, due to lack of input Al/Fe measurements at the WRRF, may explain the lower SO_4 removal found through simulation (cfr. Zhang et al., 2013). This can also explain why model predictions for COD removal and CH_4 production were good, while additional COD would be required for additional SO_4 removal by SRBs. Based on a similar reasoning, Lizarralde et al. (2010) assigned potential sulfate precipitation (which was not considered in their model) to the highly overestimated H_2S production found with their model.

An attempt to calibrate input Al in the present case study

Table 6
NRM-AD validation based on experimental results from Holmen Paper, Madrid, Spain at steady state and comparison with the Lizarralde et al. (2010) model for anaerobic S removal. ND = not determined.

Output	Variable	Unit	Experiment	Simulation NRM-AD	Simulation Lizarralde et al. (2010)
Biogas	CH_4	%	80	81	70
	CO_2	%	13	15	8
	H_2S	%	6	2	22
Digestate	pH	–	7.21	7.21	7.6
	NH_4-N	mole m^{-3}	123	130.04	ND
	PO_4-P	mole m^{-3}	12.63	12.48	ND
Removal efficiency	ηCOD	%	61	63	62
	ηSO_4	%	78	63	81

showed that a reactor concentration of 276 mol Al m^{-3} resulted in a SO_4 removal of 78% (= experimental value in Table 6) and a biogas H_2S concentration of 3%. However, in this scenario the pH lowered to a value of 6.26. The higher SO_4 removal found through addition of Al was likely the result of a combination of multiple effects. It was, for example, observed that the addition of Al affected the amount of Ca/Mg sulfates and Ca/Mg precipitates formed. The addition of Fe resulted in a lower H_2S production because of FeS precipitation, but it did not aid in SO_4 removal.

Finally, other model gaps can of course not be ruled out and one should bear in mind that the above validation is based on a one-time test.

It can be concluded that more detailed waste(water) input characterizations, including all selected components for the NRM-AD unit process (Section 2.2.1: Table 2), as well as instantaneous pH measurements in the reactor, are required in order to correctly calibrate the model for biological S removal. Nevertheless, clearly, exploration using the NRM-AD leads to increased insights and better understanding of the various interacting processes occurring in digesters.

3.4. NRM-prec validation

3.4.1. Phosphorus precipitation at different Mg:P-ratios

For validation of the NRM-Prec model, batch experiments were carried out in the lab for P recovery from two different crude digestates (Section 2.4; Appendix 6: Table A6.7). Different Mg:P-ratios obtained through dosing of $MgCl_2{:}6H_2O$ were applied aiming at the production of N-struvite ($MgNH_4PO_4{:}6H_2O$ or MAP) or K-struvite ($MgKPO_4{:}6H_2O$ or MKP) fertilizer. Initial simulation results showed a large deviation from the experimental results (Table 7). After evaluation using the full PHREEQC and MINTEQ databases, this deviation could be attributed to ion pair formation of NaH_2PO_4, a species that was initially not included in the reduced PHREEQC database, nor in the generic PHREEQC database (Table 3). Indeed, due to the high Na concentration of both digestates, Na paired with P, making it less available for precipitation. When NaH_2PO_4 was added as species to the reduced database, a very good agreement between the simulation and the experimental results was obtained for P recovery at steady state (after 12 h; Table 7).

This finding is in line with the results obtained by Li et al. (2012), who found a ± five times higher residual effluent P concentration when $NaH_2PO_4 + MgCl_2{:}6H_2O$ were dosed for struvite precipitation, compared to the dosing of $H_3PO_4 + MgCl_2{:}6H_2O$. Moreover, recently Chauhan and Joshi (2014) found that at high Na:NH_4-ratios, NaH_2PO_4 is formed instead of, or next to, $NH_4H_2PO_4$, the precursor for MAP precipitation. In turn, this compound may be transformed into Na-struvite through the following reaction:

$$NaH_2PO_4{:}2H_2O + Mg(CH_3COO)_2{:}4H_2O + H_2O \rightarrow NaMgPO_4{:}7H_2O + 2CH_3COOH$$

The formation of Na-struvite was not yet included in the NRM-Prec model due to lack of knowledge on the existence, the stoichiometry, and the kinetics of this precipitation reaction. However, knowing that current practice often involves the addition of NaOH for pH-increase prior to struvite crystallization, the case study above clearly shows the relevance of further research on Na-P ion pair formation and Na-struvite precipitation kinetics in waste(waters). The phenomenon may not only impact the effluent quality, but also the quality of the resulting recovered fertilizer product, i.e. a potential mixture of N/K- and Na-struvite may appear.

3.4.2. Exploration for process understanding and optimization

Two questions arise from the experimental and simulation results presented above (Table 7):

1. Why is the P recovery efficiency rather low for both digestates?
2. Why does increasing the Mg dose not improve the P recovery efficiency?

The ability of the models to find an answer to such questions is presented below.

First, it was observed experimentally and through simulations that the main precipitated components, next to P, were Al, Ca, Fe, K, Mg, and N(−III). Hence, the product recovered was definitely not pure MAP or MKP. A scenario analysis evaluating these components was conducted for both digestates in order to obtain more insights in the results (Fig. 6). The two tested digestate compositions under study are marked as stars in Fig. 6.

The maximum achievable P recovery as function of the input Mg and Ca content was 56.2% for digestate 1 (Fig. 6A), whereas it amounted to 90.7% for digestate 2 (Fig. 6B). This discrepancy can be attributed to the higher concentration of Fe and Al in digestate 1

Table 7
NRM-Prec validation based on experimental batch tests at lab-scale at steady state (after 12 h).

Mg:P	% P recovery digestate 1			% P recovery digestate 2	
	Experiment	NRM-Prec without NaH_2PO_4	NRM-Prec with NaH_2PO_4	Experiment	NRM-Prec with NaH_2PO_4
1:1	41	95.60	41.32	28	27.76
2:1	44	97.91	43.62	29	29.29

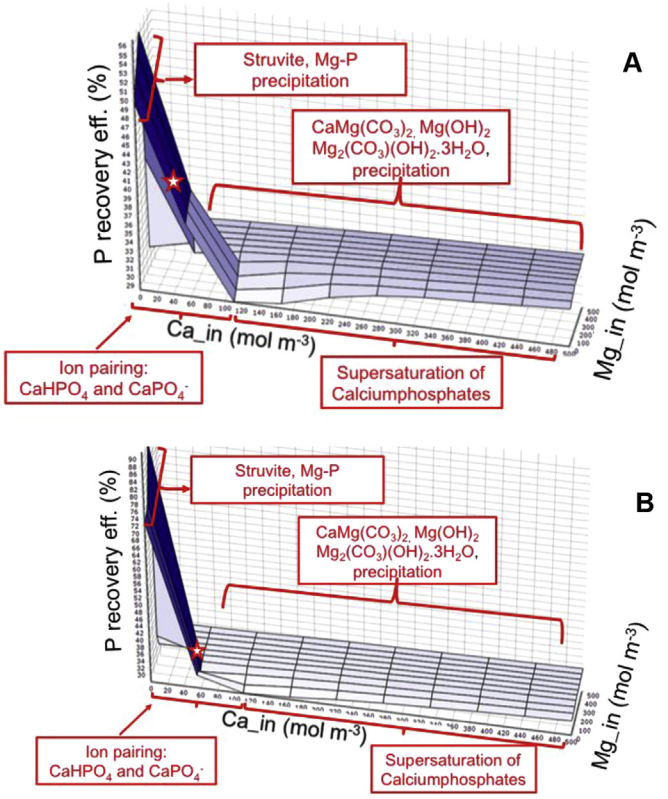

Fig. 6. P recovery efficiency (%) as function of input Mg and Ca concentration (mole m^{-3}) for streams with high (A: digestate 1) and low (B: digestate 2) Fe and Al input concentrations. Red stars indicate the digestate compositions of the case studies. (For interpretation of the references to colour in this figure legend, the reader is referred to the web version of this article.)

compared to digestate 2 (Appendix 6: Table A6.7). Indeed, at high concentrations of both Fe and Al mainly hercynite ($FeAl_2O_4$) precipitation occurs, whereas at low concentrations P recovery increases through precipitation of $AlPO_4$ and vivianite ($Fe_3(PO_4)_2$:$8H_2O$). Furthermore, the inhibition of P precipitation due to the presence of soluble Ca is very clear for both cases (see details Fig. 6). Up to ±110 mol m^{-3} of input Ca (the margin in which the digestates under study are situated), mainly ion pairing of $CaHPO_4$(aq) and $CaPO_4^-$ was observed, which decreased the amount of P available for precipitation (cfr. Lin, 2012). Above a value of ±110 mol m^{-3}, calcium phosphates became oversaturated, precipitation occurred, and P recovery increased. This effect of Ca inhibition observed through model simulations is in agreement with the experimental findings of Huchzermeier and Wendong (2012). The latter concluded that struvite purity decreased because of the formation of calcium phosphates when the Ca:P activity ratio was greater than 0.5 to 1.

Secondly, the fact that the P recovery efficiency in the presented experiment was not much influenced by increasing Mg:P-ratios can, according to the model, be attributed to the formation of dolomite ($CaMg(CO_3)_2$), as well as $Mg(OH)_2$ and $Mg_2(CO_3)(OH)_2$:$3H_2O$ at higher Ca and Mg concentrations. Indeed, higher Ca and Mg doses are associated with a pH-increase, which favours carbonate and hydroxide precipitation (Zumdahl, 2005). When the input Ca concentration would be 0, one can see an increase in P recovery with increasing Mg dose due to the formation of MKP (note: high K-concentration in the input waste stream) and Mg-phosphates. This competitive effect between Mg, Ca, and P found through NRM-Prec simulations is in agreement with the

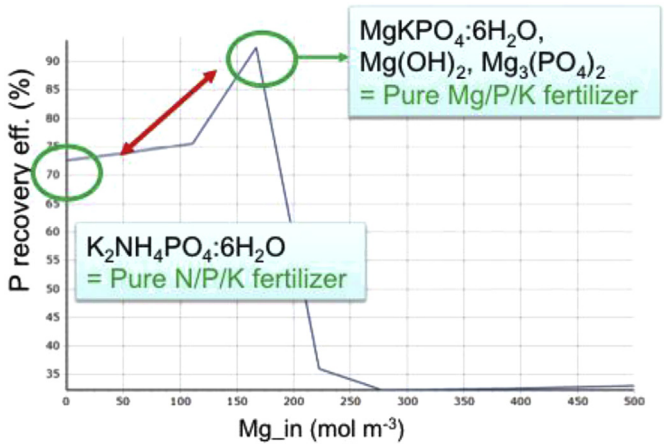

Fig. 7. P recovery efficiency (%) through precipitation as function of Mg dosing (range: 0–500 mol m^{-3}) for digestate 1 following $CaCO_3$ removal and without Fe/Al dosing in processes upstream.

findings of Lin (2012), who obtained a precipitate mixture of struvite, dolomite, $Mg(OH)_2$, calcium phosphates, and $CaCO_3$ in experiments on P recovery from digested swine manure.

Based on the above-mentioned findings, **two optimizations of the process can be proposed** if the aim would be to produce high purity struvite:

1. Removal of $CaCO_3$ through precipitation prior to the experiment, e.g., using a filtration system as in Huchzermeier and Wendong (2012);
2. Elimination or reduction of the use of Fe and Al in the WRRF processes upstream of the precipitation unit, e.g., for improved sludge dewatering. This measure could also be assessed by locating the struvite precipitation unit upstream in the WRRF, e.g., immediately after the activated sludge (AS) system (cfr. combined use of the *WASSTRIP* and *Pearl* process for improved P release and struvite recovery; Cullen et al., 2013). In fact, the AS system itself could also (partially) be replaced by a strip/scrub system.

When applying these proposed measures in a treatment train for digestate 1, the maximum achievable P recovery through simulation became 91%, consisting of MKP, $Mg(OH)_2$, and $Mg_3(PO_4)_2$. Hence, a pure Mg/P/K fertilizer would be obtained (Fig. 7). Remark that the main precipitate found, MKP, is not included in the standard PHREEQC/MINTEQ databases. Hence, again, **the extensions provided to the database are clearly relevant** (Section 2.2.1).

It should also be noted that in Fig. 7, the Mg dose was allowed to change within the range of 0–500 mol m^{-3} (so no point measurements are presented). Hence, the abrupt changes in slope are related to actual changes in precipitation mechanisms, which could, e.g., involve transitions from nucleation to particle growth and/or agglomeration and/or redissolution, and changes in precipitated species due to changes in saturation indices. Moreover, an interesting observation made through model simulations was that, without any addition of Mg, a high P recovery efficiency of 72% could be obtained. This could be appointed to the precipitation of $K_2NH_4PO_4$:$6H_2O$ (= pure N/P/K fertilizer) due to the high amounts of K available in the digestate (Appendix 6: Table A6.7). In this case, an economic analysis is recommended to select a target fertilizer, thereby taking into account local fertilizer market demands, and environmental and fertilizer regulations. On the one hand, the use

Table 8
NRM-Strip/NRM-Scrub validation based on experimental literature results (Collivignarelli et al., 1998) at different operating conditions at steady state (after 6 h).

Test	Operational factor	Input		Recovery efficiency	Output	
		Experiment	Model		Experiment (6 h)	Model (6 h)
1	V_liq (m^3)	0.84	0.84	NH_3 recovery (%)	32	34.26
	Height (m)	2	2			
	S_N_min3_in (mole m^{-3})	147	147			
	Q_air (NL L^{-1} h^{-1})[a]	120	120			
	pH	8.5	8.52[b]			
	Temperature (K)	293.15	293.15			
2[c]	Q_air (NL L^{-1} h^{-1})[a]	200	200	NH_3 recovery (%)	50	50.12
	pH	12	12.03[b]			
3[c]	Q_air (NL L^{-1} h^{-1})[a]	70	70	NH_3 recovery (%)	59	58.44
	pH	10	9.97[b]			
	Temperature (K)	323.15	323.15			

[a] NL = normalized liter: temperature = 273.15 K, pressure = 1 atm.
[b] Calculated by PHREEQC based on the (calibrated) input composition.
[c] Other factors are similar as for Test 1.

of chemical Mg may increase the operational costs of P recovery, while on the other hand a higher recovery efficiency can be obtained, with larger mean particle diameter of the recovered precipitates (mainly MKP), as predicted with the NRM-Prec. Larger particles generally increase the revenues from fertilizer sales (Vaneeckhaute et al., 2017a).

3.5. NRM-strip/NRM-scrub validation

3.5.1. NH_3 recovery at different operating conditions

During validation of the NRM-Strip and NRM-Scrub models, NH_3 stripping was found to be very sensitive to the total and relative input concentration of carbonates, Ca, and Na, since these determine the input alkalinity and pH. Since operators usually only measure NH_3 and pH (+sometimes total alkalinity), an identifiability problem arises. For example, when using the design parameters and input flow characterization (S_N_min3_, pH) of Collivignarelli et al. (1998), a good agreement was obtained between experimental and simulation results for NH_3 recovery (Table 8).

However, due to lack of some fundamental input flow characteristics for pH calculation using the NRM-Strip model, the input composition had to be calibrated in order to approximate the operational pH. Evidently, there are multiple ion combinations possible to obtain the specified pH, and the choice of the combination may influence the model outputs. Hence, in order to effectively use the NRM-Strip/NRM-Scrub models for process optimization, the initial waste flow composition should be characterized in more detail than is usually done at WRRFs today. Irrespective thereof, it can be seen in Table 8 that the model responded correctly to disturbances/operational decisions, such as an increase in pH, temperature, and air flow rate (cfr. Collivignarelli et al., 1998).

3.5.2. Treatment train for NH_3 recovery

In order to overcome the above-mentioned identifiability issue, a technical survey was sent out to key suppliers of strip/scrub units for the treatment of a particular digestate flow (Section 2.4). Using the predefined input characteristics (Appendix 6: Table A6.8), as well as the dimensions, operating conditions, effluent quality and stripping performance offered by the different suppliers, the models were again validated for the different configurations received. To this end, first a treatment train consisting of NRM-Chem, NRM-Strip, and NRM-Scrub was built to reflect a full-scale installation. Then, model simulations using the design data were conducted and scenario analyses were performed in order to compare simulation results with the experimental data obtained from the suppliers.

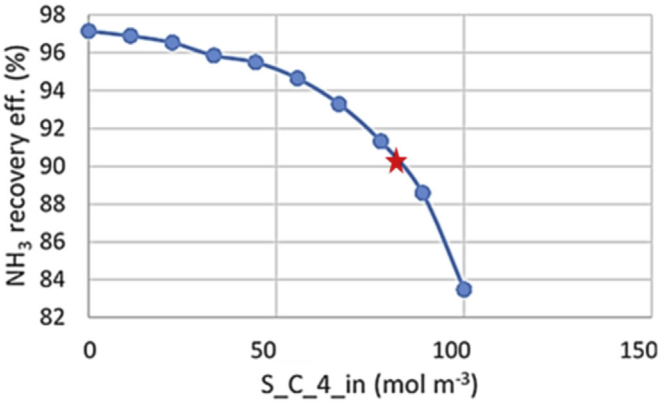

Fig. 8. Simulated NH_3 recovery efficiency (%) as function of carbonate alkalinity (S_C_4_in, mole m^{-3}) using the NRM-Strip model. The red star indicates the digestate composition under study.

The data of the supplier who provided the most detailed experimental results (RVT Process Equipment GmbH) are presented below as an example. An NH_3 recovery efficiency of ±90% at 55 °C was guaranteed by the supplier, when increasing the pH to a value of 10.3 by addition of 102.5 mol m^{-3} NaOH d^{-1} under the design conditions provided in Appendix 6 (Table A6.8). The same results were obtained through treatment train simulation (Table 9).

Finally, technology providers also advised to remove excess input carbonate buffer capacity prior to treatment, e.g., through CO_2 stripping, in order to minimize NaOH consumption for pH-increase as well as $CaCO_3$ precipitation in the reactor (Pérez, 2002). This

Table 9
Validation treatment train (NRM-Chem, NRM-Strip, NRM-Scrub) based on experimental data obtained by a technology provider for the predefined case (Appendix 6: Table A6.8).

Variable	Output Experiment	Output Model
S_NH_3_out (mole m^{-3})[a]	20	19.87
NH_3 recovery (%)	±90	90.02
Operational pH[b]	10.3	10.30
Fertilizer pH[a]	6.3–6.8	6.33

[a] Ammonium sulfate (AmS) solution = output NRM-Scrub.
[b] NRM-Strip.

recommendation could be confirmed using the NRM-Strip model: Fig. 8 shows the decreasing NH_3 recovery efficiency as function of carbonate buffer capacity, if the NaOH consumption and other operating conditions would not be adjusted.

Hence, the more carbonate is stripped off, the higher the reactor pH and the higher the NH_3 recovery efficiency. Note that, based on this principle, some technology suppliers provide an integrated CO_2 and NH_3 stripping process without using NaOH for pH-increase (Vaneeckhaute et al., 2017a).

3.6. Recommendations for further experimental research

The results show that the performance of all resource recovery systems under study is very sensitive to the input waste stream composition, e.g., through its direct effect on the pH. Therefore, in order to obtain good model predictions for a particular waste flow, the input flow should be characterized in more detail than is usually done at WRRFs today. This observation is similar to activated sludge modelling in which influent characterization is considered as the most important step for achieving accurate results (Rieger et al., 2012). It is clear that a better characterization of the input composition may help to adjust the use of consumables (e.g., chemical dose and air requirements) to a minimum, thereby reducing the operational costs. As such, the models can be used as an invaluable tool for process optimization. New experimental results, including detailed input characterizations, are currently being collected at pilot/full scale under dynamic conditions in order to further calibrate and validate the proposed NRMs.

A second issue observed is that values for the precipitation kinetics (k_T) and gas transfer coefficients ($K_{L/G}a$) used from literature are commonly determined under ideal conditions, i.e. gas transfer in clean water and precipitation in a synthetic solution containing only the target species involved in the reaction, e.g., Mg, NH_4, and P for struvite precipitation. However, the actual value of these parameters may be highly influenced by the complex matrix of the waste streams involved, e.g., through ion pairing (Section 3.4.1), concurrent and competing precipitation reactions (Section 3.4.2), and the presence of seed material. Studies evaluating kinetic rates under actual process conditions are lacking in literature, but should be focus of further research in order to correctly calibrate these parameters in the NRMs. Moreover, rates and mechanisms for nucleation, agglomeration and dissolution of various precipitates are still unknown and should be further studied. In this perspective, the use of the simple empirical equation (Eq. (3)) for liquid-solid/solid-liquid transfer in the NRMs is interesting compared to previously used approaches in wastewater treatment (e.g., Hauduc et al., 2015; Lizarralde et al., 2015; Musvoto et al., 2000).

Another important complication is related to the characterization of the precipitates formed. X-ray diffraction is the commonly used technique to characterize precipitates in pure solutions. However, it generally requires pure crystals of high regularity to solve the structure of a complicated arrangement of atoms. Also, the results usually represent a very local microstructure, and it requires a lot of work to obtain a certain statistical reliability on the results (Tanigawa et al., 2003). More research is required on the development of a generic and cost-effective experimental method to accurately characterize the different precipitated species from a complex waste matrix. Such a procedure may not only be used to determine the precipitated species in precipitation units and hence the recovered product purity (Vanrolleghem and Vaneeckhaute, 2014), but also, for example, the precipitates in the digestate leaving the digester. The latter is relevant as these precipitates may act as seed material for precipitation downstream.

Finally, interesting model extensions have been identified. They lead to the inclusion of: i) Lactate as specific substrate for biological sulfate removal in the NRM-AD, e.g., as in UCT (2007); ii) A transformer tool in the NRM-AD to allow for co-digestion of multiple input streams, e.g., the GISCOD tool (Zaher et al., 2009); iii) Biochemical transformations of EBPR sludge in the NRM-AD, e.g., as in Flores-Alsina et al. (2016), Ikumi (2011), or Wang et al. (2016); iv) Microscale flocculation in the NRM-Prec, e.g., as in Crittenden et al. (2012); v) Particle size distributions in the NRM-Prec, e.g., as in Perez et al. (2008); vi) Differential settling in the NRM-Settle and (if relevant) in the NRM-Prec, e.g., using the Stokes equation (Crittenden et al., 2012) or a particle settling velocity distribution (Bachis et al., 2015); vii) Heavy metals (and other contaminants) in all NRM models. These extensions will of course lead to further experimental data requirements.

4. Conclusions and future perspectives

- The first available generic nutrient recovery model (NRM) library including dynamic mathematical models based on both detailed chemical solution speciation calculations, as well as physicochemical and biochemical reaction kinetics, was developed through PHREEQC-Tornado/WEST coupling, and successfully validated at steady state;
- Implementation correctness was verified under steady state and dynamic conditions using a 6-step procedure, including, e.g., a comparison of the simulation outputs of two independent model implementations for each unit process: one based on individual equations and one compact matrix-based implementation;
- Using a systematic procedure for PHREEQC database reduction a 3- to 5-fold improvement of model simulation speed was obtained as compared to the use of standard thermodynamic databases, on top of the improvement obtained through tight model coupling;
- Because of gaps in existing standard thermodynamic databases, an extended database with the purpose of nutrient recovery was made available, named *'Nutricover.dat'*;
- Detailed input characterization was found to be most critical for accurate prediction of resource recovery process performance;
- Simulation results showed the high potential of the NRM library to increase understanding of nutrient recovery process interactions and to optimize integrated nutrient and energy recovery systems;
- The use of the NRM library by the various stakeholders in the field to facilitate the implementation, operation, and optimization of nutrient recovery technologies can stimulate the transition from WWTPs to more sustainable WRRFs.

Acknowledgements

This work has been funded by the Natural Science and Engineering Research Council of Canada (NSERC), the Fonds de Recherche de Québec sur la Nature et les Technologies (FRQNT) and Primodal Inc. (Québec, QC, Canada) through an industrial innovation scholarship (BMP Innovation 178263) and an NSERC Discovery Grant (RGPIN-2017-04838) awarded to the first author. Peter Vanrolleghem holds the Canada Research Chair in Water Quality Modelling. The authors would like to thank Lizarralde Izaro (CEIT, Spain) for experimental data delivery.

APPENDIX 1

Physicochemical species and reactions included in the nutrient recovery models (NRM)

Table A1.1
Dissolved species included in each nutrient recovery model (NRM) (1: NRM-AD = anaerobic digestion, 2: NRM-Prec = precipitation/crystallization, 3: NRM-Strip = stripper, 4: NRM-Scrub = scrubber) resulting from speciation calculations using PHREEQC (and Visual MINTEQ) modelling software.

Species	1	2	3	4	Species	1	2	3	4	Species	1	2	3	4	Species	1	2	3	4
$Acetate^-$	X	X	X	–	DOM	–	X	X	–	HSO_4-	–	–	–	X	NaCl (aq)	X	X	X	–
Al^{3+}	X	X	X		Fe^{2+}	X	X	X	–	H-Valerate	X	X	X	–	$NaCO_3^-$	–	X	X	–
$Al(OH)_2^+$	X	X	–	–	Fe^{3+}	X	X	X	–	K^+	X	X	X	–	$NaHCO_3$ (aq)	X	X	–	–
$Al(OH)_3$ (aq)	X	X	–	–	$FeCl^+$	–	X	–	–	K-Acetate (aq)	X	X	X	–	$NaHPO_4^-$	X	X	X	–
$Al(OH)_4^-$	X	X	X	–	$FeCO_3$	X	–	–	–	KCl (aq)	X	X	X	–	NaH_2PO_4 (aq)	X	X	–	–
$Butyrate^-$ (aq)	X	X	X	–	$FeHPO_4$ (aq)	X	X	–	–	$KHPO_4^-$	X	X	X	–	$NaNO_3$ (aq)	–	X	X	–
Ca^{2+}	X	X	X	–	$FeHS^+$	X	–	–	–	KH_2PO_4	X	X	–	–	NaOH	–	X	X	–
Ca-$Acetate^+$	X	X	X	–	$Fe(HS)_2$	X	–	–	–	KNO_3 (aq)	–	X	X	–	$NaPO_4^{2-}$	–	X	–	–
Ca-$Butyrate^+$ (aq)	X	X	X	–	$FeH_2PO_4^+$	X	–	–	–	KOH (aq)	–	X	X	–	$NaSO_4^-$	X	X	X	–
$CaCl^+$	X	X	X	–	$FeNH_3^{2+}$	X	X	X	–	KPO_4^{2-}	–	X	–	–	N_2 (aq)[a]	X	(X)	X	X
$CaCO_3$ (aq)	X	X	X	–	$Fe(NH_3)_2^{2+}$	X	X	X	–	KSO_4^-	X	X	X	–	NH_2COO^-	X	–	–	X
Ca-DOM	–	X	X	–	$Fe(NH_3)_3^{2+}$	–	X	–	–	Mg^{2+}	X	X	X	–	NH_3 (aq)	X	X	X	X
$CaHCO_3^+$	X	–	X	–	$FeOH^+$	X	X	X	–	Mg-$Acetate^+$	X	X	X	–	NH_4^+	X	X	X	X
$CaHPO_4$ (aq)	X	X	X	–	$Fe(OH)_2$ (aq)	X	X	X	–	Mg-$Butyrate^+$	X	X	X	–	$NH_4SO_4^-$	X	X	X	X
$CaH_2PO_4^+$	X	–	–	–	$Fe(OH)_3^-$	–	X	X	–	$MgCl^+$	X	X	X	–	NO_3^-	X	X	X	X
$CaNH_3^{2+}$	X	X	X	–	$FeSO_4$ (aq)	–	X	–	–	$MgCO_3$ (aq)	X	X	X	–	OH^-	X	X	X	X
$Ca(NH_3)_2^{2+}$	–	X	–	–	H^+	X	X	X	X	$Mg_2CO_3^{2+}$	–	X	X	–	O_2 (aq)	–	X	X	X
$CaNO_3^+$	–	–	X	–	H_2 (aq)	X	–	X	X	Mg-DOM	–	X	X	–	PO_4^{3-}	X	X	X	–
$CaOH^+$	–	–	X	–	H-Acetate	X	X	X	–	$MgHCO_3^+$	X	X	X	–	$Propionate^-$	X	X	X	–
$CaPO_4^-$	X	X	X	–	H-Butyrate	X	X	X	–	$MgHPO_4$ (aq)	X	X	X	–	SO_4^{2-}	X	X	X	X
Ca-$Propionate^+$	X	X	X	–	H-DOM	–	X	X	–	$Mg(NH_3)_2^{2+}$	X	X	X	–	$Valerate^-$	X	X	X	–
$CaSO_4$ (aq)	X	X	X	–	HCO_3^-	X	X	X	X	$MgOH^+$	X	X	X	–					
Ca-$Valerate^+$ (aq)	X	X	X	–	HPO_4^{2-}	X	X	X	–	$MgPO_4^-$	X	X	X	–					
CH_4	X	X	X	X	$H_2PO_4^-$	X	X	–	–	Mg-$Propionate^+$	X	X	X	–					
Cl^-	X	X	X	–	HS^-	X	–	X	X	$MgSO_4$ (aq)	X	X	X	–					
CO_2	X	X	X	X	H_2S (aq)	X	–	X	X	Na^+	X	X	X	–					
CO_3^{2-}	X	X	X	X	H-Propionate	X	X	X	–	Na-Acetate (aq)	X	X	X	–					

[a] Values between brackets represent the use of air instead of chemicals for pH-adjustment.

Table A1.2
Acid-base systems and reactions (AB) included in each nutrient recovery model (NRM). AD = anaerobic digestion; Prec = precipitation/crystallization; Strip = stripper; Scrub = scrubber; Ac = acetate; Bu = butyrate; Pro = propionate; Va = valerate.

Acid-base system	No.	Acid-base reaction	AD	Prec	Strip	Scrub
Acetate	AB1	$Ac^- + H^+ \leftrightarrow HAc$	X	X	X	–
Ammonia	AB2	NH_3 (aq) + $H^+ \leftrightarrow NH_4^+$	X	X	X	X
Butyrate	AB3	$Bu^- + H^+ \leftrightarrow HBu$	X	X	X	–
Carbonate	AB4	$CO_3^{2-} + H^+ \leftrightarrow HCO_3^-$	X	X	X	X
	AB5	$HCO_3^- + H^+ \leftrightarrow H_2CO_3$ (aq)	X	X	X	X
Phosphate	AB6	$PO_4^{3-} + H^+ \leftrightarrow HPO_4^{2-}$	X	X	X	–
	AB7	$HPO_4^{2-} + H^+ \leftrightarrow H_2PO_4^-$	X	X	–	–
	AB8	$H_2PO_4^- + H^+ \leftrightarrow H_3PO_4$	X	X	–	–
Propionate	AB9	$Pro^- + H^+ \leftrightarrow HPro$	X	X	X	–
Sulfate	AB10	$SO_4^{-2} + H^+ \leftrightarrow HSO_4^-$	–	–	–	X
Sulfide	AB11	$HS^- + H^+ \leftrightarrow H_2S$	X	–	X	X
Valerate	AB12	$Va^- + H^+ \leftrightarrow HVa$	X	X	X	–
Water	AB13	$H^+ + OH^- \leftrightarrow H_2O$	X	X	X	X

Table A1.3
Redox couples and reactions (R) included in each nutrient recovery model (NRM). AD = AD = anaerobic digestion; Prec = precipitation/crystallization; Strip = stripper; Scrub = scrubber; Ac = acetate; Bu = butyrate; Pro = propionate; Va = valerate.

Redox system	No.	Redox reaction	AD	Prec	Strip	Scrub
C(+IV) /C(−IV)	R1	$CO_3^{2-} + 10H^+ + 8e^- \leftrightarrow CH_4 + 3H_2O$	X	X	X	X
Fe(+II) /Fe(+III)	R2	$Fe^{3+} + e^- \leftrightarrow Fe^{2+}$	X	X	X	–
H(0) /H(+I)	R3	$2H^+ + 2e^- \leftrightarrow H_2$	X	–	X	X
N(-III) /N(+V)	R4	$NO_3^- + 10H^+ + 8e^- \leftrightarrow NH_4^+ + 3H_2O$	X	X	X	X
N(0) /N(+V)	R5	$2NO_3^- + 12H^+ + 10e^- \leftrightarrow N_2 + 6H_2O$	X	(X)[a]	X	X
O(−II) /O(0)	R6	$O_2 + 4H^+ + 4e^- \leftrightarrow 2H_2O$	–	X	X	X
S(−II) /S(+VI)	R7	$SO_4^{2-} + 9H^+ + 8e^- \leftrightarrow HS^- + 4H_2O$	X	–	X	X

[a] Values between brackets represent the use of air instead of chemicals for pH-adjustment.

Table A1.4
Ion pairing reactions (IP) included in each nutrient recovery model (NRM). AD = anaerobic digestion; Prec = precipitation/crystallization; Strip = stripper; Scrub = scrubber.

No.	Ion pairing reaction	AD	Prec	Strip	Scrub	No.	Ion pairing reaction	AD	Prec	Strip	Scrub
IP1	$Al^{3+} + 2OH^- \leftrightarrow Al(OH)_2^+$	X	–	–	–	IP34	$K^+ + Cl^- \leftrightarrow KCl$	X	X	X	–
IP2	$Al^{3+} + 3OH^- \leftrightarrow Al(OH)_3$	X	X	–	–	IP35	$K^+ + HPO_4^{2-} \leftrightarrow KHPO_4^-$	X	X	X	–
IP3	$Al^{3+} + 4OH^- \leftrightarrow Al(OH)_4^-$	X	X	X	–	IP36	$K^+ + NO_3^- \leftrightarrow KNO_3$	–	X	X	–
IP4	$Ca^{2+} + Ac^- \leftrightarrow CaAc^+$	X	X	X	–	IP37	$K^+ + OH^- \leftrightarrow KOH$	–	X	X	–
IP5	$Ca^{2+} + Bu^- \leftrightarrow CaBu^+$	X	X	X	–	IP38	$K^+ + PO_4^{3-} \leftrightarrow KPO_4^{2-}$	–	X	–	–
IP6	$Ca^{2+} + Cl^- \leftrightarrow CaCl^+$	X	X	X	–	IP39	$K^+ + H_2PO_4^- \leftrightarrow KH_2PO_4$	X	X	–	–
IP7	$Ca^{2+} + CO_3^{2-} \leftrightarrow CaCO_3$	X	X	X	–	IP40	$K^+ + SO_4^{2-} \leftrightarrow KSO_4^-$	X	X	X	–
IP8	$Ca^{2+} + DOM \leftrightarrow Ca\text{-}DOM$	–	X	X	–	IP41	$Mg^{2+} + Ac^- \leftrightarrow MgAc^+$	X	X	X	–
IP9	$Ca^{2+} + HCO_3^- \leftrightarrow CaHCO_3^+$	X	–	X	–	IP42	$Mg^{2+} + Bu^- \leftrightarrow MgBu^+$	X	X	X	–
IP10	$Ca^{2+} + HPO_4^{2-} \leftrightarrow CaHPO_4$	X	X	X	–	IP43	$Mg^{2+} + Cl^- \leftrightarrow MgCl^+$	X	X	X	–
IP11	$Ca^{2+} + H_2PO_4^- \leftrightarrow CaH_2PO_4^+$	X	–	–	–	IP44	$Mg^{2+} + CO_3^{2-} \leftrightarrow MgCO_3$	X	X	X	–
IP12	$Ca^{2+} + NH_3 \leftrightarrow CaNH_3^{2+}$	X	X	X	–	IP45	$2Mg^{2+} + CO_3^{2-} \leftrightarrow Mg_2CO_3^{2+}$	–	X	X	–
IP13	$Ca^{2+} + 2NH_3 \leftrightarrow Ca(NH_3)_2^{2+}$	–	X	–	–	IP46	$Mg^{2+} + DOM \leftrightarrow Mg\text{-}DOM$	–	X	X	–
IP14	$Ca^{2+} + NO_3^- \leftrightarrow CaNO_3^+$	–	–	X	–	IP47	$Mg^{2+} + HCO_3^- \leftrightarrow MgHCO_3^+$	X	X	X	–
IP15	$Ca^{2+} + OH^- \leftrightarrow CaOH^+$	–	–	X	–	IP48	$Mg^{2+} + HPO_4^{2-} \leftrightarrow MgHPO_4$	X	X	X	–
IP16	$Ca^{2+} + PO_4^{3-} \leftrightarrow CaPO_4^-$	X	X	X	–	IP49	$Mg^{2+} + 2NH_3 \leftrightarrow Mg(NH_3)_2^{2+}$	X	X	X	–
IP17	$Ca^{2+} + Pro^- \leftrightarrow CaPro^+$	X	X	X	–	IP50	$Mg^{2+} + OH^- \leftrightarrow MgOH^+$	X	X	X	–
IP18	$Ca^{2+} + SO_4^{2-} \leftrightarrow CaSO_4$	X	X	X	–	IP51	$Mg^{2+} + PO_4^{3-} \leftrightarrow MgPO_4^-$	X	X	X	–
IP19	$Ca^{2+} + Va^- \leftrightarrow CaVa^+$	X	X	X	–	IP52	$Mg^{2+} + Pro^- \leftrightarrow MgPro^+$	X	X	X	–
IP20	$Fe^{2+} + Cl^- \leftrightarrow FeCl^+$	–	X	–	–	IP53	$Mg^{2+} + SO_4^{2-} \leftrightarrow MgSO_4$	X	X	X	–
IP21	$Fe^{2+} + CO_3^{2-} \leftrightarrow FeCO_3$	X	–	–	–	IP54	$Na^+ + Ac^- \leftrightarrow NaAc$	X	X	X	–
IP22	$Fe^{2+} + HPO_4^{2-} \leftrightarrow FeHPO_4$	X	X	–	–	IP55	$Na^+ + Cl^- \leftrightarrow NaCl$	X	X	X	–
IP23	$Fe^{2+} + HS^- \leftrightarrow FeHS^+$	X	–	–	–	IP56	$Na^+ + CO_3^{2-} \leftrightarrow NaCO_3^-$	–	X	X	–
IP24	$Fe^{2+} + 2HS^- \leftrightarrow Fe(HS)_2$	X	–	–	–	IP57	$Na^+ + HCO_3^- \leftrightarrow NaHCO_3$	X	X	–	–
IP25	$Fe^{2+} + H_2PO_4^- \leftrightarrow FeH_2PO_4^+$	X	–	–	–	IP58	$Na^+ + HPO_4^{2-} \leftrightarrow NaHPO_4^-$	X	X	X	–
IP26	$Fe^{2+} + NH_3 \leftrightarrow FeNH_3^{2+}$	X	X	X	–	IP59	$Na^+ + H_2PO_4^- \leftrightarrow NaH_2PO_4\,(aq)$	X	X	–	–
IP27	$Fe^{2+} + 2NH_3 \leftrightarrow Fe(NH_3)_2^{2+}$	X	X	X	–	IP60	$Na^+ + NO_3^- \leftrightarrow NaNO_3$	–	X	X	–
IP28	$Fe^{2+} + 3NH_3 \leftrightarrow Fe(NH_3)_3^{2+}$	–	X	–	–	IP61	$Na^+ + OH^- \leftrightarrow NaOH$	–	X	X	–
IP29	$Fe^{2+} + OH^- \leftrightarrow FeOH^+$	X	X	X	–	IP62	$Na^+ + PO_4^{3-} \leftrightarrow NaPO_4^{2-}$	–	X	–	–
IP30	$Fe^{2+} + 2OH^- \leftrightarrow Fe(OH)_2$	X	X	X	–	IP63	$Na^+ + SO_4^{2-} \leftrightarrow NaSO_4^-$	X	X	X	–
IP31	$Fe^{3+} + 3OH^- \leftrightarrow Fe(OH)_3$	–	X	X	–	IP64	$NH_3 + HCO_3^- \leftrightarrow NH_2COO^- + H_2O$	X	–	–	X
IP32	$Fe^{2+} + SO_4^{2-} \leftrightarrow FeSO_4\,(aq)$	–	X	–	–	IP65	$NH_4^+ + SO_4^{2-} \leftrightarrow NH_4SO_4^-$	X	X	X	X
IP33	$K^+ + Ac^- \leftrightarrow KAc$	X	X	X	–						

Table A1.5
Liquid-solid/solid-liquid transfer reactions (P) included in each nutrient recovery model (NRM). AD = anaerobic digestion; Prec = precipitation/crystallization; P = precipitation; Strip = stripper; Scrub = scrubber.

No.	PHREEQC Phase name	Liquid-solid /solid-liquid transfer reaction	AD	Prec	Strip	Scrub
P1	Al_2O_3 (s)	$Al_2O_3(s) + 6H^+ \leftrightarrow 2Al^{3+} + 3H_2O$	X	–	–	–
P2	$AlPO_4$	$AlPO_4 \leftrightarrow Al^{3+} + PO_4^{3-}$	X	X	–	–
P3	Ammoniumsulfate	$(NH_4)_2SO_4 \leftrightarrow 2NH_4^+ + SO_4^{2-}$	–	–	–	X
P4	Anhydrite	$CaSO_4 \leftrightarrow Ca^{2+} + SO_4^{2-}$	X	–	–	–
P5	Aragonite	$CaCO_3 \leftrightarrow Ca^{2+} + CO_3^{2-}$	X	X	X	–
P6	Artinite	$MgCO_3{:}Mg(OH)_2{:}3H_2O + 2H^+ \leftrightarrow 2Mg^{2+} + CO_3^{2-} + 5H_2O$	–	X	X	–
P7	Boehmite	$AlOOH + 3H^+ \leftrightarrow Al^{3+} + 2H_2O$	X	X	–	–
P8	Brucite	$Mg(OH)_2 + 2H^+ \leftrightarrow Mg^{2+} + 2H_2O$	–	X	X	–
P9	$CaHPO_4$ (s)	$CaHPO_4 \leftrightarrow Ca^{2+} + H^+ + PO_4^{3-}$	X	X	X	–
P10	$CaHPO_4{:}2H_2O$ (s)	$CaHPO_4{:}2H_2O \leftrightarrow Ca^{2+} + H^+ + PO_4^{3-} + 2H_2O$	X	X	X	–
P11	$Ca_4H(PO_4)_3{:}3H_2O$ (s)	$Ca_4H(PO_4)_3{:}3H_2O \leftrightarrow 4Ca^{2+} + H^+ + 3PO_4^{3-} + 3H_2O$	X	X	X	–
P12	Calcite	$CaCO_3 \leftrightarrow Ca^{2+} + CO_3^{2-}$	X	X	X	–
P13	$Ca_3(PO_4)_2$ (am1)	$Ca_3(PO_4)_2 \leftrightarrow 3Ca^{2+} + 2PO_4^{3-}$	X	X	X	–
P14	$Ca_3(PO_4)_2$ (am2)	$Ca_3(PO_4)_2 \leftrightarrow 3Ca^{2+} + 2PO_4^{3-}$	X	X	X	–
P15	$Ca_3(PO_4)_2$ (beta)	$Ca_3(PO_4)_2 \leftrightarrow 3Ca^{2+} + 2PO_4^{3-}$	X	X	X	–
P16	Diaspore	$AlOOH + 3H^+ \leftrightarrow Al^{3+} + 2H_2O$	X	X	X	–
P17	Dolomite (ordered)	$CaMg(CO_3)_2 \leftrightarrow Ca^{2+} + Mg^{2+} + 2CO_3^{2-}$	X	X	X	–
P18	Dolomite (disordered)	$CaMg(CO_3)_2 \leftrightarrow Ca^{2+} + Mg^{2+} + 2CO_3^{2-}$	X	X	X	–
P19	$Fe(OH)_2$ (am)	$Fe(OH)_2 + 2H^+ \leftrightarrow Fe^{2+} + 2H_2O$	–	X	X	–
P20	FeS(ppt)	$FeS + H^+ \leftrightarrow Fe^{2+} + HS^-$	X	–	–	–
P21	Gibbsite	$Al(OH)_3 + 3H^+ \leftrightarrow Al^{3+} + 3H_2O$	X	X	–	–
P22	Hercynite	$FeAl_2O_4 + 8H^+ \leftrightarrow Fe^{2+} + 2Al^{3+} + 4H_2O$	X	X	X	–
P23	Huntite	$CaMg_3(CO_3)_4 \leftrightarrow 3Mg^{2+} + Ca^{2+} + 4CO_3^{2-}$	–	–	X	–
P24	Hydromagnesite	$Mg_5(CO_3)_4(OH)_2{:}4H_2O + 2H^+ \leftrightarrow 5Mg^{2+} + 4CO_3^{2-} + 6H_2O$	–	–	X	–
P25	Hydroxyapatite	$Ca_{10}(PO_4)_6(OH)_5 + 5H^+ \leftrightarrow 10Ca^{2+} + 6PO_4^{3-} + 5H_2O$	X	X	X	–
P26	K-struvite	$MgKPO_4{:}6H_2O \leftrightarrow Mg^{2+} + K^+ + PO_4^{3-} + 6H_2O$	X	X	X	–
P27	Mackinawite	$FeS + H^+ \leftrightarrow Fe^{2+} + HS^-$	X	–	–	–
P28	Magnesite	$MgCO_3 \leftrightarrow Mg^{2+} + CO_3^{2-}$	X	X	X	–
P29	$Mg(OH)_2$ (active)	$Mg(OH)_2 + 2H^+ \leftrightarrow Mg^{2+} + 2H_2O$	–	X	X	–

Table A1.5 (*continued*)

No.	PHREEQC Phase name	Liquid-solid /solid-liquid transfer reaction	AD	Prec	Strip	Scrub
P30	$Mg_3(PO_4)_2$ (s)	$Mg_3(PO_4)_2 \leftrightarrow 3Mg^{2+} + 2PO_4^{3-}$	X	X	X	–
P31	Newberyite	$MgHPO_4{:}3H_2O \leftrightarrow Mg^{2+} + H^+ + PO_4^{3-} + 3H_2O$	X	X	X	–
P32	Periclase	$MgO + 2H^+ \leftrightarrow Mg^{2+} + H_2O$	–	–	X	–
P33	Portlandite	$Ca(OH)_2 + 2H^+ \leftrightarrow Ca^{2+} + 2H_2O$	–	–	X	–
P34	Siderite	$FeCO_3 \leftrightarrow Fe^{2+} + CO_3^{2-}$	X	X	X	–
P35	Spinel	$MgAl_2O_4 + 8H^+ \leftrightarrow Mg^{2+} + 2Al^{3+} + 4H_2O$	–	–	X	–
P36	Struvite	$MgNH_4PO_4{:}6H_2O \leftrightarrow Mg^{2+} + NH_4^+ + PO_4^{3-}$	X	X	X	–
P37	Vaterite	$CaCO_3 \leftrightarrow Ca^{2+} + CO_3^{2-}$	–	X	X	–
P38	Vivianite	$Fe_3(PO_4)_2{:}8H_2O \leftrightarrow 3Fe^{2+} + 2PO_4^{3-} + 8H_2O$	X	X	X	–

Table A1.6
Gas-liquid / liquid-gas exchange reactions (GL) included in each nutrient recovery model (NRM). AD = anaerobic digestion; Prec = precipitation/crystallization; Strip = stripper; Scrub = scrubber.

No.	Gas-liquid /liquid-gas exchange reaction	AD	Prec	Strip	Scrub
GL1	CH_4 (aq) → CH_4 (g)	X	–	–	–
GL2	CO_2 (aq) ↔ CO_2 (g)	X	(X)[a]	X	X
GL3	H_2 (aq) ↔ H_2 (g)	X	–	X	X
GL4	H_2O (aq) ↔ H_2O (g)	X	(X)[a]	X	X
GL5	H_2S (aq) ↔ H_2S (g)	X	–	X	X
GL6	N_2 (aq) ↔ N_2 (g)	X	(X)[a]	X	X
GL7	NH_3 (aq) ↔ NH_3 (g)	X	(X)[a]	X	X
GL8	O_2 (aq) ↔ O_2 (g)	–	(X)[a]	X	X

[a] Values between brackets represent the use of air instead of chemicals for pH-adjustment.

APPENDIX 2

Detailed description of mass transfer scenarios for a) liquid-gas/gas-liquid transfer and b) liquid-solid/solid-liquid transfer

a) Liquid-gas/gas-liquid transfer

If the resistance to mass transfer is on the liquid side, the overall liquid mass transfer coefficient, $K_{L,i}$, can be perfectly adequate, while the overall gaseous mass transfer coefficient, $K_{G,i}$, provides a good estimation if the resistance is on the gas side. The relationship between the two coefficients can be represented by Equation (A1) (Chapra, 2008; Tchobanoglous et al., 2003):

$$\frac{1}{K_{L,i}} = \frac{H_{T,i} \cdot R \cdot T}{K_{G,i}} \quad \text{(A1)}$$

in which R is the universal gas law constant (0.082 l atm mol^{-1} K^{-1}) and T the temperature (K). It should be noted that the above-mentionned overall mass transfer coefficients are actually derived from the individual mass transfer coefficients by Equation (A2) (combined with Eq. (A1) for $K_{G,i}$):

$$\frac{1}{K_{Li}} = \frac{1}{k_{L,i}} + \frac{H_{T,i} \cdot R \cdot T}{k_{G,i}} \quad \text{(A2)}$$

in which $k_{L,i}$ and $k_{G,i}$ are the individual mass transfer coefficients that depend on the conditions at the interface and the bulk of the liquid and gas phase, respectively (Chapra, 2008; Tchobanoglous et al., 2003). Nevertheless, since the concentrations at the interface are difficult to measure, the overall mass transfer coefficient is generally used for practical purposes.

As such, **four potential mass transfer scenarios** were considered:

1) Active liquid-gas/gas-liquid transfer (NRM-Strip, NRM-Scrub) of low to moderately soluble gases. In this case, the penetration theory of Higbie (1935) was used to calculate the liquid mass transfer coefficient, $K_L a$ [T^{-1}]. It states that diffusion is a non-steady state process and that the molecules of the solute are in constant random motion. Clusters of these molecules arrive at the interface, remain there for a fixed period of time, and some of them penetrate while the rest mixes back into the bulk of the phase. The transfer velocity was then formulated in terms of the average contact time of a gas bubble at the interface (Eq. (A3); Chapra, 2008; Gujer, 2008):

$$K_{L/G}a = K_L a \left[T^{-1}\right] = \sqrt{\frac{4 \cdot D_l \cdot u}{\pi \cdot d}} \cdot \frac{\theta_{gas} \cdot 6 \cdot Q_{gas_{in}}}{d \cdot V_{liq}} \quad \text{(A3)}$$

in which d is the average gas bubble diameter (default = 3 mm; Gujer, 2008), u is the rise velocity of the gas bubbles (default = 0.3 m s^{-1}; Gujer, 2008), $\theta_{gas} = \frac{V_{gas}}{Q_{gas}}$ is the mean residence time of a gas bubble in the reactor [T], V_{gas} is the volume of all bubbles in the reactor or the total gas volume [L^3], and D_l is the liquid phase diffusion coefficient [L^2 T^{-1}] The latter was calculated at 298 K using the equation proposed by Schwarzenbach et al. (1993) (Eq. (A4)) based on the component's molecular weight (MW, [g mol^{-1}]):

$$D_l \left[L^2\ T^{-1}\right] = \frac{2.7 \cdot 10^{-4}}{MW^{0.71}} \quad \text{(A4)}$$

The obtained D_l values using Equation (A4) showed good equivalence with D_l values found in literature for wastewater systems (Chapra, 2008; Gujer, 2008; Tchobanoglous et al., 2003).

2) Active liquid-gas/gas-liquid transfer (NRM-Strip, NRM-Scrub) of very soluble gases. In this case, Equation (A3) was again applied, but now the gaseous phase diffusion coefficient (D_g) was used (Arogo et al., 1999).

3) Passive liquid-gas/gas-liquid transfer (NRM-AD) of low to moderately soluble gases. In this case, the mass transfer rate needs to be calibrated based on experimental results, e.g. as in Tourlousse and Ahmad (2007), because the rise velocity of gas bubbles is usually not measurable or very difficult to measure. For convenience, the

K_La is usually calculated from the K_La of oxygen gas (O_2) as a reference compound, since the latter is easy to deduce from experimental data and rate constants for volatile solutes can be assumed proportional to each other (Chapra, 2008; Ikumi, 2011; Mackay and Yeun, 1983; Munz and Roberts, 1989; Musvoto et al., 2000). However, the use of O_2 as a reference compound, as selected by Musvoto et al. (2000), is quite odd for anaerobic digestion, because normally no O_2 is present in such reactors. Therefore, in the NRM-AD model, H_2 was used as volatile reference compound occurring in digesters, similar as in (Pauss et al. (1990); Eq. (A5)):

$$K_{L/G}a = K_La\left[T^{-1}\right] = K_{L,H_2}\,a\cdot\left(\frac{D_l}{D_{l,H_2}}\right)^{0.5} \quad (A5)$$

4) Passive liquid-gas/gas-liquid transfer (NRM-AD) of very soluble gases. In this case, the mass transfer rate should be determined independently of the low to moderately soluble gases above (Sotemann et al., 2005). If no experimental data are available, the K_Ga value for NH_3 in anaerobic digestion is usually set to a very low value ranging from 1.92 to 3.2 d^{-1} (default in NRM-AD = 3.2 d^{-1}; Ikumi, 2011; Musvoto et al., 2000; Sotemann et al., 2005). This is to ensure an extremely low loss from the liquid phase through stripping. However, as the transfer rate depends much on design, operating conditions, and characteristics of the waste flow to be treated, it is advised to determine the $K_{G,NH_3}a$ under actual environmental conditions, as e.g. in Arogo et al. (1999). This is especially important for the stripper and scrubber unit processes.

b) liquid-solid/solid-liquid transfer

1) Supersaturation occurs (S > 1; SI > 0) and seed material is available. In this case, the crystallization of sparingly soluble salts in WRRFs is mainly controlled by surface spiral growth. This means that the integration of the cations into crystal lattice positions at kinks in the surface is the rate-determining molecular mechanism (Galbraith et al., 2014; Hauduc et al., 2015; Koutsoukos et al., 1980; Musvoto et al., 2000; Nielsen, 1984). The kinetic precipitation coefficient (Eq. (A6)) was then assumed to be proportional to the available seed material (cfr. Koutsoukos et al., 1980; Parkhurst and Appelo, 2013):

$$k_T\left[M\,L^{-3}\,T^{-1}\right] = k_{G,T}\cdot a_{seed}\cdot\frac{M_{seed}}{V_{liq}} \quad (A6)$$

in which $k_{G,T}$ is the temperature dependent growth rate coefficient [$M\,L^{-2}\,T^{-1}$], a_{seed} is the specific area of surface per gram of seed material before the seed crystals start to grow in the crystallizing solution [$L^2\,M^{-1}$] (default = 600 $m^2\,g^{-1}$; Parkhurst and Appelo, 2013), and M_{seed} is the time-dependent mass of seed material in the reactor [M] (default initial mass = 0.0005 kg; Parkhurst and Appelo, 2013). The latter is calculated at every time step by means of mass balances on the seed material for each precipitate (Section 2.2.4), taking in account the mass of newly formed precipitates and redissolution. The default reaction order for surface controlled growth (n_G) was set at 2, which generally provides a good approximation to represent precipitation in WRRFs (Bouropoulos and Koutsoukos, 2000; Mehta and Batstone, 2013; Musvoto et al., 2000; Nielsen, 1984).

2) Supersaturation occurs (S > 1; SI > 0), but no seed material is available and/or the crystal size is not large enough to have any influence on the process, i.e. the induction time is not exceeded. In this case, primary nucleation occurs, which was often not accounted for in previous studies (Harrison et al., 2011; Nielsen, 1984; Schneider et al., 2013), though very relevant (Bhuiyan et al., 2008). The value of $k_T$and n in Equation (3) are then switched to the nucleation rate, $k_{B,T}$(default = 10^6 nuclei $L^{-1}\,T^{-1}$; Mehta and Batstone, 2013), and the nucleation reaction order, n_B. The latter is usually higher for nucleation than for growth (3–4; default = 3; Tavare, 1995). The induction time is inversely proportional to the logarithm of S, and should be estimated experimentally for each precipitate (Bhuiyan et al., 2008; Mehta and Batstone, 2013).

3) The solution is undersaturated (S < 1; SI < 0) and precipitate is present in the system. In this case, the NRMs allow for precipitate redissolution until equilibrium is reached using the reverse reaction of Equation (3) (Morse and Arvidson, 2002). However, the kinetic dissolution rate($k_{D,T}$) and the reaction order for dissolution (n_D) may be different than those for precipitation. Significantly more work is needed to better understand the dissolution behaviour of the various precipitates in complex waste(water) matrices (Greenberg and Tomson, 1992; Morse and Arvidson, 2002).

4) Equilibrium occurs (S = 1; SI = 0).. In this case, the liquid-solid /solid-liquid transfer rate is set at 0.

Finally, for the NRM-Prec, a generic mechanism for **agglomeration and floc break-up** through the effect of mixing was included using the spherical particle model for macroscale flocculation (Crittenden et al., 2012). The net rate of floc appearance (Eq. (A7)) was written as:

$$\rho_{aggl}\left[L^{-3}\,T^{-1}\right] = K_a\cdot\overline{G}\cdot\frac{N_{part}}{V_{liq}}\cdot\frac{V_{fertilizer}}{V_{liq}} - K_b\cdot\overline{G}^{\delta} \quad (A7)$$

in which K_a [−] is the aggregation constant (= $4\alpha/\pi$ for laminar flow where α is the collision efficiency factor; default for turbulent flow = 5×10^{-4}), K_b [$T^{\delta-1}.L^{-3}$] is the floc break-up constant (= 0 for laminar flow; default for turbulent flow = 10^{-7}; Crittenden et al., 2012), $\overline{G}$ is the root mean square velocity gradient [T^{-1}] which depends on the power input (Camp and Stein, 1943), and δ is the turbulence constant. Under turbulent conditions, the values of K_a and K_b should be determined empirically in laboratory or pilot-scale tests (Argaman, 1971; Parker et al., 1972). Note that when the $\overline{G}$ value is set to 0, it is assumed that no agglomeration occurs.

APPENDIX 3

Biochemical processes and Gujer matrix included in the nutrient recovery model for the anaerobic digester (NRM-AD)

Table A3.1
Biochemical (BC) processes included in the nutrient recovery model for anaerobic digestion (NRM-AD) and extensions made as compared to the Anaerobic Digestion Model No. 1 (ADM1). Ac = acetate; Bu = butyrate; EBPR = enhanced biological phosphorus (P) removal; LCFA = long chain fatty acids; PAO = P accumulating organism; PHA = poly-hydroxy-alkanoate; PP = poly-phosphate; Pro = propionate; SRB = sulfate reducing bacteria; Va = valerate.

PHYSICOCHEMICAL PROCESSES	BIOCHEMICAL PROCESSES			
ADM1:	ADM1:	NRM-AD Extension 2:	NRM-AD Extension 3:	NRM-AD Potential extension 4:
4 Acid-base systems: NH_4^+/NH_3, CO_2/HCO_3^-, VFA/VFA^-, $H_2O/OH^-/H^+$	Disintegration, hydrolysis, acidogenesis, acetogenesis, methanogenesis (Batstone et al., 2002)	Sulfurgenesis (Knobel and Lewis, 2002; Lizarralde et al., 2010)	Release/uptake of P, K, S from bacterial cells and other biochemical components	EBPR sludge (Ikumi, 2011)
4 Gas-liquid exchange reactions: CO_2, CH_4, H_2, H_2O				
NRM-AD Extension 1:	BC1. Disintegration of complex particulates	BC20. Sulfate reduction on Ac	Inclusion in stoichiometric Gujer matrix (Table A2.2-A2.4)	BC28. Release of PP with uptake of Ac by PAOs
Acid-base systems: Table A1.2	BC2. Hydrolysis of carbohydrates	BC21. Sulfate reduction on Bu		BC29. Decay of PAOs
Redox reactions: Table A1.3	BC3. Hydrolysis of proteins	BC22. Sulfate reduction on H_2		BC30. Hydrolysis of PP + release of K, Ca, Mg
Ion pairing reactions: Table A1.4	BC4. Hydrolysis of lipids	BC23. Sulfate reduction on Pro		BC31. Hydrolysis of PHA
Solid-liquid transfer: Table A1.5	BC5. Uptake of monosaccharides	BC24. Decay of SRBs using Ac		
Gas-liquid exchange: Table A1.6	BC6. Uptake of aminoacids	BC25. Decay of SRBs using Bu		
	BC7. Uptake of LCFA	BC26. Decay of SRBs using H_2		
	BC8. Uptake of Va	BC27. Decay of SRBs using Pro		
	BC9. Uptake of Bu			
	BC10. Uptake of Pro			
	BC11. Uptake of Ac			
	BC12. Uptake of H_2			
	BC13. Decay of monosaccharide degraders			
	BC14. Decay of amino acid degraders			
	BC15. Decay of LCFA degraders			
	BC16. Decay of Va and Bu degraders			
	BC17. Decay of Pro degraders			
	BC18. Decay of Ac degraders			
	BC19. Decay of H degraders			

Table A3.2
Stoichiometry of the biochemical (BC) Gujer matrix incorporated in the nutrient recovery model for the anaerobic digester (NRM-AD). For process description: see Table A3.1. For nomenclature: see Table A3.4. For state variable description: see Appendix 5.

Component Process	S_aa kg COD m^{-3}	S_CO_2 kmol m^{-3}	S_HAc kg COD m^{-3}	S_HBu kg COD m^{-3}
BC1		C_xc - f_ch_xc.C_ch - f_si_xc.C_si - f_pr_xc.C_pr - f_xi_xc.C_xi - f_li_xc.C_li		
BC2		C_ch-C_su		
BC3	1	C_aa-C_pr		
BC4		(f_fa_li-1).C_su - f_fa_li.C_fa + C_li		
BC5		C_su - (1-Y_su).f_ac_su.C_ac - (1-Y_su).f_pro_su.C_pro - (1-Y_su).f_bu_su.C_bu - Y_su.C_biom	(1-Y_su).f_ac_su	(1-Y_su).f_bu_su
BC6	−1	C_aa - (1-Y_aa).f_ac_aa.C_ac - (1-Y_aa).f_bu_aa.C_bu - (1-Y_aa).f_pro_aa.C_pro - (1-Y_aa).f_va_aa.C_va - Y_aa.C_biom	(1-Y_aa).f_ac_aa	(1-Y_aa).f_bu_aa
BC7		C_fa - (1-Y_fa).0.7.C_ac - Y_fa.C_biom	(1-Y_fa).0.7	
BC8		C_va - (1-Y_c4).0.54.C_pro - Y_c4.C_biom - (1-Y_c4).0.31.C_ac	(1-Y_c4).0.31	
BC9		C_bu - (1-Y_c4).0.8.C_ac - Y_c4.C_biom	(1-Y_c4).0.8	−1
BC10		C_pro - (1-Y_pro).0.57.C_ac - Y_pro.C_biom	(1-Y_pro).0.57	
BC11		C_ac - Y_ac.C_biom - (1-Y_ac).C_ch4	−1	
BC12		-Y_h2.C_biom - (1-Y_h2).C_ch4		
BC13		C_biom - C_xc		
BC14		C_biom - C_xc		
BC15		C_biom - C_xc		
BC16		C_biom - C_xc		
BC17		C_biom - C_xc		
BC18		C_biom - C_xc		
BC19		C_biom - C_xc		
BC20		f_co2_ac	−1	
BC21		f_co2_bu		−1
BC22		f_co2_h		
BC23		f_co2_pro		
BC24		C_biom - C_xc		
BC25		C_biom - C_xc		
BC26		C_biom - C_xc		
BC27		C_biom - C_xc		

Table A3.2
Continuation: Stoichiometry of the biochemical (BC) Gujer matrix incorporated in the nutrient recovery model for the anaerobic digester (NRM-AD). For process description: see Table A3.1. For nomenclature: see Table A3.4. For state variable description: see Appendix 5.

Component Process	$S\_HPO_4^{2-}$ kmol m^{-3}	S_HVa kg COD m^{-3}	S_CH_4 kg COD m^{-3}	S_fa kg COD m^{-3}	S_H_2 kg COD m^{-3}	S_H_2S kmol m^{-3}	S_inert kg COD m^{-3}	S_K^+ kmol m^{-3}
BC1	P_xc - f_xi_xc.P_xi - f_si_xc.P_si - f_li_xc.P_li						f_Si_xc	
BC2								
BC3								
BC4	P_li			f_fa_li				
BC5	-Y_su.P_biom				(1-Y_su).f_h2_su			-Y_su.K_biom
BC6	-Y_aa.P_biom	(1-Y_aa).f_va_aa			(1-Y_aa).f_h2_aa			-Y_aa.K_biom
BC7	P_fa - Y_fa.P_biom			−1	(1-Y_fa).0.3			-Y_fa.K_biom
BC8	-Y_c4.P_biom	−1			(1-Y_c4).0.15			-Y_c4.K_biom
BC9	-Y_c4.P_biom				(1-Y_c4).0.2			-Y_c4.K_biom
BC10	-Y_pro.P_biom				(1-Y_pro).0.43			-Y_pro.K_biom
BC11	-Y_ac.P_biom		1-Y_ac					-Y_ac.K_biom
BC12	-Y_h2.P_biom		1-Y_h2		−1			-Y_h2.K_biom
BC13	P_biom - P_xc							K_biom - K_xc
BC14	P_biom - P_xc							K_biom - K_xc
BC15	P_biom - P_xc							K_biom - K_xc
BC16	P_biom - P_xc							K_biom - K_xc
BC17	P_biom - P_xc							K_biom - K_xc
BC18	P_biom - P_xc							K_biom - K_xc
BC19	P_biom - P_xc							K_biom - K_xc
BC20						f_s_ac		
BC21						f_s_bu		
BC22					−1	f_s_h		
BC23						f_s_pro		
BC24	P_biom - P_xc							K_biom - K_xc
BC25	P_biom - P_xc							K_biom - K_xc
BC26	P_biom - P_xc							K_biom - K_xc
BC27	P_biom - P_xc							K_biom - K_xc

Table A3.2
Continuation: Stoichiometry of the biochemical (BC) Gujer matrix incorporated in the nutrient recovery model for the anaerobic digester (NRM-AD). For process description: see Table A3.1. For nomenclature: see Table A3.4. For state variable description: see Appendix 5.

Component Process	$S\_NH_4^+$ kmol m^{-3}	S_pro kg COD m^{-3}	$S\_SO_4^{2-}$ kmol m^{-3}	S_su kg COD m^{-3}	X_aa kg COD m^{-3}	X_ac kg COD m^{-3}	X_c kg COD m^{-3}	X_c4 kg COD m^{-3}	X_ch kg COD m^{-3}	X_fa kg COD m^{-3}
BC1	N_xc - f_xi_xc.N_xi - f_si_xc.N_si - f_pr_xc.N_aa						−1		f_ch_xc	
BC2				1					−1	
BC3										
BC4				1-f_fa_li						
BC5	-N_biom.Y_su	(1-Y_su).f_pro_su	-Y_su.S_biom	−1						
BC6	N_aa - Y_aa.N_biom	(1-Y_aa).f_pro_aa	-Y_aa.S_biom		Y_aa					
BC7	-N_biom.Y_fa		-Y_c4.S_biom							Y_fa
BC8	-N_biom.Y_c4	(1-Y_c4).0.54	-Y_c4.S_biom					Y_c4		
BC9	-N_biom.Y_c4		-Y_ac.S_biom					Y_c4		
BC10	-N_biom.Y_pro	−1	-Y_pro.S_biom							
BC11	-N_biom.Y_ac		-Y_ac.S_biom			Y_ac				
BC12	-N_biom.Y_h2		-Y_h2.S_biom							
BC13	N_biom - N_xc		S_biom - S_xc				1			
BC14	N_biom - N_xc		S_biom - S_xc		−1		1			
BC15	N_biom - N_xc		S_biom - S_xc				1			−1
BC16	N_biom - N_xc		S_biom - S_xc				1	−1		
BC17	N_biom - N_xc		S_biom - S_xc				1			
BC18	N_biom - N_xc		S_biom - S_xc			−1	1			
BC19	N_biom - N_xc		S_biom - S_xc				1			
BC20			-f_s_ac							
BC21			-f_s_bu							
BC22			-f_s_h							
BC23		−1	-f_s_pro							
BC24	N_biom - N_xc		S_biom - S_xc				1			
BC25	N_biom - N_xc		S_biom - S_xc				1			
BC26	N_biom - N_xc		S_biom - S_xc				1			
BC27	N_biom - N_xc		S_biom - S_xc				1			

Table A3.2
Continuation: Stoichiometry of the biochemical (BC) Gujer matrix incorporated in the nutrient recovery model for the anaerobic digester (NRM-AD). For process description: see Table A3.1. For nomenclature: see Table A3.4. For state variable description: see Appendix 5.

Component Process	X_h2 kg COD m^{-3}	X_pr kg COD m^{-3}	X_pro kg COD m^{-3}	X_su kg COD m^{-3}	X_inert kg COD m^{-3}	X_li kg COD m^{-3}	X_srb_ac kg COD m^{-3}	X_srb_bu kg COD m^{-3}	X_srb_h kg COD m^{-3}	X_srb_pro kg COD m^{-3}
BC1		f_pr_xc			f_xi_xc	f_li_xc				
BC2										
BC3		−1								
BC4						−1				
BC5				Y_su						
BC6										
BC7										
BC8										
BC9										
BC10			Y_pro							
BC11										
BC12	Y_h2									
BC13				−1						
BC14										
BC15										
BC16										
BC17			−1							
BC18										
BC19	−1									
BC20							Y_srb_ac			
BC21								Y_srb_bu		
BC22									Y_srb_h	
BC23										Y_srb_pro
BC24							−1			
BC25								−1		
BC26									−1	
BC27										−1

Table A3.3
Biochemical (BC) kinetic equations of the Gujer matrix incorporated in the nutrient recovery model for the anaerobic digester (NRM-AD). For process description: see Table A3.1. For nomenclature: see Table A3.4. For state variable description: see Appendix 5.

Process	Kinetic equation (kg COD m^{-3} d^{-1})
BC1	$k_{dis} \cdot X_c$
BC2	$k_{hyd,X_{ch}} \cdot X_{ch}$
BC3	$k_{hyd,X_{pr}} \cdot X_{pr}$
BC4	$k_{hyd,X_{li}} X_{li}$
BC5	$km_{su} \cdot \frac{X_{su} \cdot S_{su}}{KS_{su}+S_{su}} \cdot I_{pH,bac} \cdot I_{NH,limit}$
BC6	$km_{aa} \cdot \frac{X_{aa} \cdot S_{aa}}{KS_{aa}+S_{aa}} \cdot I_{pH,bac} \cdot I_{NH,limit}$
BC7	$km_{fa} \cdot \frac{X_{fa} \cdot S_{fa}}{KS_{fa}+S_{fa}} \cdot I_{pH,bac} \cdot I_{NH,limit} \cdot I_{h2,fa}$
BC8	$km_{c4} \cdot \frac{X_{c4} \cdot S_{HVa}}{KS_{c4}+S_{HVa}} \cdot \frac{S_{HVa}}{S_{HVa}+S_{HBu}} \cdot I_{pH,bac} \cdot I_{NH,limit} \cdot I_{h2,c4}$
BC9	$km_{c4} \cdot \frac{X_{c4} \cdot S_{HBu}}{KS_{c4}+S_{HBu}} \cdot \frac{S_{HBu}}{S_{HBu}+S_{HVa}} \cdot I_{pH,bac} \cdot I_{NH,limit} \cdot I_{h2,c4}$
BC10	$km_{pro} \cdot \frac{X_{pro} \cdot S_{HPro}}{KS_{pro}+S_{HPro}} \cdot I_{pH,bac} \cdot I_{NH,limit} \cdot I_{h2,pro}$
BC11	$km_{ac} \cdot \frac{X_{ac} \cdot S_{HAc}}{KS_{ac}+S_{HAc}} \cdot I_{pH,ac} \cdot I_{NH3,ac} \cdot I_{NH,limit}$
BC12	$km_{h2} \cdot \frac{X_{h2} \cdot S_{h2}}{KS_{h2}+S_{h2}} \cdot I_{pH,h2} \cdot I_{NH,limit}$
BC13	$k_{dec,X_{su}} \cdot X_{su}$
BC14	$k_{dec,X_{aa}} \cdot X_{aa}$
BC15	$k_{dec,X_{fa}} \cdot X_{fa}$
BC16	$k_{dec,X_{c4}} \cdot X_{c4}$
BC17	$k_{dec,X_{pro}} \cdot X_{pro}$
BC18	$k_{dec,X_{ac}} \cdot X_{ac}$
BC19	$k_{dec,X_{h2}} \cdot X_{h2}$
BC20	$km_{srb,ac} \cdot \frac{X_{srb,ac} \cdot S_{HAc}}{KS_{srb,ac}+S_{HAc}} \cdot \frac{S_{SO_4}}{KS_{SO_4,ac}+S_{SO_4}} \cdot I_{pH,srb} \cdot I_{H_2S,ac}$
BC21	$km_{srb,bu} \cdot \frac{X_{srb,bu} \cdot S_{HBu}}{KS_{srb,bu}+S_{HBu}} \cdot \frac{S_{SO_4}}{KS_{SO_4,bu}+S_{SO_4}} \cdot I_{pH,srb} \cdot I_{H_2S,bu}$
BC22	$km_{srb,h2} \cdot \frac{X_{srb,h2} \cdot S_{H2}}{KS_{srb,h2}+S_{H2}} \cdot \frac{S_{SO_4}}{KS_{SO_4,h2}+S_{SO_4}} \cdot I_{pH,srb} \cdot I_{H_2S,h2}$
BC23	$km_{srb,pro} \cdot \frac{X_{srb,pro} \cdot S_{HPro}}{KS_{srb,pro}+S_{HPro}} \cdot \frac{S_{SO_4}}{KS_{SO_4,pro}+S_{SO_4}} \cdot I_{pH,srb} \cdot I_{H_2S,pro}$
BC24	$k_{dec,X_{srb,ac}} \cdot X_{srb,ac}$
BC25	$k_{dec,X_{srb,bu}} \cdot X_{srb,bu}$
BC26	$k_{dec,X_{srb,h2}} \cdot X_{srb,h2}$
BC27	$k_{dec,X_{pro}} \cdot X_{pro}$

Table A3.4
Nomenclature for Tables A3.2 and A3.3.

Symbol	Description	Unit
C_i	Carbon content of component i	kmol C kg^{-1} COD
f_product_substrate	Yield (catabolism only) of product on substrate	kg COD kg^{-1} COD
$I_{H_2,\ substrate}$	Hydrogen inhibition for substrate degradation	–
$I_{H_2S,substrate}$	Hydrogen sulfide inhibition for substrate degradation	–
$I_{NH,limit}$	Inhibition of biomass growth due to lack of inorganic nitrogen	–
$I_{pH,bac}$	pH inhibition of acetogens and acidogens	–
$I_{pH,i}$	pH inhibition of component *i*	–
$k_{dec,i}$	First order decay rate for biomass death of component *i*	d^{-1}
$k_{dis,i}$	Complex particulate first order disintegration rate of component *i*	d^{-1}
$k_{hyd,i}$	First order hydrolysis rate of component *i*	d^{-1}
K_i	Potassium content of component i	kmol K kg^{-1} COD
$k_{m,i}$	Specific Monod maximum uptake rate of component *i*	d^{-1}
Ks_i	Monod half saturation constant of component *i*	kg COD m^{-3}
N_i	Nitrogen content of component i	kmol N kg^{-1} COD
P_i	Phosphorus content of component i	kmol P kg^{-1} COD
S_i	Sulfur content of component i	kmol S kg^{-1} COD
Y_substrate	Yield of biomass on substrate	kg COD X kg^{-1} COD S

APPENDIX 4

Reactor design and the default specifications and features for each unit process

Table A4.1
Reactor design, default specifications and features for each unit in the nutrient recovery model (NRM) library. AD = anaerobic digestion; AmS = ammonium sulfate; Chem = chemical dosing; CSTR = continuously stirred tank reactor; Heat = heater; TSS = total suspended solids; P = precipitates; Prec = precipitation/crystallization; Scrub = scrubber; Settle = settler; Store = storage tank; Strip = stripper; WRRF = water resource recovery facility; X = biological particulate solids.

Unit	Reactor design	Default specifications and features
NRM-AD	CSTR (based on Gujer, 2008)	- Constant liquid volume; - Sealed gas phase at atmospheric pressure; - Gas removed to downstream treatment/process.
NRM-Prec	CSTR (as generally used for coagulation /flocculation units; Crittenden et al., 2012)	- Variable volume as function of retained precipitant volume; - Precipitate flow rate (Q_prec) extracts fraction of the precipitates continuously or at specific times when selected specifications are reached, e.g. target particle diameter, purity, etc.; - Allows to study the effect of mixing power and reactor seeding on, e.g., the mean particle/aggregate diameter; - Optional: use of gas flow instead of chemicals for pH-increase in the reactor; - Potential extension: inclusion of particle (differential) settling velocity (Crittenden et al., 2012).
NRM-Strip	Stirred tank for active liquid-gas exchange (based on Gujer, 2008)	- Continuous in- and outgoing liquid and gas flows; - Newly formed gas bubble enters the reactor at an initial gas phase concentration; - Model parameters averaged over all bubbles; - Heterogenous gas transfer throughout the reactor height; - User-selectable number of liquid layers to represent spatially dependent liquid transfer.[a]
NRM-Scrub	Stirred tank for active gas-liquid exchange (Gujer, 2008)	- Similar specifications as NRM-Strip, but: i) Default use of sulfuric acid solution at pH 1.3 for NH_3 absorption; ii) AmS recycle flow (Q_rec) with extraction as fertilizer flow when user-selected AmS specifications (usually 25–40% AmS concentration) are reached (cfr. semi-batch process).
NRM-Store	Tank with gas recovery for digestate storing	- Continued (non-controlled) anaerobic digestion and biogas recovery; - Continuously emptied to a user-specified minimum level, default = 15% (*AgriDigestore*, Ludlow, UK) → Complete digestion, energy recovery ↑, digestate nutrient availability ↑.
NRM-Settle	Point settler	- Simplified design based on TSS removal efficiency and TSS settleability (Hendricks, 2010), default = 0.5% non-settleable *X* and 10% non-settleable *P*; - Potential extension: inclusion of particle (differential) settling velocity (Crittenden et al., 2012) → No longer simplified design.
NRM-Chem	Point mixer	- Closed tank to avoid NH_3 emissions through pH-increase; - Allows addition of the most important amendments in WRRFs: i) $MgCl_2$, $Mg(OH)_2$, and $Ca(OH)_2$ prior to P precipitation, ii) NaOH and $Ca(OH)_2$ prior to stripping (goal = pH ↑, $CaCO_3$ scaling ↓); - Usually followed by NRM-Prec to allow for species precipitation and flocculation.
NRM-Heat	Point heater	- Colder fluid gaining heat from a hot gas/steam flow or a hot liquid flow; - Generic equation based on the specific heat of the fluid, the surface area of the heat exchanger, and the overall heat transfer coefficient (AIC, 2014); - Application prior to NRM-AD and NRM-Strip.

[a] Some literature studies show that hydraulic levels and reactor design have no effect on the NH_3 recovery efficiency as equilibrium conditions are reached in a very small time interval (Arogo et al., 1999; Collivignarelli et al., 1998; Gujer, 2008; Powers et al., 1987). However, other studies believe that liquid transfer should be modelled heterogeneously, i.e. spatially dependent (Yu et al., 2011). Because of this discussion, an option was included in the NRM-Strip and NRM-Scrub to calculate NH_3 removal and absorption for a user-selectable number of liquid layers. The Gujer (2008) model is based on homogeneous liquid transfer.

APPENDIX 5

State vectors used in the nutrient recovery model (NRM) library

Table A5.1
Generic state vectors used in the nutrient recovery model (NRM) library, component symbols, and descriptions.

State vector	Component symbol	Description	Component symbol	Description
Components_S1_PC	S_Acetate	soluble acetate	S_Mg	soluble magnesium
	S_Al	soluble aluminium	S_Na	soluble sodium
	S_Butyrate	soluble butyrate	S_N_min3_	soluble ammonia (N, -III)
	S_Ca	soluble calcium	S_N_0_	soluble nitrogen (N, 0)
	S_C_4_	soluble carbonate (C, +IV)	S_N_5_	soluble nitrate (N, +V)
	S_Cl	soluble chloride	S_O_0_	soluble oxygen (O, 0)
	S_C_min4_	soluble methane (C, −IV)	S_P	soluble phosphorus
	S_DOM	soluble dissolved organic matter	S_Propionate	soluble propionate
	S_Fe	soluble iron	S_S_min2_	soluble sulfide (S, -II)
	S_H_0_	soluble hydrogen (H, 0)	S_S_6_	soluble sulfate (S, +VI)
	S_K	soluble potassium	S_Valerate	soluble valerate
Components_S1_Bio	S_aa	soluble aminoacids	S_inert	soluble inerts
	S_fa	soluble long chain fatty acids	S_su	soluble sugars
Components_S2	S_C_4_	soluble carbonate (C, +IV)	S_N_5_	soluble nitrate (N, +V)
	S_C_min4_	soluble methane (C, −IV)	S_O_0_	soluble oxygen (O, 0)
	S_H_0_	soluble hydrogen (H, 0)	S_S_min2_	soluble sulfide (S, -II)
	S_N_min3_	soluble ammonia (N, -III)	S_S_6_	soluble sulfate (S, +VI)
	S_N_0_	soluble nitrogen (N, 0)		
Components_G	G_CH4	methane gas	G_H2S	hydrogen sulfide gas
	G_CO2	carbon dioxide gas	G_NH3	ammonia gas
	G_H2	hydrogen gas	G_N2	nitrogen gas
	G_H2O	water vapour	G_O2	oxygen gas
Components_P	P_Al	precipitated aluminium	P_Mg	precipitated magnesium
	P_Ca	precipitated calcium	P_N_min3_	precipitated ammonia (N, -III)
	P_C_4_	precipitated carbonate (C, +IV)	P_P	precipitated phosphorus
	P_Fe	precipitated iron	P_S_min2_	precipitated sulfide (S, -II)
	P_K	precipitated potassium	P_S_6_	precipitated sulfate (S, +VI)
Components_X	X_aa	aminoacid degraders	X_li	lipids
	X_ac	acetate degraders	X_pr	proteins
	X_c	composites	X_pro	propionate degraders
	X_ch	carbohydrates	X_su	sugar degraders
	X_c4	valerate and butyrate degraders	X_srb_ac	sulfate reducing bacteria using acetate
	X_fa	long chain fatty acid degraders	X_srb_bu	sulfate reducing bacteria using butyrate
	X_h2	hydrogen reducing bacteria	X_srb_h	sulfate reducing bacteria using hydrogen
	X_inert	particulate inerts	X_srb_pro	sulfate reducing bacteria using propionate

APPENDIX 6

Data requirements and data used for nutrient recovery model (NRM) validation

Table A6.1
Types of data required and datasets available for each key unit in the nutrient recovery model (NRM) library. AD = anaerobic digestion; Prec = precipitation/crystallization; Strip = stripper; Scrub = scrubber; N/A = not applicable.

	NRM-AD	NRM-Prec	NRM-Strip	NRM-Scrub
Input waste characteristics				
Biological components Physicochemical components	Sludge: Astals et al. (2013), Ikumi (2011), Tchobanoglous et al. (2003); Manure: Cesur and Albertson (2005), Martin (2003), Mattocks et al. (2002); Co-digestion: Zaher et al. (2009) + own data	N/A Ali and Schneider (2008), Bhuiyan et al. (2007), Harrison et al. (2011), Schneider et al. (2013) + own data	N/A Bhuiyan et al. (2007), Campos et al. (2013), Collivignarelli et al. (1998), Powers et al. (1987), Yu et al. (2011) + own data	N/A Campos et al. (2013), Collivignarelli et al. (1998), Manuzon et al. (2007), Powers et al. (1987), Yu et al. (2011) + own data
Physicochemical stoichiometric parameters				
Acid-base /ion pairing equilibrium constants (K_{ab}, K_{ip})	NIST (2001), PHREEQC	NIST (2001), PHREEQC	NIST (2001), PHREEQC	NIST (2001), PHREEQC
Water dissociation constant (K_w)	NIST (2001), PHREEQC	NIST (2001), PHREEQC	NIST (2001), PHREEQC	NIST (2001), PHREEQC

(*continued on next page*)

Table A6.1 (*continued*)

	NRM-AD	NRM-Prec	NRM-Strip	NRM-Scrub
Solubility products (K_s)	NIST (2001), PHREEQC	NIST (2001), PHREEQC	NIST (2001), PHREEQC	NIST (2001), PHREEQC
Henry's law coefficients (H)	Sander (1999)	Sander (1999)	Sander (1999)	Sander (1999)
Physicochemical kinetic parameters				
Precipitation /dissolution transfer coefficients and reaction order (k, n)	Bénézeth et al. (2008), Chauhan et al. (2011), Ikumi (2011), Inskeep and Silvertooth (1988), Johnson (1990), Musvoto et al. (1997); Musvoto et al. (2000); Nielsen (1984), NIST (2001), to mention a few	Ali and Schneider (2008), Bhuiyan et al. (2008), Galbraith et al. (2014), Harrison et al. (2011), NIST (2001), Schneider et al. (2013), to mention a few	Bénézeth et al. (2008), Chauhan et al. (2011), Ikumi (2011), Inskeep and Silvertooth (1988), Johnson (1990), Musvoto et al. (1997); Musvoto et al. (2000); Nielsen (1984), NIST (2001), to mention a few	Belcu and Turtoi (1996), NIST (2001)
Liquid-gas transfer coefficients ($K_{L/G}a$)	Batstone et al. (2002), Chapra (2008), Lizarralde et al. (2013), Musvoto et al. (1997), Munz and Roberts (1989)	If pH increase with aeration: Batstone et al. (2002), Chapra (2008), Lizarralde et al. (2013), Musvoto et al. (1997), Munz and Roberts (1989)	Collivignarelli et al. (1998), Musvoto et al. (1997), Musvoto et al. (2000), Powers et al. (1987), Yu et al. (2011)	Collivignarelli et al. (1998), Manuzon et al. (2007), Yu et al. (2011)
Biological stoichiometric parameters				
Biomass composition	Batstone et al. (2002), Ikumi (2011), Tchobanoglous et al. (2003), Zaher et al. (2009)	N/A	N/A	N/A
Pre-set fractions (f_product_substrate)	Batstone et al. (2002), Ikumi (2011), Knobel and Lewis (2002), Lizarralde et al. (2010)	N/A	N/A	N/A
Biomass substrate yield (Y_substrate)	Batstone et al. (2002), Ikumi (2011), Knobel and Lewis (2002), Lizarralde et al. (2010)	N/A	N/A	N/A
Biological kinetic parameters				
Uptake rates (k_m), disintegration rates (k_{dis}), decay rates (k_{dec}), etc.	Batstone et al. (2002), Ikumi (2011), Knobel and Lewis (2002), Lizarralde et al. (2010)	N/A	N/A	N/A
Input/output data + operational factors (temperature, pH, etc.) = calibration/validation data				
	Sludge: Astals et al. (2013); Manure: Cesur and Albertson (2005), Martin (2003), Mattocks et al. (2002), + own data + data from industry	Ali and Schneider (2008), Bhuiyan et al. (2007, 2008), Harrison et al. (2011), Schneider et al. (2013) + own data + data from industry	Campos et al. (2013), Collivignarelli et al. (1998), Powers et al. (1987), Yu et al. (2011) + own data + data from industry	Campos et al. (2013), Collivignarelli et al. (1998), Koptev (1966), Manuzon et al. (2007), Melse and Ogink (2005), Powers et al. (1987), Yu et al. (2011) + own data + data from industry

Table A6.2
Parameter categories, names, default values and units for the NRM-AD.

CATEGORY	NAME	DEFAULT VALUE	UNIT
DIMENSION			
Volume	Vol_gas	1	m^3
	Vol_liq	2.8	m^3
KINETICS			
Liquid-gas diffusion coefficient at T_diff	D[CH4_g_]	3.771E-05	m^2/d
	D[CO2_g_]	0.000156	m^2/d
	D[H2S_g_]	2.2043E-05	m^2/d
	D[H2_g_]	0.000165	m^2/d
	D[N2_g_]	0.0001536	m^2/d
	D[NH3_g_]	0.000169	m^2/d
	D_O2	0.0001608	m^2/d
Inhibitory concentration	KI_h2_c4	1E-05	kg/m^3
	KI_h2_fa	5E-06	kg/m^3
	KI_h2_pro	3.5E-06	kg/m^3
	KI_h2s_ac	0.00475	kg/m^3
	KI_h2s_bu	0.0156	kg/m^3
	KI_h2s_h2	0.00465	kg/m^3
	KI_h2s_pro	0.00889	kg/m^3
	KI_nh3_ac	0.0252	$kmol/m^3$
Saturation constant	Ks_IN	0.0001	kg/m^3
	Ks_aa	0.3	kg/m^3
	Ks_ac	0.15	kg/m^3
	Ks_c4	0.2	kg/m^3
	Ks_fa	0.4	kg/m^3
	Ks_h2	7E-06	kg/m^3
	Ks_pro	0.1	kg/m^3
	Ks_so4_ac	0.0002	kg/m^3
	Ks_so4_bu	0.00017	kg/m^3
	Ks_so4_h2	9.3E-06	kg/m^3
	Ks_so4_pro	7.7E-05	kg/m^3
	Ks_srb_ac	0.024	kg/m^3
	Ks_srb_bu	0.28672	kg/m^3
	Ks_srb_h2	2.4E-05	kg/m^3
	Ks_srb_pro	0.04944	kg/m^3
	Ks_su	0.5	kg/m^3
Temperature of diffusion coefficient	T_diff[CH4_g_]	298	K
	T_diff[CO2_g_]	293	K
	T_diff[H2S_g_]	298	K
	T_diff[H2_g_]	298	K
	T_diff[N2_g_]	293	K
	T_diff[NH3_g_]	298	K
Liquid mass transfer rate	kLa_O2	200	1/d
Liquid-solid transfer rate	k[Al2O3]	0.0001	$mol/m^2/d$
	k[AlPO4]	0.0001	$mol/m^2/d$
	k[Anhydrite]	0.0001	$mol/m^2/d$
	k[Aragonite]	0.61166516	$mol/m^2/d$
	k[Boehmite]	0.00028	$mol/m^2/d$
	k[Ca4H_PO4_3_3H2O_]	0.1	$mol/m^2/d$
	k[CaHPO4_2H2O]	14.6435	$mol/m^2/d$
	k[CaHPO4bis]	0.1	$mol/m^2/d$
	k[Calcite]	1080	$mol/m^2/d$
	k[Diaspore]	0.1	$mol/m^2/d$
	k[Dolomite]	11.22	$mol/m^2/d$
	k[FeS_ppt_]	0.0001	$mol/m^2/d$
	k[Gibbsite]	0.0001192652	$mol/m^2/d$
	k[Hercynite]	0.1	$mol/m^2/d$
	k[Hydroxyapatite]	986.64761	$mol/m^2/d$
	k[Kstruvite]	4.64E-06	$mol/m^2/d$
	k[Mackinawite]	0.0001	$mol/m^2/d$
	k[Magnesite]	0.000988416	$mol/m^2/d$
	k[Mg3_PO4_2]	0.1	$mol/m^2/d$
	k[MgHPO4_3H2O]	4.78021E-07	$mol/m^2/d$
	k[Siderite]	0.00209952	$mol/m^2/d$
	k[Struvite]	0.002037407	$mol/m^2/d$
	k[Vivianite]	1.66165E-06	$mol/m^2/d$
Decay rate	kdec_xaa	0.02	1/d
	kdec_xac	0.02	1/d
	kdec_xc4	0.02	1/d
	kdec_xfa	0.02	1/d
	kdec_xh2	0.02	1/d
	kdec_xpro	0.02	1/d
	kdec_xsrbac	0.02	1/d
	kdec_xsrbbu	0.02	1/d
	kdec_xsrbh	0.02	1/d

(*continued on next page*)

Table A6.2 (*continued*)

CATEGORY	NAME	DEFAULT VALUE	UNIT
	kdec_xsrbpro	0.02	1/d
	kdec_xsu	0.02	1/d
Dissociation rate	kdis	0.5	1/d
Hydrolysis rate	khyd_ch	10	1/d
	khyd_li	10	1/d
	khyd_pr	10	1/d
Maximum uptake rate	km_aa	50	1/d
	km_ac	9	1/d
	km_c4	20	1/d
	km_fa	6	1/d
	km_h2	35	1/d
	km_pro	9	1/d
	km_srb_ac	12.55	1/d
	km_srb_bu	14.51	1/d
	km_srb_h2	20	1/d
	km_srb_pro	20	1/d
	km_su	30	1/d
Reaction order precipitation	n[Al2O3]	2	–
	n[AlPO4]	2	–
	n[Anhydrite]	2	–
	n[Aragonite]	2	–
	n[Boehmite]	2	–
	n[Ca4H_PO4_3_3H2O_]	2	–
	n[CaHPO4_2H2O]	2	–
	n[CaHPO4bis]	2	–
	n[Calcite]	2	–
	n[Diaspore]	2	–
	n[Dolomite]	2	–
	n[FeS_ppt_]	2	–
	n[Gibbsite]	2	–
	n[Hercynite]	2	–
	n[Hydroxyapatite]	2	–
	n[Kstruvite]	2	–
	n[Mackinawite]	2	–
	n[Magnesite]	2	–
	n[Mg3_PO4_2]	2	–
	n[MgHPO4_3H2O]	2	–
	n[Siderite]	2	–
	n[Struvite]	2	–
	n[Vivianite]	2	–
pH inhibitory levels	pH_ac_ll	6.3	–
	pH_ac_ul	9	–
	pH_bac_ll	4	–
	pH_bac_ul	5.5	–
	pH_h2_ll	5.3	–
	pH_h2_ul	9	–
	pH_srb_ll	5.5	–
	pH_srb_ul	8	–
	alfa_ll	6	–
	alfa_ul	6	–
Arrhenius coefficient for temperature dependency	theta[CH4_g_]	1.024	–
	theta[CO2_g_]	1.024	–
	theta[H2S_g_]	1.024	–
	theta[H2_g_]	1.024	–
	theta[N2_g_]	1.024	–
	theta[NH3_g_]	1[a]	–
OPERATION			
Gas flow constant	K_p	50000	–
Mass of seed material	M_seed[Al2O3]	0.0005	kg
	M_seed[AlPO4]	0.0005	kg
	M_seed[Anhydrite]	0.0005	kg
	M_seed[Aragonite]	0.0005	kg
	M_seed[Boehmite]	0.0005	kg
	M_seed[Ca4H_PO4_3_3H2O_]	0.0005	kg
	M_seed[CaHPO4_2H2O]	0.0005	kg
	M_seed[CaHPO4bis]	0.0005	kg
	M_seed[Calcite]	0.0005	kg
	M_seed[Diaspore]	0.0005	kg
	M_seed[Dolomite]	0.0005	kg
	M_seed[FeS_ppt_]	0.0005	kg
	M_seed[Gibbsite]	0.0005	kg
	M_seed[Hercynite]	0.0005	kg
	M_seed[Hydroxyapatite]	0.0005	kg
	M_seed[Kstruvite]	0.0005	kg
	M_seed[Mackinawite]	0.0005	kg
	M_seed[Magnesite]	0.0005	kg

Table A6.2 (*continued*)

CATEGORY	NAME	DEFAULT VALUE	UNIT
	M_seed[Mg3_PO4_2]	0.0005	kg
	M_seed[MgHPO4_3H2O]	0.0005	kg
	M_seed[Siderite]	0.0005	kg
	M_seed[Struvite]	0.0005	kg
	M_seed[Vivianite]	0.0005	kg
Temperature	T_op	302.15	K
Surface area of seed material	a_seed	600	m^2/g
Fraction of particulate matter that leaves the reactor	f_X_Out	0.002	–
Atmospheric pressure	p_atm	1	atm
STOICHIOMETRY			
COD content	COD[Acetatemin]	64	g/mol
	COD[Butyratemin]	160	g/mol
	COD[CH4]	64	g/mol
	COD[CO2]	1	g/mol
	COD[CO3min2]	1	g/mol
	COD[H2S]	1	g/mol
	COD[H2]	16	g/mol
	COD[Kplus]	1	g/mol
	COD[NH4plus]	1	g/mol
	COD[PO4min3]	1	g/mol
	COD[Propionatemin]	112	g/mol
	COD[SO4min2]	1	g/mol
	COD[Valeratemin]	208	g/mol
Carbon content	C_SI	0.03	mol/g
	C_XI	0.03	mol/g
	C_Xc	0.02786	mol/g
	C_aa	0.03	mol/g
	C_ac	0.0313	mol/g
	C_biom	0.0313	mol/g
	C_bu	0.025	mol/g
	C_ch	0.0313	mol/g
	C_ch4	0.0156	mol/g
	C_fa	0.0217	mol/g
	C_li	0.022	mol/g
	C_pr	0.03	mol/g
	C_pro	0.0268	mol/g
	C_su	0.0313	mol/g
	C_va	0.024	mol/g
Reaction enthalphie of gas-liquid transfer	H_gas[CH4_g_]	−1700	–
	H_gas[CO2_g_]	−236534	–
	H_gas[H2S_g_]	−3000	–
	H_gas[H2_g_]	−500	–
	H_gas[N2_g_]	−1300	–
	H_gas[NH3_g_]	−4200	–
Potassium content	K_Xc	0.0001278828	mol/g
	K_biom	0.0002557656	mol/g
Nitrogen content	N_SI	0.0042857143	mol/g
	N_XI	0.0042857143	mol/g
	N_Xc	0.0026857143	mol/g
	N_aa	0.007	mol/g
	N_biom	0.0057142857	mol/g
Phosphorus content	P_Xc	0.00032285392	mol/g
	P_biom	0.00064570783	mol/g
Sulfur content	S_Xc	0.0001278828	mol/g
	S_biom	0.0002557656	mol/g
Biomass yield	Y_aa	0.08	–
	Y_ac	0.05	–
	Y_c4	0.06	–
	Y_fa	0.06	–
	Y_h2	0.06	–
	Y_pro	0.04	–
	Y_srb_ac	0.05437	–
	Y_srb_bu	0.03809	–
	Y_srb_h	0.17355	–
	Y_srb_pro	0.04081	–
	Y_su	0.1	–
Enthalpy of heat for precipitation	delta_H[Al2O3]	−258.5901	kJ/mol
	delta_H[AlPO4]	−458.6	kJ/mol
	delta_H[Anhydrite]	−7.2	kJ/mol
	delta_H[Aragonite]	−8	kJ/mol
	delta_H[Boehmite]	−117.6959	kJ/mol
	delta_H[Ca4H_PO4_3_3H2O_]	−105	kJ/mol
	delta_H[CaHPO4_2H2O]	23	kJ/mol
	delta_H[CaHPO4bis]	31	kJ/mol
	delta_H[Calcite]	−8	kJ/mol

(*continued on next page*)

Table A6.2 (*continued*)

CATEGORY	NAME	DEFAULT VALUE	UNIT
	delta_H[Diaspore]	−103.0519	kJ/mol
	delta_H[Dolomite]	−31.9	kJ/mol
	delta_H[FeS_ppt_]	−11	kJ/mol
	delta_H[Gibbsite]	−105	kJ/mol
	delta_H[Hercynite]	−313.9199	kJ/mol
	delta_H[Hydroxyapatite]	0	kJ/mol
	delta_H[Kstruvite]	−83.21	kJ/mol
	delta_H[Mackinawite]	0	kJ/mol
	delta_H[Magnesite]	20	kJ/mol
	delta_H[Mg3_PO4_2]	0	kJ/mol
	delta_H[MgHPO4_3H2O]	0	kJ/mol
	delta_H[Siderite]	−7.3	kJ/mol
	delta_H[Struvite]	0	kJ/mol
	delta_H[Vivianite]	−5.06	kJ/mol
Pre-set fraction and yield	f_SI_xc	0.1	–
	f_XI_xc	0.2	–
	f_ac_aa	0.4	–
	f_ac_su	0.41	–
	f_bu_aa	0.26	–
	f_bu_su	0.13	–
	f_ch_xc	0.1	–
	f_co2_ac	0.02955	mol/gCOD
	f_co2_bu	0	mol/gCOD
	f_co2_h	0.00542	mol/gCOD
	f_co2_pro	0.0085	mol/gCOD
	f_fa_li	0.95	–
	f_h2_aa	0.06	–
	f_h2_su	0.19	–
	f_li_xc	0.3	–
	f_pr_xc	0.52	–
	f_pro_aa	0.05	–
	f_pro_su	0.27	–
	f_s_ac	0	mol/gCOD
	f_s_bu	0.00542	mol/gCOD
	f_s_h	0	mol/gCOD
	f_s_pro	0	mol/gCOD
	f_va_aa	0.23	–
Henry coefficient at 298.15 K	kH[CH4_g_]	0.0014	mol/L/atm
	kH[CO2_g_]	0.035	mol/L/atm
	kH[H2S_g_]	0.1	mol/L/atm
	kH[H2_g_]	0.00078	mol/L/atm
	kH[N2_g_]	0.00065	mol/L/atm
	kH[NH3_g_]	61	mol/L/atm

[a] Passive liquid-gas transfer, kLa = 3.2.

Table A6.3
Parameter categories, names, default values and units for the NRM-Prec.

CATEGORY	NAME	DEFAULT VALUE	UNIT
DIMENSION			
Volume	Vol_liq	1000	m^3
Fertilizer extraction rate	Q_prec_target	10	m^3/d
KINETICS			
Liquid-solid transfer rate	k[AlPO4]	0.0001	$mol/m^2/d$
	k[Aragonite]	6.1166516	$mol/m^2/d$
	k[Artinite]	50	$mol/m^2/d$
	k[Boehmite]	0.00028	$mol/m^2/d$
	k[Brucite]	0.1	$mol/m^2/d$
	k[Ca3_PO4_2_am1]	50	$mol/m^2/d$
	k[Ca3_PO4_2_am2]	50	$mol/m^2/d$
	k[Ca3_PO4_2_beta]	50	$mol/m^2/d$
	k[Ca4H_PO4_3_3H2O_]	0.1	$mol/m^2/d$
	k[CaHPO4_2H2O]	14.6435	$mol/m^2/d$
	k[CaHPO4bis]	0.1	$mol/m^2/d$
	k[Calcite]	1080	$mol/m^2/d$
	k[Diaspore]	0.1	$mol/m^2/d$
	k[Dolomite]	11.22	$mol/m^2/d$
	k[Dolomite_dis]	0.1	$mol/m^2/d$
	k[Fe_OH_2_s]	0.1	$mol/m^2/d$
	k[Gibbsite]	0.0001192652	$mol/m^2/d$
	k[Hercynite]	0.1	$mol/m^2/d$
	k[Hydroxyapatite]	986.64761	$mol/m^2/d$

Table A6.3 (*continued*)

CATEGORY	NAME	DEFAULT VALUE	UNIT
	k[Kstruvite]	4.64E-06	mol/m^2/d
	k[Magnesite]	0.000988416	mol/m^2/d
	k[Mg3_PO4_2]	0.1	mol/m^2/d
	k[MgHPO4_3H2O]	4.78021E-07	mol/m^2/d
	k[Mg_OH_2_act]	0.1	mol/m^2/d
	k[Siderite]	0.00209952	mol/m^2/d
	k[Struvite]	0.002037407	mol/m^2/d
	k[Vaterite]	0.1	mol/m^2/d
	k[Vivianite]	1.66165E-06	mol/m^2/d
OPERATION			
Target minimum diameter of particels	D_fertilizer_target	0.001	m
Mass of seed material	M_seed[AlPO4]	0.0005	kg
	M_seed[Aragonite]	0.0005	kg
	M_seed[Artinite]	0.0005	kg
	M_seed[Boehmite]	0.0005	kg
	M_seed[Brucite]	0.0005	kg
	M_seed[Ca3_PO4_2_am1]	0.0005	kg
	M_seed[Ca3_PO4_2_am2]	0.0005	kg
	M_seed[Ca3_PO4_2_beta]	0.0005	kg
	M_seed[Ca4H_PO4_3_3H2O_]	0.0005	kg
	M_seed[CaHPO4_2H2O]	0.0005	kg
	M_seed[CaHPO4bis]	0.0005	kg
	M_seed[Calcite]	0.0005	kg
	M_seed[Diaspore]	0.0005	kg
	M_seed[Dolomite]	0.0005	kg
	M_seed[Dolomite_dis]	0.0005	kg
	M_seed[Fe_OH_2_s]	0.0005	kg
	M_seed[Gibbsite]	0.0005	kg
	M_seed[Hercynite]	0.0005	kg
	M_seed[Hydroxyapatite]	0.0005	kg
	M_seed[Kstruvite]	0.0005	kg
	M_seed[Magnesite]	0.0005	kg
	M_seed[Mg3_PO4_2]	0.0005	kg
	M_seed[MgHPO4_3H2O]	0.0005	kg
	M_seed[Mg_OH_2_act]	0.0005	kg
	M_seed[Siderite]	0.0005	kg
	M_seed[Struvite]	0.0005	kg
	M_seed[Vaterite]	0.0005	kg
	M_seed[Vivianite]	0.0005	kg
Residence time	Res_time_liq	10	d
Temperature	T_op	0	K
Surface area of seed material	a_seed	600	m^2/g
Fraction of precipitates removed from the reactor per extraction	f_prec	1	–
pH	pH_op	10	–
STOICHIOMETRY			
Enthalpy of heat for precipitation	delta_H[AlPO4]	−458.6	kJ/mol
	delta_H[Aragonite]	−8	kJ/mol
	delta_H[Artinite]	−120.2565	kJ/mol
	delta_H[Boehmite]	−117.6959	kJ/mol
	delta_H[Brucite]	−114	kJ/mol
	delta_H[Ca3_PO4_2_am1]	−94	kJ/mol
	delta_H[Ca3_PO4_2_am2]	−87	kJ/mol
	delta_H[Ca3_PO4_2_beta]	54	kJ/mol
	delta_H[Ca4H_PO4_3_3H2O_]	−105	kJ/mol
	delta_H[CaHPO4_2H2O]	23	kJ/mol
	delta_H[CaHPO4bis]	31	kJ/mol
	delta_H[Calcite]	−8	kJ/mol
	delta_H[Diaspore]	−103.0519	kJ/mol
	delta_H[Dolomite]	−31.9	kJ/mol
	delta_H[Dolomite_dis]	−46.4	kJ/mol
	delta_H[Fe_OH_2_s]	−91.62	kJ/mol
	delta_H[Gibbsite]	−105	kJ/mol
	delta_H[Hercynite]	−313.9199	kJ/mol
	delta_H[Hydroxyapatite]	0	kJ/mol
	delta_H[Kstruvite]	−83.21	kJ/mol
	delta_H[Magnesite]	20	kJ/mol
	delta_H[Mg3_PO4_2]	0	kJ/mol
	delta_H[MgHPO4_3H2O]	0	kJ/mol
	delta_H[Mg_OH_2_act]	0	kJ/mol
	delta_H[Siderite]	−7.3	kJ/mol
	delta_H[Struvite]	0	kJ/mol
	delta_H[Vaterite]	−8	kJ/mol
	delta_H[Vivianite]	−5.06	kJ/mol

Table A6.4
Parameter categories, names, default values and units for the NRM-Strip.

CATEGORY	NAME	DEFAULT VALUE	UNIT
DIMENSION			
Height	H_reactor	11.5	m
Safety factor on air requirements	SF_Air	1.5	–
Safety factor on reactor height	SF_Height	1.5	–
Volume	V_liq	81.3	m^3
Number of layers	NrOfLayers	3	–
Initial gas flow rate	Q_gas_in	2400	m^3/d
Initial liquid flow rate	Q_liq_in	1560000	m^3/d
KINETICS			
Liquid-gas diffusion coefficient at T_diff	D[CH4_g_]	3.771E-05	m^2/d
	D[CO2_g_]	0.000156	m^2/d
	D[H2S_g_]	2.2043E-05	m^2/d
	D[H2_g_]	0.000165	m^2/d
	D[N2_g_]	0.0001536	m^2/d
	D[NH3_g_]	0.000169	m^2/d
	D[O2_g_]	0.0001608	m^2/d
Temperature of diffusion coefficient	T_diff[CH4_g_]	298	K
	T_diff[CO2_g_]	293	K
	T_diff[H2S_g_]	298	K
	T_diff[H2_g_]	298	K
	T_diff[N2_g_]	293	K
	T_diff[NH3_g_]	298	K
	T_diff[O2_g_]	293	K
Liquid-solid transfer rate	k[Aragonite]	6.1166516	$mol/m^2/d$
	k[Artinite]	50	$mol/m^2/d$
	k[Brucite]	0.1	$mol/m^2/d$
	k[Ca3_PO4_2_am1]	50	$mol/m^2/d$
	k[Ca3_PO4_2_am2]	50	$mol/m^2/d$
	k[Ca3_PO4_2_beta]	50	$mol/m^2/d$
	k[Ca4H_PO4_3_3H2O_]	0.1	$mol/m^2/d$
	k[CaHPO4_2H2O]	14.6435	$mol/m^2/d$
	k[CaHPO4bis]	0.1	$mol/m^2/d$
	k[Calcite]	1080	$mol/m^2/d$
	k[Diaspore]	0.1	$mol/m^2/d$
	k[Dolomite]	11.22	$mol/m^2/d$
	k[Dolomite_dis]	0.1	$mol/m^2/d$
	k[Fe_OH_2]	0.1	$mol/m^2/d$
	k[Hercynite]	0.1	$mol/m^2/d$
	k[Huntite]	0.1	$mol/m^2/d$
	k[Hydromagnesite]	50	$mol/m^2/d$
	k[Hydroxyapatite]	986.64761	$mol/m^2/d$
	k[Kstruvite]	4.64E-06	$mol/m^2/d$
	k[Magnesite]	0.000988416	$mol/m^2/d$
	k[Mg3_PO4_2]	0.1	$mol/m^2/d$
	k[MgHPO4_3H2O]	4.78021E-07	$mol/m^2/d$
	k[Mg_OH_2_act]	0.1	$mol/m^2/d$
	k[Periclase]	0.1	$mol/m^2/d$
	k[Portlandite]	0.1	$mol/m^2/d$
	k[Siderite]	0.00209952	$mol/m^2/d$
	k[Spinel]	0.1	$mol/m^2/d$
	k[Struvite]	0.002037407	$mol/m^2/d$
	k[Vivianite]	1.66165E-06	$mol/m^2/d$
Reaction order for precipitation	n[Aragonite]	2	–
	n[Artinite]	2	–
	n[Brucite]	2	–
	n[Ca3_PO4_2_am1]	2	–
	n[Ca3_PO4_2_am2]	2	–
	n[Ca3_PO4_2_beta]	2	–
	n[Ca4H_PO4_3_3H2O_]	2	–
	n[CaHPO4_2H2O]	2	–
	n[CaHPO4bis]	2	–
	n[Calcite]	2	–
	n[Diaspore]	2	–
	n[Dolomite]	2	–
	n[Dolomite_dis]	2	–
	n[Fe_OH_2]	2	–
	n[Hercynite]	2	–
	n[Huntite]	2	–
	n[Hydromagnesite]	2	–
	n[Hydroxyapatite]	2	–
	n[Kstruvite]	2	–
	n[Magnesite]	2	–
	n[Mg3_PO4_2]	2	–
	n[MgHPO4_3H2O]	2	–

Table A6.4 (*continued*)

CATEGORY	NAME	DEFAULT VALUE	UNIT
	n[Mg_OH_2_act]	2	–
	n[Periclase]	2	–
	n[Portlandite]	2	–
	n[Siderite]	2	–
	n[Spinel]	2	–
	n[Struvite]	2	–
	n[Vivianite]	2	–
Arrhenius coefficient for temperature dependency	theta[CH4_g_]	1.024	–
	theta[CO2_g_]	1.024	–
	theta[H2S_g_]	1.024	–
	theta[H2_g_]	1.024	–
	theta[N2_g_]	1.024	–
	theta[NH3_g_]	1.024	–
	theta[O2_g_]	1.024	–
OPERATION			
Bubble size	Diam_gas	0.003	m
Target removal efficiency	Eff_target_NH3	0.9	–
Mass of seed material	M_seed[Aragonite]	0.0005	kg
	M_seed[Artinite]	0.0005	kg
	M_seed[Brucite]	0.0005	kg
	M_seed[Ca3_PO4_2_am1]	0.0005	kg
	M_seed[Ca3_PO4_2_am2]	0.0005	kg
	M_seed[Ca3_PO4_2_beta]	0.0005	kg
	M_seed[Ca4H_PO4_3_3H2O_]	0.0005	kg
	M_seed[CaHPO4_2H2O]	0.0005	kg
	M_seed[CaHPO4bis]	0.0005	kg
	M_seed[Calcite]	0.0005	kg
	M_seed[Diaspore]	0.0005	kg
	M_seed[Dolomite]	0.0005	kg
	M_seed[Dolomite_dis]	0.0005	kg
	M_seed[Fe_OH_2]	0.0005	kg
	M_seed[Hercynite]	0.0005	kg
	M_seed[Huntite]	0.0005	kg
	M_seed[Hydromagnesite]	0.0005	kg
	M_seed[Hydroxyapatite]	0.0005	kg
	M_seed[Kstruvite]	0.0005	kg
	M_seed[Magnesite]	0.0005	kg
	M_seed[Mg3_PO4_2]	0.0005	kg
	M_seed[MgHPO4_3H2O]	0.0005	kg
	M_seed[Mg_OH_2_act]	0.0005	kg
	M_seed[Periclase]	0.0005	kg
	M_seed[Portlandite]	0.0005	kg
	M_seed[Siderite]	0.0005	kg
	M_seed[Spinel]	0.0005	kg
	M_seed[Struvite]	0.0005	kg
	M_seed[Vivianite]	0.0005	kg
Initial gas temperature	T_gas_in	0	K
Stripping temperature	T_op	0	K
Surface area of seed material	a_seed	600	m^2/g
Stripping pH	pH_op	10.5	–
Rise velocity of bubbles	u	25.920	m/d
STOICHIOMETRY			
Reaction enthalphie of gas-liquid transfer	H_gas[CH4_g_]	−1700	–
	H_gas[CO2_g_]	−236.534	–
	H_gas[H2S_g_]	−3000	–
	H_gas[H2_g_]	−500	–
	H_gas[N2_g_]	−1300	–
	H_gas[NH3_g_]	−4200	–
	H_gas[O2_g_]	−1700	–
Enthalpy of heat for precipitation	delta_H[Aragonite]	−8	kJ/mol
	delta_H[Artinite]	−120.2565	kJ/mol
	delta_H[Brucite]	−114	kJ/mol
	delta_H[Ca3_PO4_2_am1]	−94	kJ/mol
	delta_H[Ca3_PO4_2_am2]	−87	kJ/mol
	delta_H[Ca3_PO4_2_beta]	54	kJ/mol
	delta_H[Ca4H_PO4_3_3H2O_]	−105	kJ/mol
	delta_H[CaHPO4_2H2O]	23	kJ/mol
	delta_H[CaHPO4bis]	31	kJ/mol
	delta_H[Calcite]	−8	kJ/mol
	delta_H[Diaspore]	−103.0519	kJ/mol
	delta_H[Dolomite]	−31.9	kJ/mol
	delta_H[Dolomite_dis]	−46.4	kJ/mol
	delta_H[Fe_OH_2]	−91.62	kJ/mol

(*continued on next page*)

Table A6.4 (*continued*)

CATEGORY	NAME	DEFAULT VALUE	UNIT
	delta_H[Hercynite]	−313.9199	kJ/mol
	delta_H[Huntite]	−107.7798	kJ/mol
	delta_H[Hydromagnesite]	−218.4466	kJ/mol
	delta_H[Hydroxyapatite]	0	kJ/mol
	delta_H[Kstruvite]	−83.21	kJ/mol
	delta_H[Magnesite]	20	kJ/mol
	delta_H[Mg3_PO4_2]	0	kJ/mol
	delta_H[MgHPO4_3H2O]	0	kJ/mol
	delta_H[Mg_OH_2_act]	0	kJ/mol
	delta_H[Periclase]	−151.23	kJ/mol
	delta_H[Portlandite]	−128.62	kJ/mol
	delta_H[Siderite]	−7.3	kJ/mol
	delta_H[Spinel]	−388.0122	kJ/mol
	delta_H[Struvite]	0	kJ/mol
	delta_H[Vivianite]	−5.06	kJ/mol
Dimensionless Henry coefficient at 298.15 K	kH[CH4_g_]	0.0342527	–
	kH[CO2_g_]	0.085632	–
	kH[H2S_g_]	2.44662	–
	kH[H2_g_]	0.019	–
	kH[N2_g_]	0.0159	–
	kH[NH3_g_]	1492	–
	kH[O2_g_]	0.0318	–

Table A6.5
Parameter categories, names, default values and units for the NRM-Scrub.

CATEGORY	NAME	DEFAULT VALUE	UNIT
DIMENSION			
Height	H_reactor	11.5	m
Safety factor on acid requirements	SF_Acid	1.5	–
Safety factor on reactor height	SF_Height	1.5	–
Volume	V_liq	81.3	m^3
KINETICS			
Liquid-gas diffusion coefficient at T_diff	D[CH4_g_]	3.771E-05	m^2/d
	D[CO2_g_]	0.000156	m^2/d
	D[H2S_g_]	2.2043E-05	m^2/d
	D[H2_g_]	0.000165	m^2/d
	D[N2_g_]	0.0001536	m^2/d
	D[NH3_g_]	0.000169	m^2/d
	D[O2_g_]	0.0001608	m^2/d
Temperature of diffusion coefficient	T_diff[CH4_g_]	298	K
	T_diff[CO2_g_]	293	K
	T_diff[H2S_g_]	298	K
	T_diff[H2_g_]	298	K
	T_diff[N2_g_]	293	K
	T_diff[NH3_g_]	298	K
	T_diff[O2_g_]	293	K
Liquid-solid transfer rate	k[NH4_2_SO4_s_]	0.001	$mol/m^2/d$
Arrhenius coefficient for temperature dependency	theta[CH4_g_]	1.024	–
	theta[CO2_g_]	1.024	–
	theta[H2S_g_]	1.024	–
	theta[H2_g_]	1.024	–
	theta[N2_g_]	1.024	–
	theta[NH3_g_]	1.024	–
	theta[O2_g_]	1.024	–
OPERATION			
Bubble size	Diam_gas	0.003	m
Target recovery efficiency	Eff_target_NH3	0.9	–
Mass of seed material	M_seed[NH4_2_SO4_s_]	0.0005	kg
Initial gas temperature	T_gas_in	0	K
Scrubbing temperature	T_op	0	K
Surface area of seed material	a_seed	600	m^2/g
Rise velocity of bubbles	u	25,920	m/d
STOICHIOMETRY			
Reaction enthalphie of gas-liquid transfer	H_gas[CH4_g_]	−1700	–
	H_gas[CO2_g_]	−236.534	–
	H_gas[H2S_g_]	−3000	–
	H_gas[H2_g_]	−500	–
	H_gas[N2_g_]	−1300	–

Table A6.5 (*continued*)

CATEGORY	NAME	DEFAULT VALUE	UNIT
	H_gas[NH3_g_]	−4200	–
	H_gas[O2_g_]	−1700	–
Enthalpy of heat for precipitation	delta_H[NH4_2_SO4_s_]	0	kJ/mol
Dimensionless Henry coefficient at 298.15 K	kH[CH4_g_]	0.0342527	–
	kH[CO2_g_]	0.085632	–
	kH[H2S_g_]	2.44662	–
	kH[H2_g_]	0.019	–
	kH[N2_g_]	0.0159	–
	kH[NH3_g_]	1492	–
	kH[O2_g_]	0.0318	–

Table A6.6
Input sludge characteristics, reactor design, initial values, and operating conditions for the anaerobic digester at Holmen Paper Madrid (Spain). Data used for validation of the nutrient recovery model for the anaerobic digester (NRM-AD). COD = chemical oxygen demand. COD input fractionation was conducted following the procedure proposed by Grau et al. (2007). For state variable description: see Appendix 5. COD = chemical oxygen demand; HRT = hydraulic residence time; Q_liq = liquid flow rate; T_liq = liquid temperature; T_operational = operational temperature; V_liq = liquid volume.

INPUT FLOW				REACTOR (DESIGN + INITIAL VALUES + OPERATION)			
S_aa (kg COD m^{-3})	0	S_Acetate (mol m^{-3})	2.85	S_aa (kg COD m^{-3})	0.0172	S_Acetate (mol m^{-3})	0.0347
S_fa (kg COD m^{-3})	0.217	S_Al (mol m^{-3})	Unknown	S_fa (kg COD m^{-3})	0.0113	S_Al (mol m^{-3})	unknown
S_inert (kg COD m^{-3})	0.170	S_Butyrate (mol m^{-3})	1.14	S_inert (kg COD m^{-3})	0.480	S_Butyrate (mol m^{-3})	0.322
S_su (kg COD m^{-3})	1.05	S_C_4_ (mol m^{-3})	12.8	S_su (g COD m^{-3})	0.569	S_C_4_ (mol m^{-3})	60.1
X_aa (kg COD m^{-3})	0	S_C_min4_ (mol m^{-3})	0	X_aa (kg COD m^{-3})	0.112	S_C_min4_ (mol m^{-3})	1.23
X_ac (kg COD m^{-3})	0	S_Ca (mol m^{-3})	2.85	X_ac (kg COD m^{-3})	0.0178	S_Ca (mol m^{-3})	7.10
X_c4 (kg COD m^{-3})	0	S_Cl (mol m^{-3})	0.0357	X_c4 (kg COD m^{-3})	1.33	S_Cl (mol m^{-3})	0.0357
X_c (kg COD m^{-3})	0	S_Fe (mol m^{-3})	Unknown	X_c (kg COD m^{-3})	31.3	S_Fe (mol m^{-3})	unknown
X_ch (kg COD m^{-3})	0.187	S_H_0_ (mol m^{-3})	0	X_ch (kg COD m^{-3})	4.03	S_H_0_ (mol m^{-3})	0.0344
X_fa (kg COD m^{-3})	0	S_K (mol m^{-3})	0.0350	X_fa (kg COD m^{-3})	2.30	S_K (mol m^{-3})	6.39
X_h2 (kg COD m^{-3})	0	S_Mg (mol m^{-3})	2.41	X_h2 (kg COD m^{-3})	0.127	S_Mg (mol m^{-3})	2.69
X_inert (kg COD m^{-3})	0.0936	S_N_0_ (mol m^{-3})	0	X_inert (kg COD m^{-3})	13.8	S_N_0_ (mol m^{-3})	0.000256
X_li (kg COD m^{-3})	0.140	S_N_5_ (mol m^{-3})	0	X_li (kg COD m^{-3})	6.98	S_N_5_ (mol m^{-3})	0.00100
X_pr (kg COD m^{-3})	0	S_N_min3_ (mol m^{-3})	7.36	X_pr (kg COD m^{-3})	0.998	S_N_min3_ (mol m^{-3})	4.57
X_pro (kg COD m^{-3})	0	S_Na (mol m^{-3})	0.0357	X_pro (kg COD m^{-3})	0.0178	S_Na (mol m^{-3})	0.0357
X_srb_ac (kg COD m^{-3})	0	S_O_0_ (mol m^{-3})	3.98	X_srb_ac (kg COD m^{-3})	0.469	S_O_0_ (mol m^{-3})	0
X_srb_bu (kg COD m^{-3})	0	S_P (mol m^{-3})	0.309	X_srb_bu (kg COD m^{-3})	4.99	S_P (mol m^{-3})	0.245
X_srb_h (kg COD m^{-3})	0	S_Propionate (mol m^{-3})	1.63	X_srb_h (kg COD m^{-3})	43.6	S_Propionate (mol m^{-3})	0.0451
X_srb_pro (kg COD m^{-3})	0	S_S_6_ (mol m^{-3})	5.42	X_srb_pro (kg COD m^{-3})	16.6	S_S_6_ (mol m^{-3})	1.16
X_su (kg COD m^{-3})	0	S_S_min2_ (mol m^{-3})	0.0106	X_su (kg COD m^{-3})	7.20	S_S_min2_ (mol m^{-3})	6.35
		S_Valerate (mol m^{-3})	0.878			S_Valerate (mol m^{-3})	0.402
Q_liq (m^3 d^{-1})	15.0	T_liq (K)	28.9	Fraction of solids in effluent	0.002	V_liq (m^3)	2.80
pH (–)	6.66			T_operational (K)	302.15	HRT (h)	4.48

Table A6.7
Input digestate characteristics and operating conditions used for the lab-scale experiments on struvite precipitation. Data used for validation of the nutrient recovery model for the precipitation/crystallization unit (NRM-Prec). For state variable description: see Appendix 5.

Variable	Digestate 1	Digestate 2	Variable	Digestate 1	Digestate 2
S_Acetate[a] (mol m^{-3})	0.100	0.100	S_Mg (mol m^{-3})	26.1	26.4
S_Al (mol m^{-3})	0.0100	1.00	S_N_5_ (mol m^{-3})	98.0	127
S_Butyrate[a] (mol m^{-3})	0.100	0.100	S_N_min3_ (mol m^{-3})	362	346
S_C_4_ (mol m^{-3})	10.0	10.0	S_Na (mol m^{-3})	100	127
S_C_min4_[a] (mmol m^{-3})	0.100	0.100	S_P (mol m^{-3})	38.8	45.5
S_Ca (mol m^{-3})	42.1	57.1	S_Propionate[a] (mol m^{-3})	0.0100	0.0100
S_Cl (mol m^{-3})	73.3	25.0	S_S_6_ (mol m^{-3})	40.0	20.0
S_Fe (mol m^{-3})	170	0.100	S_S_min2_ (mol m^{-3})	0.100	0.100
S_K (mol m^{-3})	104	122	S_Valerate[a] (mol m^{-3})	0.100	0.100
pH (–)	8.43	7.83	Temperature (K)	293.15	293.15

[a] Estimated from the soluble chemical oxygen demand (COD) content following the procedure described in Cesur and Albertson (2005).

Table A6.8
Input flow composition and operating conditions used for validation of the treatment train: NRM-Chem / NRM-Strip / NRM-Scrub. Operational data were obtained from a technical inquiry at company X. Chem = chemical dosing unit; Strip = stripper; Scrub = scrubber. For state variable description: see Appendix 5. DOM = dissolved organic matter; P_gas = gas pressure; Q_gas = gas flow rate; Q_liq = liquid flow rate.

Input flow (after NaOH-dose)[a]		Operation NRM-Strip		Operation NRM-Scrub	
S_Al (mol m^{-3})	20	Q_liq_in (m^3 d^{-1})	2004	H_2SO_4-dose (m^3 d^{-1})	20.16
S_C_4_ (mol m^{-3})	80	Q_gas_in (m^3 d^{-1})	1,560,000	Q_gas_in (m^3 d^{-1})	=Output NRM-Strip
S_C_min4_ (mol m^{-3})	0.0080	Column height (m)	11.5	Column height (m)	11.5
S_Ca (mol m^{-3})	60	Temperature (K)	328.15	Temperature (K)	=Output NRM-Strip
S_Cl (mol m^{-3})	80	pH (−)	10.3	pH acid (−)	1.3
S_DOM (mol m^{-3})	10	Vol_liq (m^3)	81.3	Vol_liq (m^3)	20.16
S_Fe (mol m^{-3})	1.2	P_gas_in (atm)	2.42	P_gas_in (atm)	=Output NRM-Strip
S_H_0_ (mol m^{-3})	0.0010				
S_K (mol m^{-3})	33				
S_Mg (mol m^{-3})	43				
S_N_0_ (mol m^{-3})	0.10				
S_N_5_ (mol m^{-3})	59				
S_N_min3_ (mol m^{-3})	199				
S_Na (mol m^{-3})	102				
S_O_0_ (mol m^{-3})	0				
S_P (mol m^{-3})	33				
S_S_6_ (mol m^{-3})	40				
S_S_min2_ (mol m^{-3})	0				
Temperature (K)	293.15				

[a] Dose of 4.1 kg NaOH m^{-3} as specified by company X.

APPENDIX 7

Model verification/validation examples

Table A7.1
Model verification/validation against prior knowledge: some dynamic simulation tests and effects. All results were found to be realistic. For state variable description: see Appendix 5. AD = anaerobic digestion; Prec = precipitation/crystallization; Scrub = scrubber; SRB = sulfate reducing bacteria; Strip = stripper; VFA = volatile fatty acids.

NRM-AD	NRM-Prec	NRM-Strip	NRM-Scrub
S_C_4_in (alkalinity) ↓ ⇒ (delayed) pH ↓, S_C_4_out ↓, VFA ↑, biogas production ↓	S_P_in ↓ ⇒ struvite precipitation ↓	Reactor height ↓ ⇒ no influence on performance	Reactor height ↓ ⇒ no influence on performance
pH ↑ ⇒ CO_3 precipitation ↑ pH ↓ ⇒ CO_2 stripping ↑ (not biologically mediated)	S_Mg_in ↓ ⇒ pH ↓, S_P_out ↑, phosphorus recovery efficiency ↓	Temperature ↑ ⇒ S_N_min3_out ↓, p_NH_3_out (gas phase partial pressure) ↑, NH_3 recovery efficiency ↑, effluent pH ↓	p_NH_3_in (gas phase partial pressure) ↑ ⇒ fertilizer alkalinity ↓ (NH_2COO^- formation), N % fertilizer ↑
Modification: pH-inhibition level SRBs = 5, other bacteria = 6 ⇒ H_2S production ↑ if pH < 6	S_P_in ↑ ⇒ phosphorus precipitation ↑ (supersaturation ↑)	Q_liq_in ↑ ⇒ residence time ↓, $CaCO_3$ precipitation ↓, scaling potential ↓	
Temperature ↑ ⇒ biogas production ↑	pH ↓ (input nutrient contents ↓) ⇒ fertilizer density ↓ and molecular weight ↓		

NRM-AD:

- Reducing the input alkalinity to the digester results in a (delayed) pH decrease (less carbonate buffer) because of volatile fatty acid accumulation. Methanogenic bacteria are very sensitive to pH decreases (Vanrolleghem and Lee, 2003). Hence, a reduction of the biogas production is observed. Obviously, the output alkalinity decreases as well.
- Increasing the input pH results in an increased formation of carbonate precipitates in the digester, whereas decreasing the pH stimulates the stripping of CO_2 (see carbonate equilibria as function of pH; Zumdahl, 2005).
- Setting the pH inhibition level of sulfate reducing bacteria (SRBs) at 5, but for the other bacteria at 6, leads to increased H_2S production if the pH in the digester becomes lower than 6. Hence, the other bacteria are inhibited, whereas the SRBs still work at pH values lower than 6.
- Increasing the temperature in the digester stimulates the production of biogas. The increased temperatures facilitate faster reaction rates, and thus more biogas can be produced from the organic matter in an equal amount of time (Tchobanoglous et al., 2003).

NRM-Prec

- Decreasing the P concentration in the input waste flow reduces the potential for struvite ($MgNH_4PO_4$:$6H_2O$) precipitation.
- Decreasing the Mg concentration in the input waste flow decreases the pH in the reactor, which is obvious as a Mg source is

often added to induce P precipitation (Le Corre et al., 2007). Hence, less Mg-P precipitates are formed, the effluent P concentration increases, while the P recovery efficiency decreases.
- Increasing the P concentration in the input waste flow at a particular (neutral to high) pH increases the amount of P precipitates formed (precipitation is driven by supersaturation).
- Decreasing the pH by decreasing the concentration of nutrients, such as Mg and Ca, in the input waste flow reduces the resulting fertilizer density and molecular weight (fewer and less heavy P precipitates).

NRM-Strip

- Decreasing the reactor height has no influence on the N recovery efficiency because the NH_3-NH_4^+ equilibrium between a gas bubble and the surrounding water is reached in a very small time interval (Gujer, 2008).
- Increasing the temperature increases the NH_3 stripping performance (Wang et al., 2007). Hence, lower effluent NH_4-N concentrations and higher NH_3 partial pressures in the gas phase are found. The more NH_3 is stripped out, the lower the effluent pH.
- Increasing the liquid flow rate, reduces the residence time in the system. As such, the (slow) formation of $CaCO_3$ precipitates in the reactor is reduced, and thus also the scaling potential.

NRM-Scrub

- Decreasing the reactor height has no influence on the N recovery efficiency because the NH_3-NH_4^+ equilibrium between a gas bubble and the surrounding water is reached in a very small time interval (Gujer, 2008).
- Increasing the partial pressure of NH_3 in the incoming gas phase (coming from the stripper) decreases the fertilizer alkalinity (through NH_2COO^- formation) and increases the N concentration in the resulting ammonium sulfate solution. Hence, more N can be recovered in an equal amount of time.

References

AIC, 2014. Heat Exchange Concepts and Heat Exchangers [Internet]. AIC Alliance, Oakville, Ontario, Canada [cited February 10 2014]. http://www.aicheatexchangers.com/heat_exchanger_design_theory.html.

Ali, M.I., Schneider, P.A., 2008. An approach of estimating struvite growth kinetic incorporating thermodynamic and solution chemistry, kinetic and process description. Chem. Eng. Sci. 63 (13), 3514–3525.

Allison, J.D., Brown, D.S., Novo Gradac, K.J., 1991. MINTEQA2/PRODEFA2. A Geochemical Assessment Model for Environmental Systems. Version 3.0. EPA/600/3–91/021. USEPA, Washington DC, USA.

Al-Zuhair, S., Al-Naas, M.H., Al-Hassani, H.A., 2008. Sulfate inhibition effect on sulfate reducing bacteria. J. Biochem. Tech. 1 (2), 39–44.

Argaman, Y.A., 1971. Pilot-plant studies of flocculation. J. Awwa 63 (12), 775–777.

Arogo, J., Zhang, R.H., Riskowski, G.L., Christianson, L.L., Day, D.L., 1999. Mass transfer coefficient of ammonia in liquid swine manure and aqueous solutions. J. Agric. Eng. Res. 73, 77–86.

Astals, S., Esteban-Gutierrez, M., Fernandez-Arevalo, T., Aymerich, E., Garcia-Heras, J.L., Mata-Ahiarez, J., 2013. Anaerobic digestion of seven different sewage sludges: a biodegradability and modelling study. Water Res. 47 (16), 6033–6043.

Bachis, J., Maruejouls, B., Tik, S., Vanrolleghem, P., 2015. Modelling and characterization of primary settlers in view of whole plant and resource recovery modelling. Water Sci. Technol. 72 (12), 2251–2261.

Batstone, D.J., Keller, J., Angelidaki, I., Kalyuzhnyi, S.V., Pavlostathis, S.G., Rozzi, A., Sanders, W.T.M., Siegrist, H., Vavilin, V.A., 2002. The IWA anaerobic digestion model No 1 (ADM1). Water Sci. Technol. 45 (10), 65–73.

Batstone, D.J., Amerlinck, Y., Ekama, G., Goel, R., Grau, P., Johnson, B., Kaya, I., Steyer, J.-P., Tait, S., Takacs, I., Vanrolleghem, P.A., Brouckaert, C.J., Volcke, E., 2012. Towards a generalized physicochemical framework. Water Sci. Technol. 66 (6), 1147–1161.

Belcu, M., Turtoi, D., 1996. Simulation of the fluidized-bed crystallizers: 1. Influence of parameters. Cryst. Res. Technol. 31 (8), 1015–1023.

Bénézeth, P., Palmer, D.A., Wesolowski, D.J., 2008. Dissolution/precipitation kinetics of boehmite and gibbsite: application of a pH-relaxation technique to study near-equilibrium rates. Geochim. Cosmochim. Acta 72, 2429–2453.

Bhuiyan, M.I.H., Mavinic, D.S., Beckie, R.D., 2007. A solubility and thermodynamic study of struvite. Environ. Technol. 28 (9), 1015–1026.

Bhuiyan, M.I.H., Mavinic, D.S., Beckie, R.D., 2008. Nucleation and growth kinetics of struvite in a fluidized bed reactor. J. Cryst. Growth 310 (6), 1187–1194.

Bouropoulos, N.C., Koutsoukos, P.G., 2000. Spontaneous precipitation of struvite from aqueous solutions. J. Cryst. Growth 213, 381–388.

Brouckaert, C.J., Ikumi, D.S., Ekama, G.A., 2010. A Three Phase Anaerobic Digestion Model. Proceedings 12th IWA Anaerobic Digestion Conference (AD12), Guadalajara, Mexico.

Brown, P.N., Byrne, G.D., Hindmarsh, A.C., 1989. VODE, A variable-coefficient ODE solver. SIAM J. Sci. Stat. Comput. 10 (5), 1038–1051.

Camp, T.R., Stein, P.C., 1943. Velocity gradients and hydraulic work in fluid motion. J. Boston Soc. Civ. Eng. 30, 203–221.

Campos, J.C., Moura, D., Costa, A.P., Yokoyama, L., da Fonseca Araujo, F.V., Cammarota, M.C., Cardillo, L., 2013. Evaluation of pH, alkalinity and temperature during air stripping process for ammonia removal from landfill leachate. J. Environ. Sci. Heal. A. 48 (9), 1105–1113.

Cesur, D., Albertson, M.L., 2005. Modification of Anaerobic Digestion Model No. 1 for Accumulation and Biomass Recycling (Proceedings AGU Hydrology Days, Denver, CO, USA).

Chapra, S.C., 2008. Surface Water-quality Modeling. Waveland Press Inc., Long Grove, IL, USA.

Charlton, S.R., Parkhurst, D.L., 2011. Modules based on the geochemical model PHREEQC for use in scripting and programming languages. Comput. Geosci. 37 (10), 1653–1663.

Chauhan, C.K., Joshi, M.J., 2014. Growth and characterization of struvite-Na crystals. J. Cryst. Growth 401, 221–226.

Chauhan, C.K., Vyas, P.M., Joshi, M.J., 2011. Growth and characterization of struvite-K crystals. Cryst. Res. Technol. 46 (2), 187–194.

Claeys, F.H.A., Fritzson, P., Vanrolleghem, P.A., 2006. Using Modelica Models for Complex Virtual Experimentation with the Tornado Kernel. Proceedings The Modelica Association, Vienna, Austria.

Claeys, F.H.A., 2008. A Generic Software Framework for Modelling and Virtual Experimentation with Complex Biological Systems. PhD Thesis. Department of Applied Mathematics, Biometrics and Process Control, Ghent University, Belgium.

Collivignarelli, C., Bertanza, G., Baldi, M., Avezzu, F., 1998. Ammonia stripping from MSW landfill leachate in bubble reactors: process modeling and optimization. Waste Manage. Res. 16 (5), 455–466.

Crittenden, J.C., Trussell, R.R., Hand, D.W., Howe, K.J., Tchobanoglous, G., 2012. MWH's Water Treatment: Principles and Design. John Wiley & Sons Inc., New York, NY, USA.

Cullen, N., Baur, R., Schauer, P., 2013. Three years of operation of North America's first nutrient recovery facility. Water Sci. Technol. 68 (4), 763–768.

De Corte, J., 2012. Removal of Phosphorus from Manure and Digestate Derivatives through Struvite Precipitation. MSc Thesis. Ghent University, Ghent, Belgium.

Dochain, D., Vanrolleghem, P.A., 2001. Dynamic Modelling and Estimation in Wastewater Treatment Processes. IWA Publishing, London, UK.

Elmqvist, H., Bachmann, B., Boudaud, F., Broenink, J., Bruck, D., Ernst, T., Franke, R., Fritzson, P., Jeandel, A., Grozman, P., 1999. Modelica – a Unified Object-oriented Language for Physical Systems Modeling. Tutorial and rationale. The Modelica Association, Lund, Sweden.

Flores-Alsina, X., Mbamba, C.K., Solon, K., Vrecko, D., Tait, S., Batstone, D.J., Jeppsson, U., Gernaey, K.V., 2015. A plant-wide aqueous phase chemistry module describing variations and ion speciation/pairing in wastewater treatment process models. Water Res. 85, 255–265.

Flores-Alsina, X., Solon, K., Mbamba, C.K., Tait, S., Gernaey, K.V., Jeppsson, U., Batstone, D.J., 2016. Modelling phosphorus (P), sulfur (S) and iron (Fe) interactions for dynamic simulations of anaerobic digestion processes. Water Res. 95, 370–382.

Galbraith, S.C., Schneider, P.A., Flood, A.E., 2014. Model-driven experimental evaluation of struvite nucleation, growth and aggregation kinetics. Water Res. 56, 122–132.

Gernaey, K.V., van Loosdrecht, M.C.M., Henze, M., Lind, M., Jorgensen, S.B., 2004. Activated sludge wastewater treatment plant modelling and simulation: state of the art. Environ. Model. Softw. 19 (9), 763–783.

Grau, P., de Gracia, M., Vanrolleghem, P.A., Ayesa, E., 2007. A new plant-wide modelling methodology for WWTPs. Water Res. 41, 4357–4372.

Greenberg, J., Tomson, M., 1992. Precipitation and dissolution kinetics and equilibria of aqueous ferrous carbonate vs temperature. Appl. Geochem 7, 185–190.

Gujer, W., 2008. Systems Analysis for Water Technology. Springer Verlag Berlin Heidelberg, Berlin, Germany.

Hafner, S.D., Bisogni, J.J., 2009. Modeling of ammonia speciation in anaerobic digesters. Water Res. 43 (17), 4105–4114.

Harned, H.S., Hamer, W.J., 1933. The ionization constant of water. J. Am. Chem. Soc. 51, 2194.

Harrison, M.L., Johns, M.R., White, E.T., Mehta, C.M., 2011. Growth rate kinetics for struvite crystallisation. Chem. Eng. Trans. 25, 309–314.

Hauduc, H., Takács, I., Smith, S., Szabo, A., Murthy, S., Daigger, G.T., Sperandio, M., 2015. A dynamic physicochemical model for chemical phosphorus removal. Water Res. 73, 157–170.

Hendricks, D., 2010. Fundamentals of Water Treatment Unit Processes. CRC Press, Boca Raton, Florida, USA.
Henze, M., Gujer, W., Mino, T., van Loosdrecht, M.C.M., 2000. Activated Sludge Models ASM1, ASM2, ASM2d and ASM3. IWA Scientific and Technical Report No 9. IWA Publishing, London, UK.
Higbie, R., 1935. The rate of absorption of a pure gas into a still liquid during short periods of exposure. Am. Inst. Chem. Eng. 31, 365–388.
Hillel, D., 2008. Soil in the Environment: Crucible of Terrestrial Life. Academia Press, New York.
Huchzermeier, M.P., Wendong, T., 2012. Overcoming challenges to struvite recovery from anaerobically digested dairy manure. Water Environ. Res. 84 (1), 34–41.
Ikumi, D.S., 2011. The Development of a Three Phase Plant-wide Mathematical Model for Sewage Treatment. PhD Thesis. Water Research Group, University of Cape Town, South Africa.
Inskeep, W.P., Silvertooth, J.C., 1988. Kinetics of hydroxyapatite precipitation at pH 7.4 to 8.4. Geochim. Cosmochim. Acta 52, 1883–1893.
Johnson, M.L., 1990. Ferrous Carbonate Precipitation Kinetics – a Temperature Ramped Approach. PhD Thesis. Rice University, Houston, Texas, USA.
Knobel, A.N., Lewis, A.E., 2002. A mathematical model of a high sulphate wastewater anaerobic treatment system. Water Res. 36 (1), 257–265.
Koptev, 1966. The solubility of ammonium sulphate and saturator washing conditions. Coke Chem. Works 2, 32–33.
Koutsoukos, P., Amjad, Z., Tomson, M.B., Nancollas, G.H., 1980. Crystallization of calcium phosphates- constant composition study. J. Am. Chem. Soc. 102 (5), 1553–1557.
Kozic, A., Hutnik, N., Matynia, A., Gluzinska, W.J., Piotrowski, G.K., 2011. Recovery of phosphate (V) ions from liquid waste solutions containing organic impurities. Chemik 65 (7), 675–686.
Le Corre, K.S., Valsami-Jones, E., Hobbs, P., Parsons, S.A., 2007. Impact of reactor operation on success of struvite precipitation from synthetic liquors. Environ. Technol. 28 (11), 1245–1256.
Li, Z., Ren, X., Zuo, J., Liu, Y., Duan, E., Yang, J., Chen, P., Wang, Y., 2012. Struvite precipitation for ammonia nitrogen removal in 7-aminocephalosporanic acid wastewater. Molecules 17, 2126–2139.
Lin, A.Y., 2012. Precipitation of Phosphate Minerals from Effluent of Anaerobically Digested Swine Manure. PhD Thesis. University of South Florida, Tampa, Florida, USA.
Lizarralde, I., Brouckaert, C.J., Ekama, G.A., Grau, P., 2013. Incorporating water chemistry into the steady-state models for wastewater treatment processes: case study anaerobic reactor in the SANI process. In: Proceedings, 13th World Congress on Anaerobic Digestion (AD-13): Recovering (bio) Resources for the World, Santiago de Compostela, Spain, June 25–28 2013.
Lizarralde, I., de Gracia, M., Sancho, L., Ayesa, E., Grau, P., 2010. New Mathematical Model for the Treatment of Wastewaters Containing High Sulphate Concentration. Proceedings 1st Spain National Young Water Professionals Conference, Barcelona, Spain.
Lizarralde, I., Fernández-Arévalo, T., Brouckaert, C., Vanrolleghem, P.A., Ikumi, D.S., Ekama, G.A., Ayesa, E., Grau, P., 2015. A new general methodology for incorporating physico-chemical transformations into multi-phase wastewater treatment process models. Water Res. 74, 239–256.
Martin, J.H., 2003. An Assessment of the Performance of the Colorado Pork LLC Anaerobic Digestion and Biogas Utilization System (Report submitted to the State of Colorado Governor's Office of Energy Management and Conservation, Denver, CO, USA).
Mackay, D., Yeun, A.T.K., 1983. Mass transfer coefficients correlations for volatilization of organic solutes from water. Environ. Sci. Technol. 17, 211–233.
Manuzon, R.B., Zhao, L.Y., Keener, H.M., Darr, M.J., 2007. A prototype acid spray scrubber for absorbing ammonia emissions from exhaust fans of animal buildings. Trans. ASABE 50 (4), 1395–1407.
Mattocks, R., Swanson, G., Torres, M., 2002. Monitoring the Performance of a Commercial Housed Swine Operation Biogas System (Final report submitted to the State of Colorado Governor's Office of Energy Management and Conservation, Denver, CO, USA).
Mbamba, C.K., Flores-Alsina, X., Batstone, D.J., Tait, S., 2016. Validation of a plant-wide phosphorus modelling approach with minerals precipitation in a full-scale WWTP. Water Res. 100, 169–183.
Mehta, C.M., Batstone, D.J., 2013. Nucleation and growth kinetics of struvite crystallization. Water Res. 47, 2890–2900.
Melse, R.W., Ogink, N.W.M., 2005. Air scrubbing techniques for ammonia and odor reduction at livestock operations: review of on-farm research in the Netherlands. T. Asae. 48 (6), 2303–2313.
Morel, F.M.M., Herring, J.G., 1993. Principles and Applications of Aquatic Chemistry. John Wiley and Sons, New York.
Morse, J.W., Arvidson, R.S., 2002. The dissolution kinetics of major sedimentary carbonate minerals. Earth-Sci. Rev. 58 (1–2), 51–84.
Müller, M., Parkhurst, D.L., Charlton, S.R., 2011. Programming PHREEQC Calculations with C++ and Python a Comparative Study. Proceedings MODFLOW and More 2011: Integrated Hydrologic Modeling, Golden, Colorado.
Munz, C., Roberts, P.V., 1989. Gas and liquid phase mass transfer resistances of organic compounds during mechanical surface aeration. Water Res. 23 (5), 589–601.
Musvoto, E.V., Wentzel, M.C., Loewenthal, R.E., Ekama, G.A., 1997. Kinetic based model for weak acid/base systems. Water SA 23 (4), 311–322.
Musvoto, E.V., Wentzel, M.C., Loewenthal, R.E., Ekama, G.A., 2000. Integrated chemical-physical processes modelling - I. Development of a kinetic-based model for mixed weak acid/base systems. Water Res. 34 (6), 1857–1867.
Nielsen, A.E., 1984. Electrolyte crystal growth mechanisms. J. Cryst. Growth 67, 289–310.
NIST, 2001. Standard Reference Database 46. National Institute of Standards and Technology, Gaithersburg, MD, USA.
Nopens, I., Torfs, E., Ducoste, J., Vanrolleghem, P.A., Gernaey, K.V., 2014. Population balance models: a useful complementary modelling framework for future WWTP modelling. Water Sci. Technol. 71 (2), 159–167.
Oh, S.T., Martin, A.D., 2010. Long chain fatty acids degradation in anaerobic digester: thermodynamic equilibrium consideration. Process Biochem. 45, 335–345.
Ohlinger, K.N., Young, T.M., Schroeder, E.D., 1998. Predicting struvite formation in digestion. Water Res. 32 (12), 3607–3614.
Oyekola, O.O., van Hille, R.P., Harrison, S.T.L., 2007. Effect of sulphate concentration on the community structure and activity of sulphate reducing bacteria. Adv. Mat. Res. 20–21, 513–515.
Parker, D.S., Kaufmann, W.J., Jenkins, D., 1972. Floc breakup in turbulent flocculation processes. J. Sanit. Eng. Dic. 98, 79–99.
Parkhurst, D.L., Appelo, C.A.J., 2013. Chapter A43: Description of Input and Examples for PHREEQC Version 3 – a Computer Program for Speciation, Batch-reaction, One-dimensional Transport, and Inverse Geochemical Calculations (U.S. Geological Survey Techniques and Methods, USA).
Pauss, A., Andre, G., Perrier, M., Guiot, S.R., 1990. Liquid-to-gas mass transfer in anaerobic processes: inevitable transfer limitation of methane and hydrogen in the biomethanisation process. Appl. Environ. Microbiol. 56, 1636–1644.
Pérez, D.P., 2002. Performance of an Ammonia Stripper for Wastewater Treatment (Ammonosulf Method). Master Thesis. Department of Chemical Engineering and Technology, Helsinki University of Technology, Finland.
Perez, M., Dumont, M., Acevedo-Reyes, D., 2008. Implementation of classical nucleation and growth theories for precipitation. Acta Mater 56 (9), 1219–2132.
Powers, S.E., Collins, A.G., Edzwald, J.K., Dietrich, J.M., 1987. Modeling an aerated bubble ammonia stripping process. J. Water Pollut. Control. Fed. 59 (2), 92–100.
Press, W.H., Flannery, B.P., Teukolsky, S.A., Vetterling, W.T., 1992. 'Runge-Kutta method' and 'adaptive step size control for runge-kutta'. In: Numerical Recipes in FORTRAN: the Art of Scientific Computing, second ed. Cambridge University Press, Cambridge, UK.
Rahaman, M.S., Mavinic, D.S., Meikleham, A., Ellis, N., 2014. Modelling phosphorus removal and recovery from anaerobic digester supernatants through struvite crystallization in a fluidized bed reactor. Water Res. 51, 1–10.
Reiter, S.L.W., Piccot, S.S.D., 2004. Environmental Technology Verification Report for the Paques THIOPAQ Gas Purification Technology. Report SRI/USEPA-GHG-VR-32. USEPA. http://www.epa.gov/etv/pubs/sriusepaghgvr32.pdf.
Rieger, L., Gillot, S., Langergraber, G., Ohtsuki, T., Shaw, A., Takács, I., Winkler, S., 2012. Guidelines for Using Activated Sludge Models. IWA Scientific and Technical Report No.22. IWA Publishing, London, UK.
Rosen, C., Jeppsson, U., 2006. Aspects on ADM1 Implementation within the BSM2 Framework. Technical report. Department of Industrial Electrical Engineering and Automation, Lund University, Lund, Sweden.
Sander, R., 1999. Compilation of Henry's Law Constants for Inorganic and Organic Species of Potential Importance in Environmental Chemistry. Report. Air Chemistry Department, Max-Planck Institute of Chemistry, Mainz, USA.
Schneider, P.A., Wallace, J.W., Tickle, J.C., 2013. Modelling and dynamic simulation of struvite precipitation from source-separated urine. Water Sci. Technol. 67 (12), 2724–2732.
Schwarzenbach, R.P., Gschwend, P.M., Imboden, D.M., 1993. Environmental Organic Chemistry. Wiley-Interscience, New York City, New York, USA.
Solon, K., Flores-Alsina, X., Kazadi Mbamba, C., Volcke, E.I.P., Tait, S., Batstone, D.J., Gernaey, K.V., Jeppsson, U., 2015. Effects of ionic strength and ion pairing on (plant-wide) modelling of anaerobic digestion processes. Water Res. 70, 235–245.
Sotemann, S.W., Musvoto, E.V., Wentzel, M.C., Ekama, G.A., 2005. Integrated biological, chemical and physical processes kinetic modelling Part 1-Anoxic-aerobic C and N removal in the activated sludge system. Water S.A 31 (4), 529–544.
Sotemann, S.W., Wentzel, M.C., Ekama, G.A., 2006. Mass balance based plant-wide wastewater treatment plant models - Part 4: aerobic digestion of primary and waste activated sludges. Water SA 32 (3), 297–306.
Stumm, W., Morgan, J.J., 1996. Aquatic Chemistry: Chemical Equilibria and Rates in Natural Waters. John Wiley & Sons Inc., New York.
Takács, I., Murthy, S., Smith, S., McGrath, M., 2006. Chemical phosphorus removal to extremely low levels: experience of two plants in the Washington, DC area. Water Sci. Technol. 53 (12), 21–28.
Tanigawa, H., Sakasegawa, H., Payzant, E.A., Zinkle, S.J., Klueh, R.L., 2003. X-ray Diffraction Analysis on Precipitates of 11J Irradiated RAGS. Research report. Kyoto University, Japan. http://web.ornl.gov/sci/physical_sciences_directorate/mst/fusionreactor/pdf/dec2003/3_FERRITIC/pg%2037-40.PDF.
Tavare, N.S., 1995. Industrial Crystallization. Plenum Press, New York City, New York, USA.
Tchobanoglous, G., Burton, F., Stensel, H.D., 2003. Metcalf & Eddy Wastewater Engineering: Treatment and Reuse. McGraw Hill, New York.
Till, A.R., 2010. Sulphur and Sustainable Agriculture. International Fertilizer Association (IFA), Paris, France.
Tourlousse, D., Ahmad, F., 2007. Design of an Experimental Unit for the Determination of Oxygen Gas-liquid Volumetric Mass Transfer Coefficients Using the Dynamic Re-oxygenation Method. Research report. Michigan State University, East Lansing, MI, USA. http://www.egr.msu.edu/~hashsham/courses/ene806/docs/Oxygen%20Uptake%20Rate.pdf.

UCT, 2007. An Extended Investigation into the Mechanism and Kinetics of Bacterial Sulphate Reduction. WRC Report No. 1251/1/07. University of Cape Town, Cape Town, South Africa.
USEPA, 1999. MINTEQA2/PRODEFA2. A Geochemical Assessment Model for Environmental Systems. User Manual Supplement for Version 4.0. EPA/600/3-91/021. USEPA, Washington.
Vaneeckhaute, C., Janda, J., Vanrolleghem, P.A., Tack, F.M.G., Meers, E., 2016. Phosphorus use efficiency in bio-based fertilizers: a bio-availability and fractionation study. Pedosphere 26 (3), 310–325.
Vaneeckhaute, C., Lebuf, V., Michels, E., Belia, E., Tack, F.M.G., Vanrolleghem, P.A., Meers, E., 2017a. Nutrient recovery from digestate: systematic technology review and product classification. Waste Biomass Valor (in press).
Vaneeckhaute, C., Meers, E., Michels, E., Buysse, J., Tack, F.M.G., 2013. Ecological and economic benefits of the application of biobased mineral fertilizers in modern agriculture. Biomass Bioenerg. 49, 239–248.
Vaneeckhaute, C., Meers, E., Michels, E., Christiaens, P., Tack, F.M.G., 2012. Fate of macronutrients in water treatment of digestate using vibrating reversed osmosis. Water Air Soil Poll. 223 (4), 1593–1603.
Vaneeckhaute, C., Meers, E., Tack, F.M.G., Belia, E., Vanrolleghem, P.A., 2017b. Modelling and optimization of nutrient recovery systems: advances and limitations. In: Meers, E., Velthof, G. (Eds.), The Recovery and Use of Mineral Nutrients from Organic Residues. Wiley, West Sussex (in press).
Vaneeckhaute, C., Ghekiere, G., Michels, E., Vanrolleghem, P., Tack, F.M.G., Meers, E., 2014. Assessing nutrient use efficiency and environmental pressure of macronutrients in bio-based mineral fertilizers: a review of recent advances and best practices at field scale. Adv. Agron. 128, 137–180.
Vanhooren, H., Meirlaen, J., Amerlinck, Y., Claeys, F., Vangheluwe, H., Vanrolleghem, P.A., 2003. Modelling biological wastewater treatment. J. Hydroinform 5, 27–50.
Vanrolleghem, P.A., Lee, D.S., 2003. On-line monitoring equipment for wastewater treatment processes: State of the art. Water Sci. Technol. 47 (2), 1–34.
Vanrolleghem, P.A., Vaneeckhaute, C., 2014. Resource Recovery from Wastewater and Sludge: Modelling and Control Challenges (Proceedings, IWA Specialist Conference on Global Challenges : Sustainable Wastewater Treatment and Resource Recovery, Kathmandu, Nepal).
Vlaco, 2012. Characterisation End Products of Biological Treatment. Report. Flemish Compost Agency (Vlaco), Mechelen, Belgium. (in Dutch).
Wang, K.L., Hung, Y.T., Shammas, N.K., 2007. Advanced physicochemical treatment processes. In: Handbook of Environmental Engineering 4. Springer Science & Business Media, CBS Publishers, New Dehli, India.
Wang, R.Y., Li, Y.M., Chen, W.L., Zou, J.T., Cheng, Y.G., 2016. Phosphate release involving PAOs activity during anaerobic fermentation of ESPR sludge and the extension of ADM1. Chem. Eng. J. 287, 436–447.
Yu, L., Zhao, Q., Jiang, A., Chen, S., 2011. Analysis and optimization of ammonia stripping using multi-fluid model. Water Sci. Technol. 63 (6), 1143–1152.
Zaher, U., Li, R., Jeppson, U., Steyer, J.-P., Chen, S., 2009. GISCOD: general integrated solid waste co-digestion model. Water Res. 43 (10), 2717–2727.
Zhang, J., Zhang, Y., Chang, J., Quan, X., Li, Q., 2013. Biological sulfate reduction in the acidogenic phase of digestion under dissimilatory Fe(III) reducing conditions. Water Res. 47 (6), 2033–2040.
Zumdahl, S.S., 2005. Chemical Principles, fifth ed. Houghton Mifflin Company, Boston, Massachusetts.